Pascal Time

The Hidden Geometry of Emergence from Cells to Cosmos

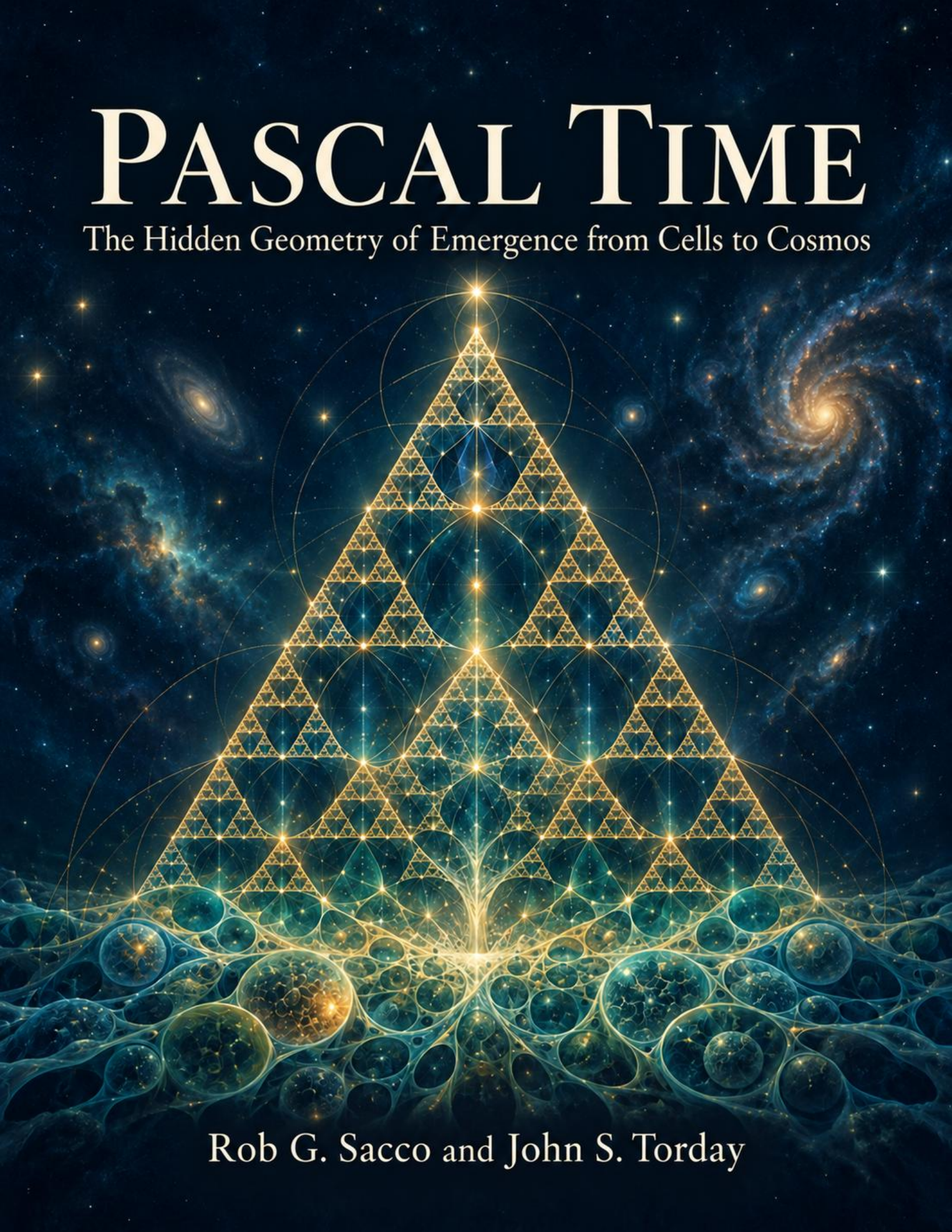

Rob G. Sacco and John S. Torday

Pascal Time: The Hidden Geometry of Emergence from Cells to Cosmos

Rob G. Sacco and John S. Torday

Abstract

This book proposes a framework for emergence across biological, cognitive, and cosmic scales using recursive combinatorics, modular patterns, information entropy, and Fibonacci scaling. Pascal's triangle provides exact examples of how simple rules generate structured possibilities; the application of those structures to physical time remains a hypothesis. The book distinguishes mathematical identities from exploratory comparisons involving development, evolution, orbital periods, and cosmological milestones. Its scientific tables retain the indexing conventions, conversion assumptions, comparison data, and limitations needed to assess these proposals. A research program specifies how independent data, alternative models, and predictions fixed before testing could determine whether the observed correspondences have explanatory or predictive value.

Contents

Part I Foundations and Mathematical Framework

Chapter 1 Emergence Constraint and Possibility

Chapter 2 Pascal Recursion and Fractal Structure

Part II Entropy Time and Scaling

Chapter 3 Entropy Symmetry and Pattern Regimes

Chapter 4 Recursive Time Memory and Layer Formation

Chapter 5 Fibonacci Scaling Energy and Temporal Models

Part III Physical Systems

Chapter 6 Solar and Planetary Dynamics

Chapter 7 Cosmological Structure and Timelines

Part IV Life Development and Evolution

Chapter 8 Biological Rhythms and Organization

Chapter 9 Development Aging and Lifespan

Chapter 10 Evolutionary Transitions and Timelines

Part V Mind Consciousness and Meaning

Chapter 11 Neural Organization and Consciousness

Chapter 12 Synchronicity and Meaning

Part VI Synthesis and Scientific Evaluation

Chapter 13 A Unified Framework and Its Scientific Tests

Chapter 14 Implications and Research Directions

Glossary of Key Terms

Appendix A Fibonacci Time Tables and Indexing

Appendix B Anatomical and Developmental Patterns

Appendix C Formal Foundations

References

Preface

This book asks whether a simple recursive structure can help describe the organization of change across biological and physical systems. Pascal's triangle provides a tractable starting point: local addition generates combinatorial growth, while modular filtering reveals nested geometry. These mathematical properties motivate a broader investigation of emergence under constraint.

Our proposal is that recursive constraints may help organize the timing and form of transitions across scales. We develop this proposal through entropy measures, Fibonacci indexing, and comparisons with biological and cosmological timelines. The mathematical constructions are explicit; their extension to natural systems remains a hypothesis to be tested.

The framework complements mechanistic explanations by asking whether they share measurable structural regularities. Its value depends on transparent mappings, meaningful alternatives, and predictive performance. The tables preserve the comparisons on which the discussion rests, including deviations and uncertainties, so that readers can assess the proposal independently.

Rob G. Sacco, Ph.D.

John S. Torday, M.Sc., Ph.D.

Reader's Guide

Parts I–II establish emergence, Pascal recursion, entropy, time, and scaling. Part III examines physical systems; Part IV covers life, development, and evolution; Part V considers mind and meaning. Part VI brings the framework together and specifies its scientific tests. The glossary and appendices provide reference material.

Key Terms

Recursion generates a new state from previous states by a repeated rule. In Pascal's triangle, each interior entry is the sum of two neighboring entries above it (Graham et al., 1994).

Modular arithmetic replaces an integer by its remainder after division by a chosen modulus. Modulo 2 retains parity: even values become 0 and odd values become 1. This transformation exposes the Sierpiński pattern within Pascal's triangle.

Entropy here usually means Shannon entropy of the symbol frequencies in a filtered row. It measures distributional diversity, not spatial arrangement or physical entropy production. Connections to thermodynamics are analogies unless a physical mapping is specified (Shannon, 1948; Cover & Thomas, 2006).

An attractor is a set toward which nearby trajectories approach under specified dynamics. Where the book uses "structural attractor" for a recurring pattern or scaling relationship, that descriptive usage does not by itself establish a dynamical attractor (Strogatz, 2015).

Constraint space is the set of configurations allowed by a system's rules and limitations. Energetic, informational, and structural constraints restrict which transitions are possible.

How to Read the Book

Equations state the construction; figures show its geometry; tables present the comparisons. Mathematical identities, physical analogies, and empirical hypotheses should be evaluated separately. The timing tables retain their stated index conventions and conversion rules; Appendix A distinguishes zero-based Pascal rows from one-based row labels.

Part I Foundations and Mathematical Framework

Chapter 1 Emergence Constraint and Possibility

Emergence requires an account of how interactions produce organized behavior and how constraints limit what can occur. This chapter develops the vocabulary of possibility spaces, trajectories, and attractors used throughout the book.

1.1 Emergence Across Scales

Components and Collective Organization

Reductionist methods explain components and local interactions, but system-level organization also requires an account of how those interactions combine. The problem of emergence concerns properties that are absent from components considered in isolation (Holland, 1998).

Metabolic regulation depends on biochemical networks, cognition on coordinated neural activity, and cosmological structure on collective gravitational dynamics. These examples motivate models that connect local mechanisms with organized outcomes (Noble, 2008; Bassett & Gazzaniga, 2011; Mo et al., 2010).

Testable Emergence

Claims about emergence become testable when initial conditions, update rules, and observables are specified. Cellular automata and recursive mathematical constructions allow researchers to reproduce global patterns generated by local interactions (Wolfram, 2002).

In such systems, local interactions generate global patterns without centralized control. For instance, flocking behavior in birds arises from simple behavioral rules followed by individuals, yet produces coordinated collective motion exhibiting stability and adaptability (Camazine et al., 2001). Likewise, fractal geometries emerge from repeated application of simple transformations, demonstrating scale-invariant structure generated algorithmically rather than externally imposed (Mandelbrot, 1982).

Organization Across Scales

One of the defining characteristics of emergent systems is continuity across scales. Processes operating at microscopic levels propagate upward through intermediate organizational layers to produce macroscopic structure. This hierarchical organization allows emergent properties at one level to become foundational components at the next (Nicolis & Prigogine, 1989).

In biology, molecular interactions give rise to cellular behavior, cells organize into tissues, and tissues form organisms exhibiting coordinated physiology. Each level introduces new properties—metabolism, regulation, cognition—that cannot be reduced entirely to lower levels (West et al., 1997). Similarly, neural circuits form cognitive networks, which in turn support consciousness and social behavior (Kandel et al., 2013).

Cosmological evolution exhibits analogous scaling relationships. Local gravitational interactions produce stars, stars organize into galaxies, and galaxies form clusters and large-scale cosmic structures (McKee & Ostriker, 2007). Across domains, recurring mathematical patterns such as

fractals and Fibonacci scaling suggest that similar generative principles may operate regardless of physical substrate (Livio, 2002).

Structured Novelty

The guiding question is how local interactions generate structured novelty without a blueprint. Self-organization offers one route: feedback can amplify fluctuations and stabilize collective patterns under energetic and environmental constraints (Kauffman, 1993).

Self-organizing systems operate far from thermodynamic equilibrium, maintaining structure through continuous energy flow and interaction with their environments (Prigogine & Stengers, 1984). Under these conditions, small fluctuations can be amplified through nonlinear feedback, producing new stable configurations or attractor states. Importantly, these structures are neither imposed nor random; they are consequences of the system's internal rule space.

1.2 Evolution and Constraint

Evolution Under Constraint

Evolution combines variation, selection, and inheritance within physical and developmental limits. Recurring forms and scaling relationships motivate a complementary question: which configurations are accessible, and which constraints channel transitions between them (Darwin, 1859/2009; Kauffman, 1993; West et al., 1997)?

The search is open-ended because new configurations remain possible, yet bounded by energetic costs, informational capacity, developmental history, and ecological interactions. Constraint shapes the available variation rather than specifying a predetermined evolutionary destination.

Developmental pathways restrict morphology, metabolic costs limit viable adaptations, and ecological interactions define feasible niches. Such constraints can also enable novelty by stabilizing combinations that would otherwise fail to persist (Gould, 2002).

Types of Evolutionary Constraints

Constraints operate across multiple domains simultaneously. For analytical clarity, they may be grouped into energetic, informational, and structural categories. Although conceptually distinct, these constraint classes interact continuously in living systems.

Energetic Constraints

All biological systems exist far from thermodynamic equilibrium and must continuously exchange energy with their environments to maintain organization (Schrödinger, 1944). The Second Law of Thermodynamics imposes unavoidable limits on energy transformations, ensuring that every metabolic process produces entropy and dissipates usable energy (Hayflick, 2007).

Energetic constraints shape evolution by favoring configurations that optimize energy throughput relative to maintenance costs. Metabolic scaling laws demonstrate that organismal structure follows predictable relationships between energy consumption and body size, suggesting that energy distribution imposes deep organizational constraints (West et al., 1997). Similarly,

ecological systems evolve toward energy-efficient trophic structures that stabilize resource flows (Odum & Pinkerton, 1955).

Informational Constraints

Life depends fundamentally on information storage, transmission, and interpretation. Genetic systems encode instructions governing development and function, but informational capacity is finite. Biological information must therefore remain compressible, interpretable, and robust against noise (Adami, 2016).

Information theory provides a framework for understanding these constraints. Shannon entropy measures uncertainty in symbolic systems, demonstrating that efficient codes balance redundancy and compression to maintain reliability (Shannon, 1948). Genetic coding systems exhibit precisely this balance: redundancy protects against mutation, while compression enables efficient storage of functional information (Maynard Smith, 2000).

Predictability also constrains evolution. Developmental processes must reliably produce viable organisms despite environmental variability. Gene regulatory networks therefore evolve architectures that stabilize outcomes through feedback loops and modular organization (Alon, 2007). These informational constraints restrict evolutionary exploration to configurations capable of maintaining coherent developmental trajectories.

Structural Constraints

Physical structure imposes another layer of constraint. Biological forms must obey geometric and topological laws governing material stability and spatial organization. For example, vascular networks exhibit fractal branching patterns that minimize transport energy while maximizing coverage, reflecting optimization under geometric constraints (Mandelbrot, 1982; West et al., 1997).

Topology further constrains connectivity. Neural and ecological networks must balance integration with robustness; excessive connectivity increases energetic cost, whereas insufficient connectivity reduces functional coordination (Sporns, 2011). Evolution repeatedly converges on modular architectures because modularity allows systems to adapt locally without destabilizing global organization (Simon, 1962).

Representing Possibility Space

If evolution operates as a constrained search, then the concept of **possibility space** becomes central. Possibility space refers to the set of all configurations accessible to a system under governing rules. Without formal representation of this space, explanations of evolutionary novelty remain descriptive rather than predictive.

Traditional evolutionary theory often treats variation implicitly, assuming an undefined pool of potential forms. However, complexity research demonstrates that the structure of possibility space strongly determines evolutionary outcomes (Kauffman, 1993). Some configurations are densely reachable through small changes, while others are effectively inaccessible because intermediate states are nonviable.

Formalizing possibility space enables several advances:

1. **Prediction of evolutionary pathways** based on accessible transitions.
2. **Identification of attractor regions** where stable configurations cluster.
3. **Quantification of novelty** as movement into previously unoccupied regions.
4. **Comparison across scales**, linking biological, cognitive, and physical evolution.

Pascal Recursion as a Minimal Model

Pascal recursion supplies a minimal mathematical example of growth within fixed rules. Each row expands the set of entries while local addition determines every coefficient. Its relevance here is methodological: it lets us study generation, filtering, and pattern measurement in a system whose rules are completely explicit.

Several properties make Pascal recursion particularly relevant as a conceptual model:

1. **Local Rule, Global Complexity**

Complex patterns emerge from repeated application of a minimal rule, paralleling evolutionary processes driven by local interactions.

2. **Intrinsic Constraint Structure**

Each new state depends strictly on prior states, limiting accessible configurations while preserving open-ended growth.

3. **Entropy Gradients**

Recursive depth produces transitions from uniformity to patterned complexity, analogous to evolutionary diversification.

1.3 States Trajectories and Attractors

States and Trajectories

The study of emergence begins with a shift in perspective. Traditional descriptions of nature focus on objects located in physical space. A planet occupies a position; a pendulum swings through an arc; a biological organism exists within an environment. Yet prediction and explanation require more than location alone. What determines future behavior is not merely where a system is, but **what state it occupies**.

A system's state consists of all variables necessary to determine its future evolution. For a pendulum this includes position and velocity; for planetary motion, position and momentum; for neural systems, distributed activation patterns across networks. The collection of all possible states forms an abstract mathematical space known as **phase space** (Arnold, 1989; Strogatz, 2015).

Phase space replaces the intuition of objects moving through space with trajectories moving through possibility. Each axis represents an independent degree of freedom rather than a spatial direction. The evolution of a system can then be written generically as:

$$state_{t+1} = F(State_t)$$

where the function F describes the recursive update rule governing the system.

In this formulation, time indexes successive transformations of state. Emergence therefore occurs not primarily in physical space but within the geometry traced by these evolving trajectories.

This shift—from objects to states—marks one of the foundational insights of modern dynamical systems theory (Guckenheimer & Holmes, 1983).

Attractors

When trajectories evolve in phase space, they rarely wander arbitrarily. Instead, many systems converge toward structured regions known as **attractors**—sets of states toward which nearby trajectories evolve over time (Strogatz, 2015).

Several canonical attractor types appear across disciplines:

Fixed Points — Static Order

Systems settle into equilibrium states, such as chemical balance or thermal rest. In phase space, these appear as single points.

Limit Cycles — Periodic Recursion

Oscillatory systems trace closed loops corresponding to exact repetition. Biological rhythms and mechanical oscillators exemplify this regime.

Toroidal Attractors — Coupled Cycles

When two independent periodic processes coexist, trajectories form toroidal structures. Such dynamics arise in coupled oscillations, magnetic dynamos, and quasi-periodic motion (Ott, 2002).

Strange Attractors — Structured Complexity

Nonlinear feedback can stretch and fold trajectories, producing fractal structures associated with deterministic chaos. These attractors exhibit bounded unpredictability and sensitive dependence on initial conditions (Lorenz, 1963; Gleick, 1987).

Constraint and Entropy

Attractors arise because systems operate under constraint. Conservation laws, energetic limits, and interaction rules restrict accessible regions of phase space. Constraints sculpt the geometry of possible evolution much as gravity shapes a physical landscape.

Statistical entropy depends on the distribution of accessible microstates, while dynamical descriptions track trajectories through phase space (Boltzmann, 1877; Penrose, 2004). These

perspectives can be related in specified models. They do not establish a general ranking in which fixed points, tori, and fractal attractors necessarily have increasing entropy.

Such transitions align naturally with recursive systems in which iterative rules generate expanding possibility under constraint. Later chapters will show how Pascal recursion provides a discrete analogue of these processes, allowing entropy dynamics to be studied in a combinatorial setting.

Universality and Time

One of the most powerful consequences of the phase-space viewpoint is **universality**. Systems as diverse as fluids, ecosystems, neural networks, and astrophysical plasmas exhibit similar attractor geometries despite radically different underlying mechanisms (Mitchell, 2009).

Within this framework, time itself acquires a geometric interpretation. Rather than acting solely as an external dimension, time orders motion along trajectories in phase space. The history of a system becomes a curve; prediction becomes continuation of that curve.

This interpretation does not replace physical time but provides a powerful descriptive framework widely used in dynamical systems, statistical mechanics, and neuroscience (Kelso, 1995).

Chapter 2 Pascal Recursion and Fractal Structure

Pascal recursion provides the mathematical construction underlying the framework. We move from binomial growth to modular fractals and higher-dimensional representations, distinguishing exact identities from comparisons with physical and biological systems.

2.1 Binomial Recursion and Combinatorial Growth

Binomial Recursion

Pascal's triangle is generated by local addition: each interior entry equals the sum of the two entries immediately above it. With n denoting the zero-based row index, the binomial coefficients satisfy (Graham et al., 1994):

$$\binom{n}{k} = \binom{n-1}{k-1} + \binom{n-1}{k}, \binom{k}{n} = \binom{k-1}{n-1} + \binom{k}{n-1}$$

with boundary conditions defined by unity along the edges. This rule represents a principle of **local additivity**, where new states emerge solely from neighboring prior states without centralized coordination.

The recursive construction also encodes path dependence. Each value reflects the cumulative history of preceding interactions, meaning that later structure is constrained by earlier configurations. Such dependence parallels evolutionary systems, where present forms arise through accumulated historical contingencies constrained by prior states (Kauffman, 1993).

Counting Growth and Probability

The same array connects counting, growth, and probability. Three properties are especially useful here.

First, Pascal's triangle encodes exponential expansion. Each row corresponds to coefficients of the binomial expansion $(a + b)\hat{}n$, demonstrating how iterative combination generates increasingly complex distributions from simple initial conditions. This property parallels growth processes in biology and physics, where repeated interactions amplify variation while maintaining structural coherence (Prigogine & Stengers, 1984).

Every row is symmetric because choosing k elements from n is equivalent to choosing the n − k elements left out. Filtering preserves some features of this symmetry while exposing patterns of parity and residue classes.

Third, the triangle naturally generates probability distributions. The binomial distribution converges toward the normal distribution as row number increases, illustrating how statistical regularities arise from repeated discrete interactions (Feller, 1968). This convergence demonstrates that ordered macroscopic patterns can emerge from simple combinatorial processes without centralized optimization.

Plant growth offers a visual analogy for repeated local construction under spatial constraints. Romanesco broccoli illustrates approximate self-similarity; it does not establish that plant development implements Pascal arithmetic.

Figure 2.1 — Romanesco broccoli. Repeated growth at the meristem produces approximately self-similar florets and spiral packing. This is a biological illustration of constrained growth, not a derivation from Pascal recursion. Source: Wikipedia (2021).

Diagonal Sums

Summing shallow diagonals of Pascal's triangle gives the Fibonacci sequence (Livio, 2002). Its recurrence is:

The Fibonacci sequence obeys its own recursion:

$$F_n = F_{n-1} + F_{n-2}$$

The diagonal identity connects two recursive constructions without introducing a separate empirical assumption. It will later motivate, but does not validate, the use of Fibonacci values as a temporal indexing scheme.

Ratios of consecutive Fibonacci numbers approach the golden ratio. This relation is mathematically exact in the limit; whether a natural process follows a related scaling law requires a separate model and evidence (Livio, 2002).

This perspective may be extended by considering generalized Fibonacci recursions, in which each term depends on not two but p preceding values. As the number of contributing prior states increases, the resulting sequences interpolate between Fibonacci growth and exponential doubling. In the limit where each term aggregates all previous values, the recursion approaches powers of two, producing the sequence 1,2,4,8,16,…Pascal's triangle implicitly contains this entire spectrum: diagonal aggregations yield Fibonacci scaling, while row sums produce exponential expansion. Different growth laws therefore arise not from different generative rules but from different modes of aggregation within the same recursive structure.

Recursion Grammars

A recursion grammar specifies transformations that generate new states from earlier ones. Pascal addition is one example; symbolic production rules and cellular automata provide others (Chomsky, 1956; Wolfram, 2002). Repeated rules can produce increasingly elaborate outputs without becoming more elaborate themselves.

Complexity science demonstrates that hierarchical organization naturally arises from recursive processes operating across levels (Simon, 1962). Each layer becomes the substrate for further recursion, producing nested structures characteristic of living and cosmic systems.

Figurate Numbers and Dimensions

Pascal's diagonals also enumerate figurate numbers. They connect the accumulation of discrete units with a hierarchy of geometric objects.

Each entry of Pascal's triangle is a binomial coefficient,

$$(nk), \binom{n}{k}, (kn)$$

where *n* represents recursion depth and *k* identifies position within the row. Traditionally, these coefficients are interpreted as counting combinations. However, an equally fundamental interpretation arises when they are viewed geometrically: the index *k* corresponds to dimensionality within a hierarchy of simplex structures.

A simplex is the simplest possible geometric object in a given dimension:

- a point in 0 dimensions,
- a line segment in 1 dimension,
- a triangle in 2 dimensions,
- a tetrahedron in 3 dimensions,
- and higher-dimensional analogues beyond ordinary spatial intuition.

Table 2.1 — Figurate numbers and simplex dimensions in Pascal's triangle

Dimension	Geometric Object	Figurate Numbers	Pascal Coefficient
0D	Point	1	$\binom{n}{0}$
1D	Line	Counting numbers	$\binom{n}{1}$
2D	Triangle	Triangular numbers	$\binom{n}{2}$
3D	Tetrahedron	Tetrahedral numbers	$\binom{n}{3}$
4D	4-Simplex (Pentatope)	Pentatope numbers	$\binom{n}{4}$
…	Higher simplices	Higher figurate numbers	$\binom{n}{k}$

Fixing a diagonal selects a family of figurate numbers; moving along it increases the size of the corresponding discrete construction. Table 2.1 lists the dimensional associations and coefficients.

Triangular numbers sum successive linear counts, tetrahedral numbers sum triangular counts, and higher simplex numbers continue the construction. This is a combinatorial model of dimensional stacking, not a physical derivation of spatial dimensions.

The familiar recursion,

$$\binom{n}{k} = \binom{n-1}{k-1} + \binom{n-1}{k}$$

acquires a geometric meaning under this view. Each new structure forms from the union of two adjacent predecessor structures, analogous to adding successive layers of a growing geometric object. Local addition becomes dimensional stacking.

2.2 Modular Filtering and Fractals

Modular Arithmetic

Modular reduction replaces each integer by its remainder after division by a fixed positive integer. It discards magnitude while retaining congruence classes, exposing regularities that are difficult to see among rapidly growing coefficients (Koblitz, 1994).

Formally, for integers *a* and *n*, the expression *a mod n* returns the remainder after division by *n*. While simple, this operation reorganizes numerical systems into equivalence classes known as congruence classes. These classes expose periodicities and symmetries that are otherwise obscured by numerical growth.

$$F_n = F_{n-1} + F_{n-2}$$

The Sierpiński Pattern

One of the most striking demonstrations of modular filtering occurs when Pascal's triangle is evaluated modulo 2. Each entry is replaced by either 0 (even) or 1 (odd). When odd values are visualized as filled cells and even values as empty cells, a fractal structure—the **Sierpiński triangle**—emerges (Mandelbrot, 1982).

The appearance of this fractal is remarkable because no geometric rule was introduced. The only governing principle remains binomial recursion:

$$\binom{n}{k} = \binom{n-1}{k-1} + \binom{n-1}{k}, \qquad \binom{k}{n} = \binom{k-1}{n-1} + \binom{k}{n-1}$$

combined with modular reduction. The fractal pattern therefore arises entirely from deterministic arithmetic operations.

Successive iterations reveal how geometric structure unfolds progressively through recursion, with each level introducing new self-similar voids while preserving the global triangular form (Figure 2.2).

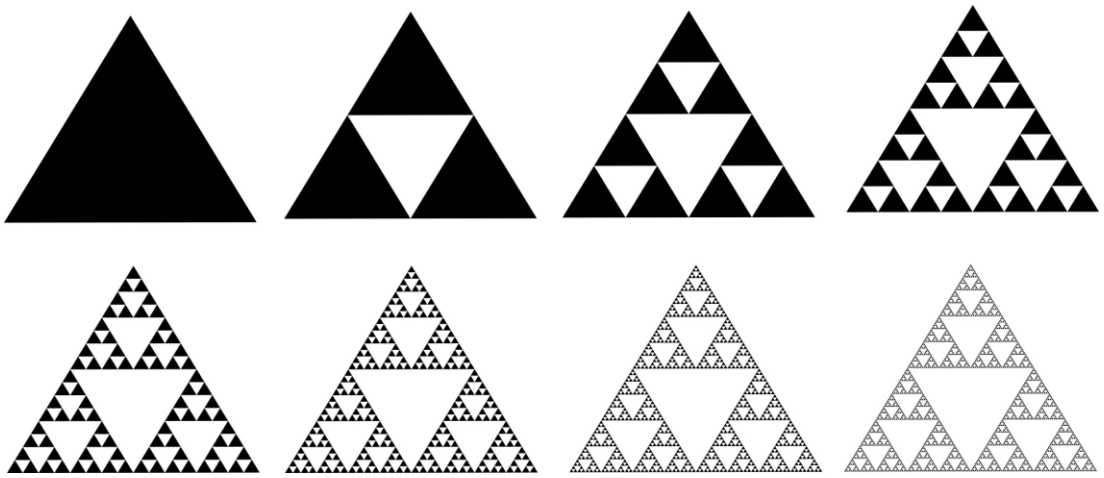

Figure 2.2 — Sierpiński structure from Pascal parity. Filled cells represent odd coefficients and empty cells even coefficients. Repeated binomial addition followed by reduction modulo 2 generates the nested pattern.

Each larger triangle contains smaller copies of itself indefinitely, demonstrating scale invariance. Importantly, this structure emerges without randomness or probabilistic input. Complexity is generated purely through repeated local rules.

Higher Moduli and Addresses

Higher moduli introduce larger residue alphabets and different pattern families. Their structure depends on both the modulus and the arithmetic properties of the coefficients (Granville, 1997).

Unlike the strict binary structure of mod 2, higher moduli introduce multiple residue classes, expanding the system's symbolic alphabet. Each residue class acts as a distinct state, allowing richer combinatorial interactions. Visualization of these classes generates multicolored fractal fields displaying layered self-similarity.

For a prime modulus p, Lucas's theorem relates a binomial coefficient to the digits of its indices in base p. This explains recurring arithmetic structure across scales (Fine, 1947).

These results illustrate an important principle: fractal complexity depends not only on recursion but also on the **filter applied to observation**. Different modular lenses expose different invariant structures within the same underlying system. Complexity therefore becomes observer-relative in a formal mathematical sense—not subjective, but dependent on transformation.

A symbolic address identifies each subtriangle by a sequence of choices: top, left, or right. This records its location within the recursive hierarchy and connects deterministic subdivision with the random vertex choices used in the Chaos Game.

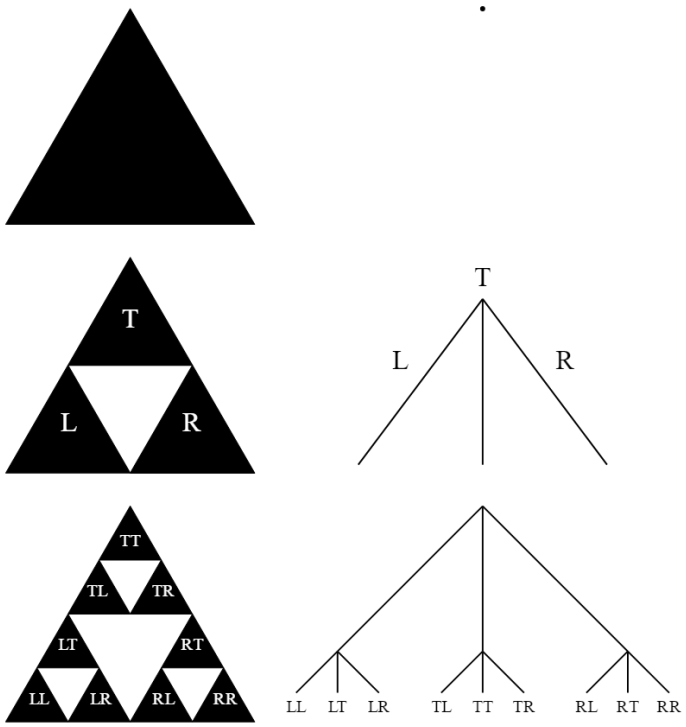

Figure 2.3 — Addresses in the Sierpiński triangle. T, L, and R identify top, left, and right subtriangles. Longer addresses identify smaller nested regions.

Probability and Quantum Comparisons

Binomial coefficients count paths through repeated binary branching. Under independent, equally probable left and right choices, normalizing a row by its sum gives the corresponding endpoint probabilities.

The Galton board makes this interpretation concrete. Balls encounter successive pegs and move left or right; an idealized independent fair-choice model gives a binomial endpoint distribution. The array counts routes, while the probabilistic assumptions determine how frequently they are taken.

Recent work extends this relationship into quantum mechanics. Bannink and Buhrman (2017) demonstrated that quantum analogues of Pascal structures arise in quantum walks, where superposition replaces classical branching. Under modular reduction, these systems generate fractal patterns such as the Sierpiński triangle (mod 2) and Sierpiński carpet (mod 3), revealing that recursive combinatorial structure persists even within quantum dynamics.

Similarly, Carney and Varcoe (2022) introduced a quantum implementation of the Galton board within a “universal statistical simulator.” By exploiting quantum superposition and entanglement, their model reproduces binomial distributions while achieving exponential computational speed-up relative to classical simulations. In this framework, probability amplitudes propagate simultaneously along multiple paths, generalizing the classical branching process encoded by Pascal recursion.

Engineered Fractal Constraints

Recent experimental work demonstrates that fractal geometry can directly influence physical behavior at microscopic scales. Kempkes et al. (2018) constructed a Sierpiński triangle by positioning carbon monoxide molecules on a copper surface, thereby confining electrons within a deliberately engineered fractal potential landscape. Measurements revealed that electronic states followed the non-integer dimensionality of the structure (fractal dimension ≈ 1.58), showing that spatial constraint alone can reorganize quantum behavior.

Importantly, the experiment does not imply that nature universally adopts fractal geometries. Rather, it demonstrates a more general principle: when particles are restricted to recursively structured environments, their accessible state space changes accordingly. Geometry acts as a constraint on dynamics.

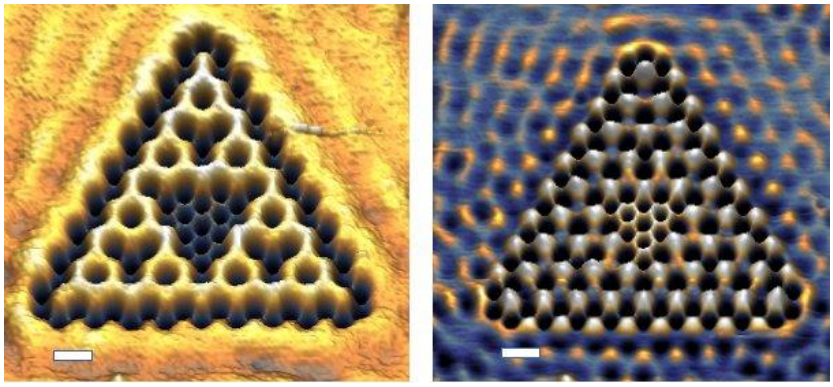

Figure 2.4 — Electronic states in an engineered Sierpiński lattice. Scanning tunneling images show bonding and non-bonding geometries that constrain electronic states. Source: Kempkes et al. (2018).

Exact and Statistical Self Similarity

Deterministic cellular automata provide a concrete illustration. Wolfram's Rule 30, governed by a minimal binary update rule, produces patterns statistically similar to random noise even though every state follows strict deterministic causation (Wolfram, 2002). Local predictability coexists with global unpredictability. Systems governed by simple recursive laws can therefore appear stochastic when observed at larger scales. The emergence of fractal structure in Pascal mod-2 recursion reflects the same principle: deterministic local addition generates large-scale complexity without introducing chance.

Exact self-similarity in mathematical fractals differs from the approximate or statistical self-similarity of natural forms. Environmental perturbations and developmental variation change local details while sometimes preserving broader scaling relationships.

Branching vasculature, shell growth, and plant organization illustrate this distinction: developmental constraints delimit families of forms, while light, nutrients, temperature, and mechanical stress alter individual realizations (Thompson, 1942; West, Brown, & Enquist, 1997). Such examples motivate comparisons with recursive models without establishing a shared mechanism.

2.3 Higher Dimensions and Biological Information

Higher Dimensional Recursion

Pascal's pyramid extends binomial recursion to a trinomial array. Each layer contains coefficients associated with three possible contributions, and an interior entry sums three predecessors (Graham, Knuth, & Patashnik, 1994; Figure 2.5).

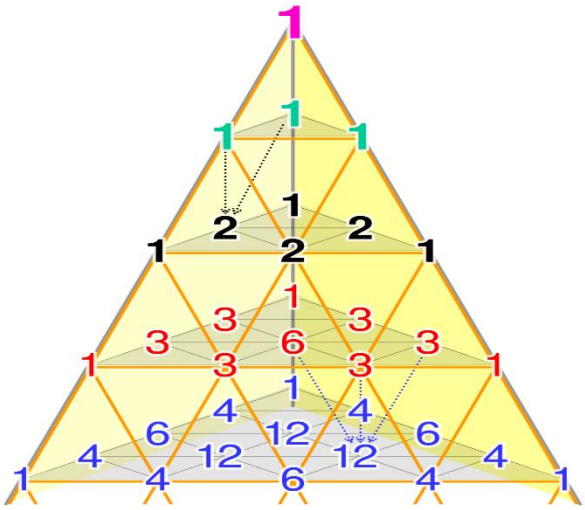

Figure 2.5 — Pascal's pyramid. Trinomial coefficients accumulate through local addition across successive triangular layers, extending the planar binomial construction.

Where Pascal's triangle encodes binomial coefficients, Pascal's pyramid encodes trinomial and, more generally, multinomial coefficients. Each element of the pyramid equals the sum of three adjacent elements from the previous layer, extending local additivity into three spatial directions. This preserves the essential recursive rule while increasing dimensional freedom.

An orthogonal lattice offers another representation of additive recursion (Figure 2.6). The coordinates and neighborhood rule must be specified for each embedding; similar appearances do not make different constructions interchangeable.

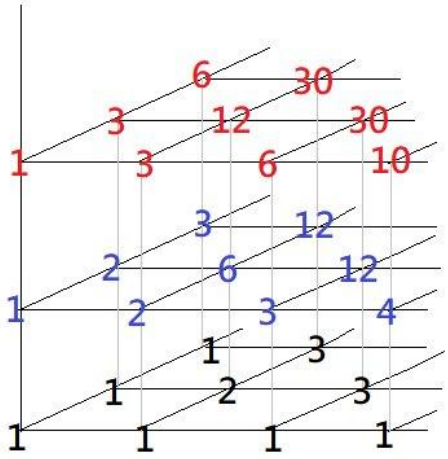

Figure 2.6 — Pascal cube. Additive propagation on an orthogonal lattice provides a spatial representation of combinatorial accumulation.

Invariants and Changes

What remains constant

Several foundational properties persist:

1. **Local additivity**: Each element is generated from neighboring predecessors.
2. **Deterministic recursion**: No randomness is introduced.
3. **Hierarchical growth**: Larger structures emerge through repeated iteration.
4. **Combinatorial interpretation**: Entries count pathways or configurations.

What changes

What changes is the geometry of constraint:

- Growth becomes volumetric rather than planar.
- Interaction neighborhoods expand.
- Pathways multiply combinatorially.
- Symmetry groups increase in complexity.

In Pascal's triangle, diagonals generate Fibonacci-like sequences. In Pascal's pyramid, analogous structures emerge along planes and spatial diagonals, producing families of higher-order recurrence relations. The combinatorial landscape becomes exponentially richer while remaining rule-bound.

Fractal Analogues

Just as Pascal's triangle produces the Sierpiński triangle under modular filtering, Pascal's pyramid generates higher-dimensional fractal analogues when evaluated modulo *n*. Applying modulo 2 to Pascal's pyramid reveals the Sierpiński tetrahedron, a three-dimensional fractal exhibiting recursive self-similarity across scales (Mandelbrot, 1982).

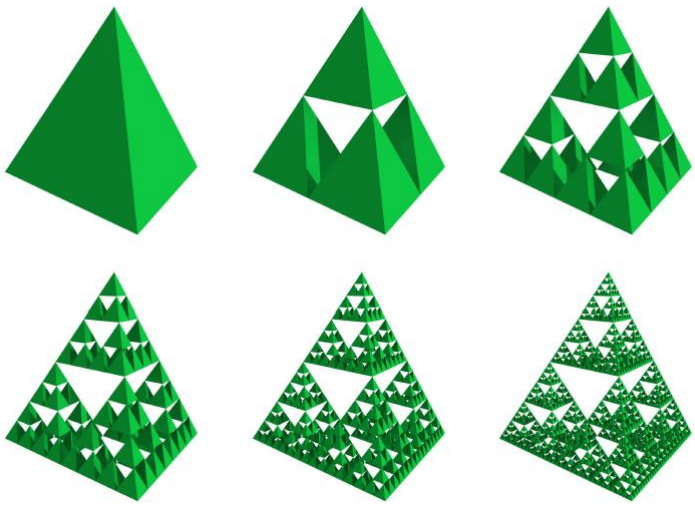

Figure 2.7 — Sierpiński tetrahedron. Repeated subdivision retains four corner tetrahedra while removing the central region, generating a self-similar three-dimensional construction.

Higher moduli generate increasingly complex volumetric patterns, forming intricate lattices and interference-like structures. These can be interpreted mathematically as **constraint manifolds**—regions of state space permitted by recursive and modular rules.

A constraint manifold represents the subset of configurations consistent with governing rules. In dynamical systems theory, attractors occupy such manifolds within phase space (Strogatz, 2015). Pascal recursion demonstrates a discrete analogue: combinatorial growth explores possibility space, while modular constraints carve out structured subsets exhibiting fractal organization.

Pascal Space

"Pascal space" denotes the family of binomial and multinomial constructions considered here. Increasing the number of components expands the configuration space; filtering or projection then selects the features to measure. This distinction between generation and observation is central to the entropy analysis that follows.

Fractal Dimension and Scaling

Fractal dimension quantifies scaling with magnification. It provides a measure distinct from both embedding dimension and the symbol-frequency entropy introduced later.

Classical geometric objects possess integer dimensions. A line has dimension 1, a square dimension 2, and a cube dimension 3. Fractals differ fundamentally in that their structure occupies space unevenly across scales, producing **non-integer dimensionality**.

The Cantor set provides a minimal illustration of recursive scaling. At each iteration, a line segment divides into two surviving intervals, producing counts that grow as 1, 2, 4, 8,… = 2^n. This exponential branching mirrors the combinatorial expansion encoded in Pascal's triangle, where successive rows enumerate binary pathway accumulation. Although the constructions differ—geometric removal versus additive aggregation—both express the same underlying principle: complexity emerging through repeated binary recursion under constraint. In this context, the Hausdorff dimension provides a quantitative measure of how completely recursive processes populate space, capturing the balance between structural order and fragmentation across scales.

Table 2.2 summarizes representative fractal structures and their associated Hausdorff dimensions.

Table 2.2 — Fractal Hausdorff Dimensions and Scaling Relationships

Type of Fractal	Euclidean Dimension	Hausdorff Dimension	Random Hausdorff Dimension	Euclidean Analogue
Cantor set	0	0.630929	0.618033	Line
Sierpiński triangle	2	1.584962	1.618033	Square
Sierpiński cube	3	2.726833	2.618033	Cube
Random 4-D Cantor set	4	4.236068	4.236067	Hypercube

Note. Data adapted from Ho, El Naschie, and Vitiello (2015).

The "random Hausdorff dimension" describes fractals generated under partial stochastic perturbation rather than strict deterministic iteration. Remarkably, these values approximate powers of the golden ratio ($\varphi \approx 1.618$):

- the Cantor set approaches $1/\varphi$,
- the Sierpiński gasket approaches φ,
- higher-dimensional analogues approximate φ^2 and φ^3.

Table 2.2 reproduces the dimensional comparisons attributed to Ho, El Naschie, and Vitiello (2015). The reported "random Hausdorff dimensions" depend on the particular stochastic constructions used by that source; they are not universal values for perturbed versions of the named fractals. Their proximity to powers of φ is a proposed correspondence, not an independently established scaling law.

The golden ratio possesses a unique mathematical property: it represents the most difficult proportion to approximate using rational numbers. As a result, φ minimizes repetitive alignment and interference across iterative processes. Systems evolving through repeated subdivision or growth may therefore gravitate toward φ-like scaling because such ratios distribute structure efficiently while avoiding degeneracy.

Biological Information Spaces

Information Geometry of the Genetic Code

The genetic code provides a concrete biological realization of a finite combinatorial space. DNA encodes information using four nucleotides arranged in triplets, producing $4^3 = 64$ possible codons that map onto amino acids and regulatory signals. Although biochemical rather than mathematical in origin, this structure forms a constrained multinomial system: each codon emerges from sequential positional choices drawn from a fixed symbolic alphabet.

Mathematically, codon space is equivalent to a 4-ary Hamming cube of dimension three, in which each codon occupies a discrete point and distances correspond to the number of nucleotide substitutions required to transform one codon into another (Lenstra, 2015).

The codon Hamming-distance matrix has a nested block structure determined by its three symbolic positions (Lenstra, 2015; Figure 2.8). The motifs illustrate combinatorial organization but are not, by themselves, a strict mathematical fractal.

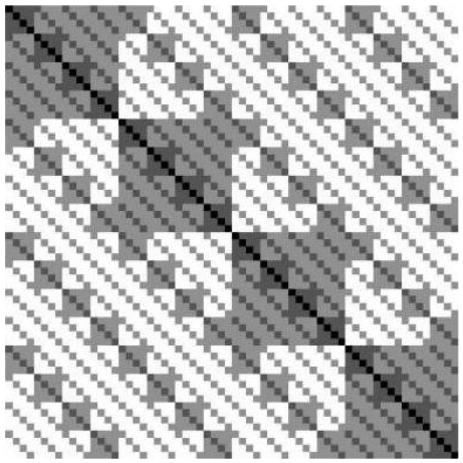

Figure 2.8 — Codon Hamming-distance matrix. Cells give the number of differing nucleotide positions between codon pairs. The block structure follows the Cartesian-product organization of three positions. Adapted from Lenstra (2015).

The origin of this global organization becomes clearer when codon space is examined locally. Sets of codons differing in only one nucleotide position form structured adjacency neighborhoods governed by minimal transformation rules. A representative cube subgraph (Figure 2.9), adapted from Lenstra (2015), illustrates how single substitutions define nearest neighbors, while larger substitution distances produce higher-order geometric relations.

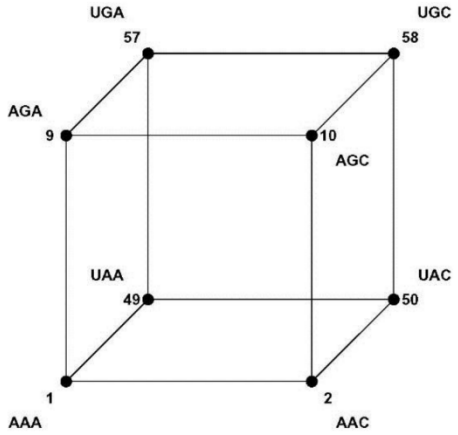

Figure 2.9 — Local codon adjacency. Edges connect the illustrated codons that differ by one nucleotide. Adapted from Lenstra (2015).

Codon geometry and Pascal recursion illustrate different ways to organize discrete possibilities. The former uses symbolic substitutions; the latter uses additive coefficients. Similar motifs do not imply causal or mechanistic equivalence.

The correspondence should therefore be understood as **structural convergence rather than derivation**. DNA does not implement Pascal arithmetic, nor does Pascal recursion encode biological mechanisms. Instead, both instantiate a shared organizational principle: complex informational order can emerge through iterative exploration of constrained combinatorial possibilities.

Part II Entropy Time and Scaling

Chapter 3 Entropy Symmetry and Pattern Regimes

Entropy calculations describe selected properties of a distribution, while symmetry and arrangement require additional information. This chapter establishes those distinctions before presenting the parity classifications and their tables.

3.1 Entropy and Configuration Space

Entropy Across Domains

Thermodynamic entropy constrains energy transformations; statistical entropy characterizes microscopic distributions; Shannon entropy measures uncertainty over symbols. These quantities share mathematical connections, but their physical interpretations depend on the state space, probabilities, and units (Shannon, 1948; Callen, 1985).

Thermodynamic entropy emerged historically from the study of heat engines, where it served as a state variable governing the direction of physical processes. Systems evolve toward states compatible with a larger number of microscopic arrangements, producing the familiar association between entropy and irreversibility (Callen, 1985). Statistical mechanics later clarified this relationship through Boltzmann's formulation, $S = klogW$ where W represents the number of accessible microstates consistent with macroscopic constraints (Pathria & Beale, 2011). Entropy therefore reflects not disorder per se, but multiplicity—the size of configuration space permitted by physical laws.

Information theory generalized this insight beyond physics. Shannon entropy measures the uncertainty of symbol distributions in a message:

$$\mathrm{H} = -\sum_{i=1}^{n} p(x_i)\log_2 p(x_i)$$

Here entropy quantifies informational diversity rather than energetic dispersion (Shannon, 1948). Crucially, randomness is not required; entropy depends only on distributional structure rather than causal origin (Cover & Thomas, 2006).

Counting Configurations

Pascal's triangle counts binary-choice pathways through deterministic addition. The path count grows with row depth, but this does not imply that the entropy of a filtered row increases monotonically. Path multiplicity and symbol-frequency entropy are different observables (Graham, Knuth, & Patashnik, 1994).

Filtering and Observation

While Pascal recursion generates combinatorial abundance, structure becomes most visible when the system is viewed through constraints. Modular arithmetic provides such a constraint by filtering numerical values into symbolic classes.

Under modulus 2, each coefficient reduces to either 0 or 1, transforming numerical rows into binary information sequences. Higher moduli produce larger symbolic alphabets. The modulus therefore acts as an observational lens selecting particular symmetries while suppressing others.

A modulus fixes the symbol alphabet and therefore the frequency distribution being measured. Changing the modulus can change the entropy of the same numerical row. The values must always be reported together with the filter and row convention.

Describing Pattern Regimes

Successive parity rows include uniform, alternating, and more differentiated arrangements. Their symbol-frequency entropies follow deterministically from their numbers of zeros and ones. Section 3.3 compares these patterns; the structural classes require information about arrangement as well as entropy.

"Phase" is used here for a descriptive pattern regime. Similarity to phase transitions in physical systems is an analogy and does not establish a thermodynamic transition in the array (Anderson, 1972; Strogatz, 2015).

3.2 Measuring Symbol Entropy

Binary Rows

Formally, the *n*-th row of Pascal's triangle under mod 2 can be expressed as a binary string:

$$R_n = (r_0, r_1, r_2, \dots, r_n), \quad r_i \in \{0,1\}$$

Shannon Entropy and Symbol Balance

Shannon entropy provides a quantitative measure of uncertainty or informational diversity within a symbolic sequence. For a binary sequence with probabilities p_0 and p_1 for symbols 0 and 1, entropy is defined as:

$$H = -(p_0 \log_2 p_0 + p_1 \log_2 p_1)$$

The probabilities in this calculation are the relative frequencies of 0 and 1 within a row. The sequence is generated deterministically; entropy describes the uncertainty of a symbol sampled from that row, not uncertainty about the rule that generated it.

Low entropy occurs when symbol distribution is highly uneven—for example, rows composed entirely of ones. Such sequences are maximally ordered and highly predictable. High entropy arises when zeros and ones appear in roughly equal proportions, increasing informational diversity.

Shannon entropy at this single-symbol level ignores arrangement. An alternating sequence and an irregular sequence can have the same value if their symbol counts match. Entropy alone therefore cannot establish structural complexity, randomness, or a developmental stage (Cover & Thomas, 2006).

Entropy as a Diagnostic

Entropy can help describe transitions between row patterns, provided it is paired with arrangement-sensitive measures. Uniform rows have H = 0; near-balanced rows, including alternating rows, have H close to one bit. “Intermediate” in a structural classification must not be confused with intermediate numerical entropy.

Distribution and Arrangement

Sequences with identical symbol frequencies can differ in periodicity, correlations, and compressibility. A complete pattern description therefore needs both distributional and arrangement information.

This distinction highlights a limitation of purely statistical entropy measures. Structural organization depends not only on symbol proportions but also on relational positioning. In recursive systems, arrangement encodes generative history.

Pascal recursion preserves correlations across positions because each entry derives from neighboring predecessors. These correlations generate long-range dependencies visible in fractal geometry. Consequently, arrangement reflects constraint propagation through recursion depth.

Information theory addresses this distinction through concepts such as mutual information and algorithmic complexity, which capture relational structure beyond frequency counts (Cover & Thomas, 2006). In recursive combinatorics, pattern identity emerges from these relational constraints.

3.3 Parity Patterns and Entropy Tables

Uniform Rows and Indexing

In this section and Table 3.2, R denotes a one-based row label: R = n + 1, where n is the zero-based binomial index. Uniform all-odd rows occur at R = 2^m, equivalently n = $2^m - 1$. Thus row labels 32 and 64 refer to binomial indices 31 and 63. This distinction is essential when comparing the prose, formulas, and tables.

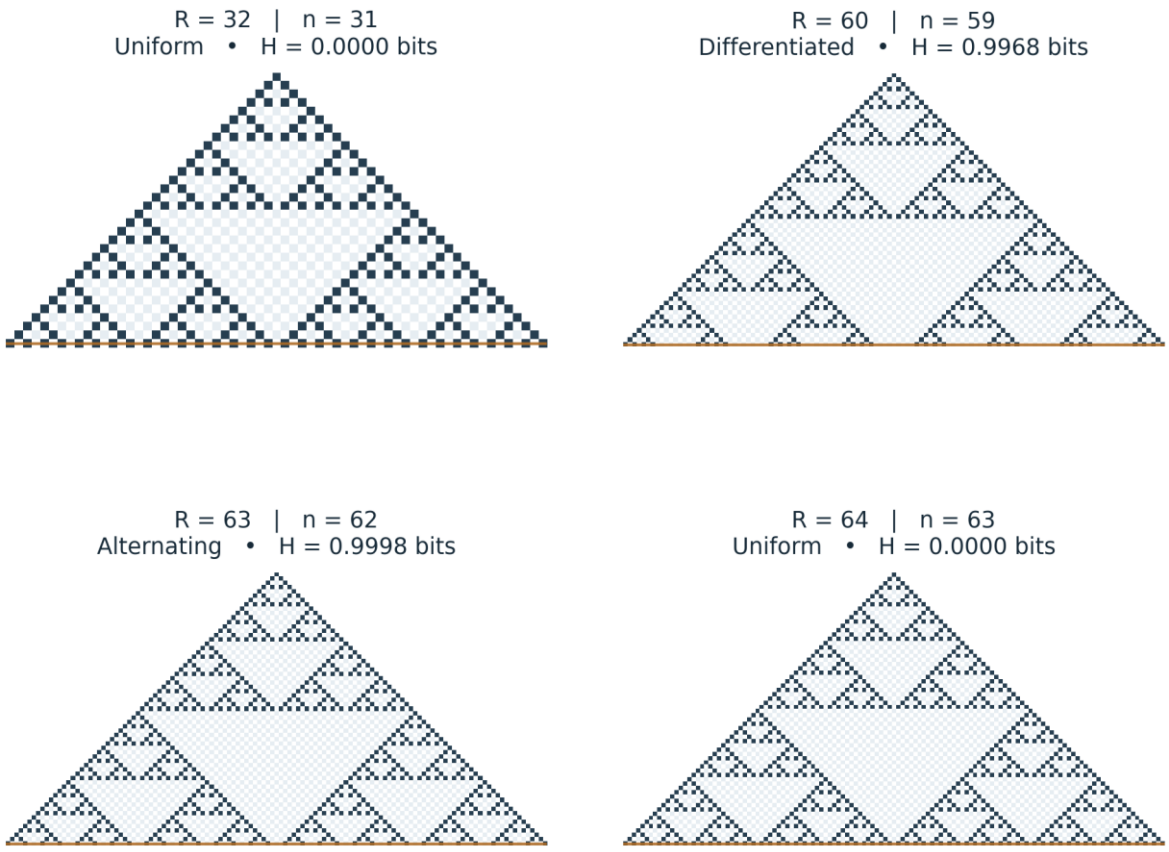

Figure 3.1 — Comparison of Pascal parity rows. Panels show one-based rows R = 32, 60, 63, and 64, corresponding to zero-based indices n = 31, 59, 62, and 63. The full triangles provide context; the bottom row is the row being compared. Uniformity, differentiation, and alternation describe arrangement, while H measures only symbol balance.

Because only one symbol is present, the Shannon entropy of the sequence equals zero: H=0.

Uniformity recurs at the one-based power-of-two labels. It is a property of the parity representation, not a fixed point of the growing array or a cessation of recursion.

Alternation and High Symbol Entropy

One-based row R = 63 (n = 62) alternates between 1 and 0. Its 32 ones and 31 zeros give H ≈ 0.9998 bits. This is a highly ordered arrangement with near-maximal single-symbol entropy, illustrating why the two concepts must be distinguished.

Differentiated Rows

One-based rows 60–62 contain other structured parity arrangements. Row 60 has H ≈ 0.9968, row 61 H ≈ 0.8302, and row 62 H ≈ 0.9992, as reported in Table 3.2. Their deterministic correlations are visible in Figure 3.1, but are not quantified by those entropy values alone.

Other Moduli

Changing the modulus changes the alphabet and the residue frequencies. Moduli 3, 4, and higher therefore produce different pattern and entropy landscapes while leaving the unfiltered binomial recursion unchanged.

Modulo 2 provides the smallest nontrivial alphabet. Higher moduli retain additional distinctions, and prime and composite moduli can behave differently. Entropy comparisons across alphabets require the modulus and normalization to be stated.

This demonstrates a central principle: **entropy is not an intrinsic property of recursion alone but of recursion viewed through a constraint filter.** The modulus functions as an observational lens that selects particular symmetries while suppressing others, analogous to frequency filtering in signal analysis or coarse-graining in statistical mechanics (Cover & Thomas, 2006).

Reading the Entropy Tables

Table 3.1 classifies arrangement; Table 3.2 reports entropy and qualitative labels. Read together, they distinguish symbol balance from periodicity and differentiation. The local sequence is:

- Rows 60–62: differentiated patterns with varying entropy.
- Row 63: alternation with near-maximal symbol entropy.
- Row 64: a uniform all-ones row with zero symbol entropy.

This local sequence is not a monotonic law of increasing complexity with depth. It is a reproducible feature of binomial parity. Extensions to biological or cosmic phases require an explicit mapping and independent tests.

The class labels A–D are descriptive pattern categories, not statistical evidence of physical phase transitions. The original table header uses n for its row label; those labels are one-based R, with binomial calculations using n = R − 1. The numerical values are preserved.

Table 3.1 — Structural Regime Taxonomy (mod 2)

Regime	Defining feature	Entropy signature
Uniform	all 1s	H = 0
Alternation	period-2 pattern	H ≈ 1 but structured
Differentiated	non-periodic fractal bands	H high, correlation-rich
Symmetric	long runs + symmetry	H moderate

Table 3.2 — Entropy measurements and structural classification for one-based rows R = 30–64

Row (n)	Entropy (H)	Structural Class
30	0.9968	D – Differentiated
31	0.9992	B – Alternation

Row (n)	Entropy (H)	Structural Class
32	0.0000	A – Uniform (Zero Entropy)
33	0.3298	C – Symmetric
34	0.5226	C – Symmetric
35	0.5127	C – Symmetric
36	0.7642	D – Differentiated
37	0.4942	C – Symmetric
38	0.7425	D – Differentiated
39	0.7321	D – Differentiated
40	0.9710	D – Differentiated
41	0.4612	C – Symmetric
42	0.7025	D – Differentiated
43	0.6931	D – Differentiated
44	0.9457	D – Differentiated
45	0.6752	D – Differentiated
46	0.9321	D – Differentiated
47	0.9252	D – Differentiated
48	0.9183	D – Differentiated
49	0.4079	C – Symmetric
50	0.6343	D – Differentiated
51	0.6268	C – Symmetric
52	0.8905	D – Differentiated
53	0.6122	C – Symmetric
54	0.8767	D – Differentiated
55	0.8699	D – Differentiated
56	0.9852	D – Differentiated
57	0.5852	C – Symmetric
58	0.8498	D – Differentiated
59	0.8432	D – Differentiated
60	0.9968	D – Differentiated
61	0.8302	D – Differentiated
62	0.9992	D – Differentiated
63	0.9998	B – Alternation
64	0.0000	A – Uniform (Zero Entropy)

Row (n)	Entropy (H)	Structural Class
Note. A = Uniform (H = 0), B = Alternation (period-2 dominance), C = Symmetric/low-moderate H, D = Differentiated/fragmented (high H)		

3.4 Symmetry and Structural Change

Symmetry means invariance under a specified transformation. Pascal rows retain reflection symmetry before and after modular reduction, even when the distribution of symbols changes. The relevant transformation must therefore be identified before calling a transition "symmetry breaking" (Graham, Knuth, & Patashnik, 1994).

Defining Symmetry

A uniform row is invariant under any permutation of its entries. Differentiated rows retain fewer such invariances, although their bilateral symmetry remains. This gives a precise sense in which uniformity is lost without implying that every symmetry disappears.

Physical symmetry breaking involves a specified dynamical model and an order parameter. Pascal parity supplies an analogy for differentiation, but changing row patterns is not itself evidence of equilibrium, instability, or a physical phase transition (Anderson, 1972).

Generated Low Entropy States

Low symbol entropy can arise within an ongoing deterministic construction rather than being imposed only at its beginning. This observation concerns a mathematical representation; it does not solve the separate problem of low initial gravitational entropy in cosmology (Carroll, 2010).

Table 3.2 shows recurring uniform rows at one-based labels R = 32 and R = 64. The general condition is R = 2^m, or zero-based n = $2^m - 1$. Subsequent rows differentiate again under the same addition rule.

Recent developments in quantum information theory suggest that entropy-based ordering principles extend even to the quantum domain. Regula and Lami (2024) demonstrated that transformations of quantum entanglement can be governed by a unique entropy measure analogous to thermodynamic constraints, establishing conditions under which entanglement manipulation becomes reversible. Rather than describing disorder alone, entropy in this context functions as a constraint determining which state transitions are physically permissible. This result reinforces a broader interpretation advanced here: entropy acts not merely as a measure of randomness but as a regulator of transformation across recursive systems, from combinatorial structures to quantum correlations.

Cross Domain Analogies

Comparable trajectories appear across natural systems. In cosmology, early large-scale uniformity gives way to gravitational instability, leading to galaxy and cluster formation (Peebles, 1993). In biology, embryonic development begins with relatively homogeneous cell populations that differentiate into specialized tissues through regulatory interactions (Alberts et

al., 2015). In cognitive systems, neural networks initially exhibit diffuse connectivity before functional specialization emerges through learning and plasticity (Kandel et al., 2013).

Table 3.3 — Cross-Domain Analogy of Constraint-Guided Emergence from Symmetry Breaking

Domain	Local Rule	Constraint	Emergent Structure
Pascal triangle	additive recursion	combinatorial rules	fractal hierarchy
Atmosphere	fluid interaction	rotation + thermodynamics	spiral vortex
Biology	cellular signaling	mechanical & genetic limits	differentiated organism
Cognition	synaptic updating	energy & connectivity	functional networks

Table 3.3 compares organizational descriptions across domains. Hurricanes follow fluid mechanics, biological differentiation follows regulatory interactions, and Pascal patterns follow arithmetic. Similar outcomes can motivate questions about constraint, but cannot substitute for a mapping between the mechanisms.

Criteria for Cross Domain Mapping

Four criteria help distinguish meaningful analogy from metaphor:

1. Structural correspondence requires specified relationships between variables or operations, beyond visual resemblance.

2. Generative correspondence requires a model linking the processes being compared. Similar outputs alone do not establish it.

3. **Scale Consistency**
Mappings should preserve relational behavior across scales. Recursive systems exhibit scale invariance, allowing cautious comparison with fractal and hierarchical phenomena (Mandelbrot, 1982).

4. Predictive utility requires a mapping to constrain observable outcomes. A useful descriptive analogy may guide inquiry without yet satisfying this stronger criterion.

Chapter 4 Recursive Time Memory and Layer Formation

A recursive sequence supplies an ordering of states; a physical model must also explain histories, transition rules, and elapsed time. The discussion moves from iteration and memory to temporal phases, attractors, and proposed layer formation.

4.1 Iteration and Historical Dependence

Iteration as an Ordering Coordinate

A recursion can be ordered by discrete update steps. This provides a model of temporal succession without assuming that physical time itself is discrete (Newton, 1687/1999; Wolfram, 2002).

In Pascal's triangle, row n is generated from row $n - 1$. The index is therefore a construction coordinate. Converting it into seconds, days, or years requires an additional rule that must be justified separately.

This interpretation aligns with computational models in which time corresponds to successive updates of system states (Wolfram, 2002). Cellular automata, for example, treat each update step as a discrete moment, demonstrating how complex structures can arise from repeated rule application. Similarly, recursive combinatorics shows that temporal order may be defined operationally through transformation rather than assumed as an independent dimension.

Historical Dependence

Later rows depend on earlier rows through the recurrence. The complete triangular array records that construction history, while a filtered view retains only selected features. Historical dependence does not imply that every past state remains recoverable from a chosen summary.

The preservation of history parallels processes observed in biological and physical systems. In evolutionary biology, new traits emerge through modification of existing structures rather than independent creation, producing layered historical inheritance (Mayr, 2001). Similarly, developmental biology shows that later organismal stages retain traces of earlier developmental constraints through regulatory networks (Alberts et al., 2015).

Pascal updating is Markovian when the full current row is the state: that row determines the next one. A current state can encode past influences while still satisfying this property. History-dependent transition restrictions are examined separately in Section 4.2.

Depth and Resolution

Plotting more rows at a fixed overall scale reveals finer nested structure. This relates construction depth to visual resolution; it does not mean that every later row has greater entropy or complexity.

In fractal geometry, self-similar structures become visible only at appropriate scales of observation (Mandelbrot, 1982). Analogously, deeper recursive iterations expose structural relationships that are invisible at earlier stages. Time can therefore be interpreted as a process that progressively reveals latent organization.

Coarse-graining likewise changes which features are visible at a chosen scale (Wilson, 1979). The comparison is about levels of description, not an identity between iteration count, spatial scale, and elapsed physical time.

Structural Change and Elapsed Time

Equal increments in row index can yield unequal changes in a pattern measure. An iteration coordinate can therefore distinguish structural transitions that a simple count of steps would not describe.

Nonlinear conceptions of time appear in several scientific domains. In thermodynamics, irreversible processes introduce temporal asymmetry through entropy production (Prigogine & Stengers, 1984). In dynamical systems, bifurcation points mark qualitative shifts in system behavior despite continuous parameter change (Strogatz, 2015). Cognitive neuroscience similarly shows that subjective temporal experience varies with informational processing and neural dynamics (Buonomano & Rovelli, 2021).

The proposed “fractal time” interpretation concerns nested organization in sequences of change. Extending it to physical temporality requires a dynamical mapping and evidence; the recursive construction alone does not replace continuous-time models.

4.2 Memory Constraints and Permitted Histories

Probabilistic Convergence

Local uncertainty can coexist with reliable aggregate behavior. Here “probabilistic convergence” names the approach to a stable distribution, and “convergent predictability” names the resulting reliability of aggregate observations.

Repeated interactions may concentrate probability within particular regions of state space when dynamics and constraints support convergence. This is a model-dependent outcome, not a consequence of iteration alone.

Individual trajectories can remain uncertain even when a macroscopic distribution is stable. A convergence claim therefore needs a specified observable, timescale, and dynamical model.

Experiments with agitated dice illustrate how boundary conditions and repeated motion can produce ordered packing (Asencio et al., 2017). The example concerns collective organization rather than predictability of every individual trajectory.

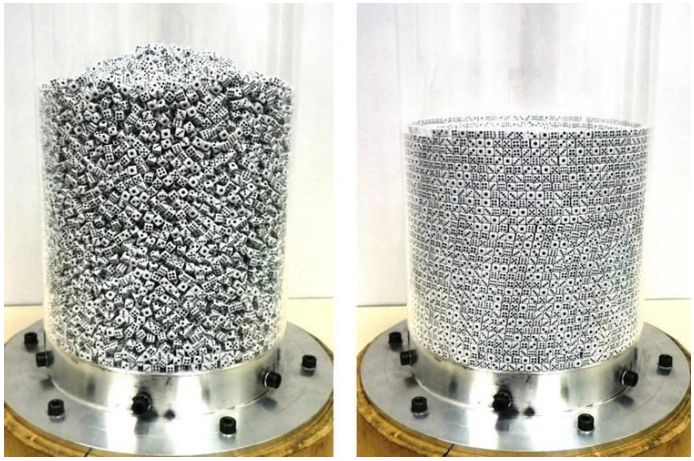

Figure 4.1 — Dice packing under repeated agitation. The comparison illustrates collective ordering despite uncertain individual rearrangements. Adapted from Asencio et al. (2017).

Memory Constraints

An unconstrained binary-choice tree has 2^n paths of length n. Pascal coefficients group these paths by endpoint. A rule depending only on the current state can be Markovian while that state still embodies effects of earlier interactions; "memoryless" does not mean history has had no influence (Cover & Thomas, 2006).

A constraint on allowed transition sequences reduces the path count. This gives a precise combinatorial meaning to memory: the next permitted choice can depend on a retained feature of the preceding choices.

Restricted Paths and Fibonacci Growth

For example, forbid two consecutive 1s in a binary string. Strings ending in 0 can follow any allowed shorter string; strings ending in 1 must extend an allowed string with 01. The counts therefore satisfy $a_n = a_{n-1} + a_{n-2}$, with $a_0 = 1$ and $a_1 = 2$. Thus $a_n = F_{n+2}$. Forbidding both 00 and 11 would instead leave only two alternating strings, so the precise restriction matters.

The constrained count grows asymptotically as φ^n rather than 2^n. It remains exponential, but its growth rate is smaller.

For an equiprobable ensemble of allowed strings, entropy is the base-2 logarithm of the path count: n bits without the restriction, and approximately n $\log_2\varphi$ plus a constant with it. This ensemble entropy differs from the within-row symbol entropy used in Sections 3.2 and 3.3.

In biological systems, prior gene activation, signaling, and differentiation can constrain later transitions (Maynard Smith & Szathmáry, 1995). The binary-string example demonstrates how a particular history constraint changes scaling; it does not imply that all biological memory produces Fibonacci growth.

Implications of Constrained Histories

History-dependent restrictions offer a way to model staged change. Applying the idea to evolution or cosmology requires identifying the retained state, permitted transitions, and time conversion. The combinatorial construction alone does not derive physical time or its arrow.

Pascal recursion serves as a formal analogue for exploring such restrictions. Its empirical usefulness depends on whether the chosen representation explains measured transitions better than alternatives.

The continuity between cosmological and biological emergence may also be understood through material inheritance. The chemical elements composing living systems were produced through stellar nucleosynthesis, establishing the periodic structure of matter prior to the emergence of life itself. These processes defined the space of chemically possible interactions available to biological organization. At a deeper physical level, this ordering reflects quantum-mechanical constraints such as the Pauli exclusion principle, which deterministically restricts how electrons occupy atomic states and thereby generates the periodic structure of the elements (Griffiths, 2018). Quantum systems nonetheless exhibit probabilistic outcomes at the level of interaction and measurement, illustrating how deterministic constraint and stochastic variation coexist within a single framework.

Biological systems inherit this constrained chemical landscape. Cellular processes follow lawful biochemical dynamics while gene expression, mutation, and molecular interactions display stochastic variation. Stability therefore emerges not from pure determinism or randomness alone but from constrained systems in which fluctuations operate within well-defined structural limits. Homeostasis may be understood as the stabilization of complex chemical dynamics within this inherited framework, maintaining organization despite continual environmental and energetic change. Evolution, in this view, represents exploration within constrained possibility spaces rather than unrestricted variation.

Within this context, symbiogenesis (Section 13.1) can be interpreted as a biological analogue of coupling in physics: new levels of organization arise when previously independent systems stabilize into integrated wholes. This interpretation illustrates how the emergence of higher-order organization across domains may reflect a shared principle of constraint-mediated integration.

4.3 Temporal Phases

Entropy Profiles Across Iterations

A sequence of entropy values provides one description of change through recursion. The values in Table 3.2 fluctuate deterministically rather than following a universal low–moderate–high progression. Alternation can have near-maximal entropy, while uniformity recurs at specific one-based row labels.

Attractors and Bifurcations

Attractors and bifurcations provide useful comparison concepts, but require dynamical definitions. A recurring row pattern is not automatically an attractor: a basin of approach and an appropriate state space would have to be established (Strogatz, 2015).

Likewise, an abrupt difference between adjacent rows is a structural transition, not necessarily a bifurcation. A stronger claim requires identification of a control parameter and a qualitative change in the system’s invariant dynamics.

Defining Phase Epochs

A “phase epoch” may be defined operationally as a contiguous interval sharing specified entropy and arrangement criteria. Those criteria, window lengths, and tolerances must be fixed before testing an empirical sequence. An algorithm should report both qualifying intervals and failures; retrospective selection of appealing intervals cannot establish a temporal law.

4.4 Recursive Models and Attractors

Construction and Dynamics

The expansion of recursion across domains—from symbolic iteration to dynamical behavior—may be summarized as shown in Table 4.1.

Table 4.1
Expansion of Recursion Across Domains and Resulting Geometry

Level	Recursion Domain	Resulting Geometry
2D	Rule iteration	Fractal triangle
3D	Spatial subdivision	Fractal tetrahedron
Dynamical	Time iteration	Toroidal attractor

Note. “Dynamical” indicates recursion unfolding through time, where geometry becomes visible in phase space.

Table 4.1 distinguishes symbolic constructions from dynamical state spaces. Iteration can generate a static geometric object or describe evolving trajectories. Attractors belong to the latter setting and depend on the update law, topology, and notion of convergence (Strogatz, 2015).

Comparing Generators

Different substrates can support mathematically comparable dynamics. Establishing this requires a correspondence between state variables and evolution rules, not merely similar shapes (Kauffman, 1993; Strogatz, 1994).

Figure 4.2 compares symbolic, cellular-automaton, and subdivision constructions that produce Sierpiński-type patterns. Their relationship is clearest at the level of explicit generation rules.

Symbolic Grammar *(recursive rules)*	Cellular Automaton *(Rule 90 fractal)*	Geometric Subdivision *(triangle recursion → tetrahedral recursion*
A ↓ **A B** ↓ **A B A** ↓ **A B A A B**	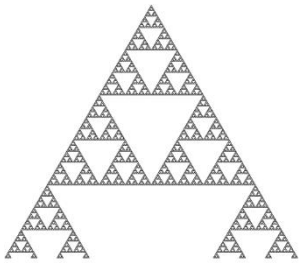	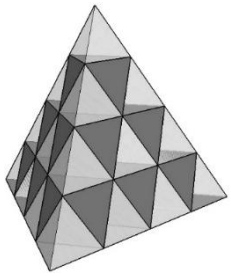
Sierpiński-like attractor	**Sierpiński-like attractor**	**Sierpiński-like attractor**

Figure 4.2 — Alternative constructions of Sierpiński-type structure. Symbolic grammar, cellular automata, and geometric subdivision illustrate comparable patterns generated in different representations.

A Classification of Recursive Models

Table 4.2 organizes possible geometries by the kind of model used. It is a conceptual classification, not a theorem requiring each system to progress through every level.

Table 4.2
The Recursion Ladder and Associated Geometrical Regimes

Stage	Recursion Type	Domain	Characteristic Geometry
Symbolic	Combinatorial iteration	Discrete rules	Fractal triangle
Spatial	Subdivision	Three-dimensional space	Fractal tetrahedron
Temporal	Cyclic evolution	Dynamical systems	Torus
Interacting	Nonlinear feedback	Coupled dynamics	Strange attractor

Note. "Interacting" recursion refers to multiple feedback loops whose coupling produces bounded, nonrepeating trajectories in phase space.

Symbolic rules can generate patterns; spatial embeddings display geometric organization; temporal models generate trajectories. Periodic motion traces a loop. Independent incommensurate phases can trace a torus, while suitable nonlinear dynamics can generate strange attractors (Arnold, 1989; Lorenz, 1963; Ott, 2002). None of these outcomes follows merely from adding dimensions or feedback.

Layer Formation as a Hypothesis

The layer-formation hypothesis proposes that constraints can favor a new description or organization when the existing one saturates. Table 4.2 provides candidate regimes for

investigation. Demonstrating a transition requires a measure of saturation, a rule for reorganization, and evidence that the new regime improves the description. Entropy increase alone is insufficient.

Forms of Stability

In spatial recursion, stability appears as invariance across scale. Fractals alter local detail while preserving global organization (Mandelbrot, 1982). In living systems, functional stability is maintained through continual turnover and regulation; vascular networks, bronchial trees, and neural branching exhibit fractal-like organization supporting efficient transport and adaptive resilience (Goldberger et al., 2002). The analogy is conceptual rather than literal, but both cases express the same principle: organization persists when constraints guide transformation.

Dynamical stability concerns behavior under perturbation and evolution. It differs from the visual self-similarity of a static fractal, even when both can be described using invariant relationships.

The Galton board illustrates statistical stability: many variable paths yield a reproducible endpoint distribution under specified conditions. This is an analogy for constraint-shaped outcomes, not a proof that a binomial distribution is a dynamical attractor.

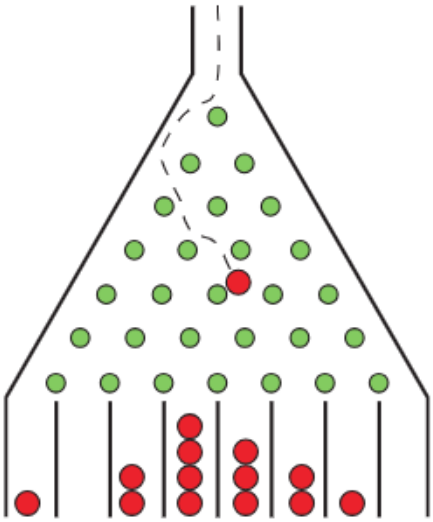

Figure 4.3 — Galton board. Repeated branching produces a stable aggregate endpoint distribution under the idealized binomial model. Adapted from Wolfram MathWorld, “Galton Board.”

4.5 Thresholds and Layer Formation

Defining Thresholds

Recursive entropy thresholding is proposed as a hypothesis about reorganization when a constrained representation approaches saturation. It extends the descriptive row analysis; it is not implied by Shannon entropy alone.

A threshold must be operationally defined. Candidate markers include declining marginal diversity, increasing compressibility, or an abrupt change in a specified correlation measure. A low-entropy row by itself does not require a system to adopt a new representational layer.

Definition (working): *Recursive entropy thresholding* occurs when a recursively generated configuration space, viewed through a constraint filter, approaches a regime in which additional recursion produces decreasing marginal diversity (entropy) or collapses into highly compressible structure—thereby selecting for a reorganization into a new representational "layer" (Cover & Thomas, 2006; Wolfram, 2002).

Layer Formation

If thresholding is real, the next question is why it would yield *layer formation* rather than simply stagnation. The proposed answer is **capacity expansion by reparameterization**: once a given regime saturates (in the constrained view), continued evolution that preserves coherence requires either (a) a richer alphabet, (b) a higher-dimensional embedding, or (c) a new coarse-graining that reorganizes correlations into fresh degrees of freedom (Prigogine & Stengers, 1984; Strogatz, 2015).

Pascal arrays provide a toy model for comparing representations. Changing the modulus, embedding, or coarse-graining changes the observable patterns. To interpret such a change as a physical reset, a model must explain what selects it and how it corresponds to measured variables (Graham et al., 1994; Mandelbrot, 1982).

Candidate Fibonacci Scaling

Fibonacci values arise through diagonal sums in Pascal's triangle. That identity makes them a candidate scaling family within the construction, but does not establish that threshold intervals in nature must follow them (Graham et al., 1994).

The empirical hypothesis is statistical: independently specified transition intervals might cluster near Fibonacci-derived values more often than under suitable alternatives. Exact matches, chosen after inspection, cannot establish this claim (Livio, 2002).

Tests and Failure Conditions

For recursive entropy thresholding to be scientifically useful, it must generate **testable predictions** and clear failure modes. The empirical program should therefore distinguish three levels: (i) detection of threshold signatures in Pascal systems, (ii) mapping to candidate empirical systems, and (iii) evaluation against null models and established mechanisms.

A. What would support it (minimum evidentiary standard)

1. **Operational threshold markers in Pascal space**
Demonstrate repeatable depth indices where constrained entropy (or related measures such as mutual information across positions) shows discontinuities, saturation plateaus, or structured resets under specified filters (Cover & Thomas, 2006; Wolfram, 2002).

2. **Scaling regularities robust to reparameterization**
Show that candidate transition spacing is not an artifact of a single choice of modulus or visualization, but persists across reasonable families of constraint lenses (Graham et al., 1994; Mandelbrot, 1982).

3. **Cross-system statistical clustering beyond nulls**
In target domains (biological cycles, stellar cycles, developmental transitions), show clustering

near predicted scaling families compared against null distributions that preserve autocorrelation and measurement uncertainty (Strogatz, 2015).

4. **Predictive value**
Demonstrate prospective improvement: a thresholding-based predictor should outperform baseline models that assume stationary periodicity, pure noise around a mean period, or flexible post hoc fitting (Cover & Thomas, 2006).

B. Example test case domain: solar and stellar magnetic cycles (as a *test*, not a proof)
Solar activity exhibits quasi-periodic cycling (≈11 years sunspot cycle; ≈22 years Hale polarity cycle), with variability rather than perfect periodicity (Hathaway, 2015). Stellar observations likewise report magnetic cycles across many active stars, with distributions of cycle lengths that vary with rotation and stellar parameters (Oláh et al., 2016). These systems are already modeled physically via dynamo theory and nonlinear feedback; therefore, a Pascal-thresholding account must be evaluated as **additional structure** (a scaling signature) rather than a replacement mechanism (Hathaway, 2015; Oláh et al., 2016). The right question is: do cycle-length *ratios and transition timings* show statistically detectable clustering consistent with a constrained-recursion scaling family, beyond what dynamo-driven variability models predict?

C. What would undermine it

1. **No robust threshold signatures** in Pascal entropy measures once arrangement-sensitive metrics are used and finite-size effects are controlled (Cover & Thomas, 2006).

2. **Apparent scaling disappears under proper null models**, or is explainable as selection effects, measurement error, or autocorrelation artifacts (Strogatz, 2015).

3. **Post hoc flexibility dominates**: if the hypothesis can "fit" any dataset by choosing modulus, windowing, or scaling constants without pre-registered constraints, it loses explanatory power.

4. **Established mechanisms fully account for the timing structure** with better predictive accuracy (e.g., dynamo-based forecasts outperforming any thresholding-based signal extraction in solar data) (Hathaway, 2015).

Chapter 5 Fibonacci Scaling Energy and Temporal Models

Fibonacci identities connect recursive constructions, but temporal applications require explicit choices of index, unit, and time origin. This chapter brings the identities together with candidate timing models, energy flows, and their failure conditions.

5.1 Fibonacci Identities and Scaling

The Diagonal Sum Identity

The shallow-diagonal sum identity, introduced in Chapter 2 and tabulated in Appendix C, connects binomial coefficients with Fibonacci numbers (Graham, Knuth, & Patashnik, 1994). The two recurrences are:

Pascal's triangle is generated through local additive rules:

$$C(n,k) = C(n-1,k-1) + C(n-1,k)$$

Each entry represents the sum of two adjacent entries from the preceding row. The Fibonacci sequence follows a formally analogous recurrence relation:

$$F_{n+1} = F_n + F_{n-1}$$

Convergence to the Golden Ratio

The Fibonacci sequence is closely associated with the golden ratio, φ (phi), defined as:

$$\phi = \frac{1+\sqrt{5}}{2}$$

As Fibonacci numbers increase, ratios of successive terms converge toward φ. This asymptotic behavior reflects a stable scaling relation that arises naturally in recursive growth processes (Livio, 2002).

Aggregation

Diagonal summation aggregates several binomial coefficients into one number. It can be viewed as a reduced description of the array, comparable in this limited sense to coarse-graining (Kadanoff, 2000).

Pascal's triangle contains rich combinatorial information distributed across two dimensions. Diagonal summation effectively compresses this information, collapsing multiple binomial relationships into a single scalar sequence. The Fibonacci sequence therefore represents a reduced description of deeper binomial interactions.

Identity and Application

The identity is deterministic and reproducible. Its application to an empirical timeline is a different claim: the choice of time unit, origin, index, and tolerance must be justified independently. An intrinsic mathematical relationship does not remove the possibility of selection bias in natural data.

5.2 Milestone Indexing and Predictions

Candidate Milestone Scales

Fibonacci milestone indexing proposes a set of candidate scales at which empirical transitions might cluster. The proposal is motivated by the diagonal identity and the asymptotic ratio φ; transition clustering does not follow from those mathematical facts alone.

The empirical question is whether this indexing predicts transition locations or intervals better than alternatives of comparable flexibility. The following chapters retain both agreements and discrepancies so that this claim can be assessed.

Direct and Cumulative Mappings

Direct and cumulative indexing are distinct transformations. Appendix A tabulates both. Each can be computed unambiguously, but the choice between them must be made before evaluating a dataset.

Snapshots (Structural Shells)

Direct indexing assigns the selected Fibonacci value itself to the scale being modeled. In the timing tables, an explicit conversion then expresses that value in physical units. The conversion is part of the model, not part of the Fibonacci identity.

Integrated Buildup (Temporal Accumulation)

Cumulative indexing sums successive Fibonacci terms through the chosen index. It represents accumulated intervals under the adopted convention. Because it changes predicted times, switching between direct and cumulative values after inspecting an event introduces an additional fitting choice.

Predictions

For Fibonacci indexing to function as a scientific framework rather than a descriptive analogy, it must generate testable predictions. The key predictive claim is not that events occur exactly at Fibonacci numbers, but that **transitions cluster statistically near Fibonacci-scaled intervals** within recursively evolving systems.

Several forms of prediction follow from this principle:

1. Scaling predictions specify which ratios or intervals should cluster near Fibonacci-derived values and define an acceptable error range before examining outcomes.

2. **Cross-Scale Consistency**
If Fibonacci indexing reflects underlying recursion, similar scaling relationships should appear across levels of organization—for example, developmental stages, ecological cycles, or astrophysical processes—without direct causal linkage.

3. **Predictive Windows Rather Than Exact Dates**
Because real systems include noise and secondary constraints, Fibonacci indices define probabilistic windows in which transitions become more likely rather than deterministic timestamps.

4. **Compression Efficiency**
Models incorporating Fibonacci indexing should reduce descriptive complexity by explaining multiple transitions with fewer parameters, consistent with principles of model parsimony (Cover & Thomas, 2006).

Empirical testing therefore involves statistical comparison between observed transition distributions and null models lacking recursive scaling. If Fibonacci indexing captures genuine structural properties, observed transitions should show non-random clustering relative to Fibonacci-derived scales.

Failure Conditions

A scientifically meaningful framework must specify conditions under which it could be falsified. Several criteria would undermine Fibonacci-indexed interpretations:

1. **Random Distribution of Transitions**
If empirical transition points show no statistically significant clustering near Fibonacci-scaled intervals, the indexing hypothesis would lack explanatory value.

2. **Superior Alternative Scaling Laws**
If another scaling framework consistently predicts transitions more accurately with equal or fewer assumptions, Fibonacci indexing would be superseded.

3. **Lack of Generative Mechanism**
If systems exhibiting Fibonacci correlations cannot be connected to recursive or additive processes, the theoretical justification for indexing collapses.

4. **Parameter Overfitting**
If Fibonacci alignment requires arbitrary rescaling, selective data inclusion, or post hoc adjustment, the framework becomes unfalsifiable and therefore non-scientific.

5. **Failure of Cross-Domain Generalization**
A core claim of recursive emergence is cross-scale applicability. If Fibonacci indexing applies only narrowly to isolated datasets, its proposed universality would be rejected.

5.3 Energy Flow and Cyclic Dynamics

Energy Flow and Cycles

Sustained energy flow supports organized dynamics in systems far from equilibrium. Morowitz's account emphasizes cycling in biological organization (Morowitz, 1968). The relevance to a particular system depends on its reaction pathways, feedback, and boundary conditions; energy throughput alone does not establish a Fibonacci period.

Cycles arise because energy gradients cannot be dissipated instantaneously. Instead, systems develop intermediate structures that regulate energy transfer through repeated pathways. Atmospheric vortices, ocean currents, and convection cells exemplify this principle, maintaining organized motion through continuous energy exchange. Similar behavior appears in biological

metabolism, where cyclic reaction networks such as the Krebs cycle stabilize energy transformation while preserving system integrity (Schneider & Sagan, 2005).

From a dynamical perspective, cycles represent constrained motion within state space. Rather than exploring all possible configurations, system trajectories repeatedly return to bounded regions determined by energetic and structural constraints. These recurring trajectories correspond to dynamical attractors—stable patterns toward which system behavior converges despite local variability (Strogatz, 2015).

Cyclic Dynamics

A recursive dynamical model specifies how states update and which transitions are allowed. Depending on the rule and parameters, trajectories may converge, cycle, diverge, or display more complex behavior. Constraints do not automatically produce an attractor.

In dynamical systems theory, these stable regions are known as attractors—sets toward which system states evolve over time (Ott, 2002). Cyclic attractors arise when recursive updates repeatedly map system states onto closed trajectories. Importantly, attractors do not eliminate variability; instead, they channel variability into bounded patterns.

Proposed Fibonacci Harmonics

The specific binary-string restriction in Section 4.2 produces Fibonacci counts. More generally, memory changes growth according to the permitted transitions. It need not produce the same recurrence in every system.

Mathematically, Fibonacci growth scales approximately as φ^n, where φ is the golden ratio, producing expansion slower than unconstrained doubling yet preserving generative capacity (Livio, 2002). This compression of combinatorial growth reduces entropy increase while maintaining structural richness.

"Fibonacci harmonics" is used here for proposed relationships among recurrence scales. It should be distinguished from harmonics in the conventional sense of integer frequency multiples. The appearance of φ in a counting rule does not establish a quasiperiodic oscillator or a stability advantage.

To test such organization, one must specify the measured periods, allowed ratios, fitting tolerance, and comparison model. Connections with phyllotaxis or branching can motivate candidate mechanisms, but spatial packing and temporal coordination require separate evidence (West, Brown, & Enquist, 1997).

Cross Scale Comparisons

Morowitz's emphasis on biological cycling motivates the search for relationships among nested rhythms. The proposed extension to Fibonacci-related timing is a further hypothesis, to be assessed against established mechanisms and alternative scaling families.

These cycles frequently interact, producing harmonic relationships between nested processes. Biological rhythms illustrate this clearly: circadian cycles interact with ultradian and seasonal cycles, forming layered temporal organization. Ecosystems likewise exhibit coupled nutrient cycles, while planetary systems display resonance relationships among orbital periods.

Part III Physical Systems

Chapter 6 Solar and Planetary Dynamics

Solar cycles, geomagnetic reversals, and orbital periods offer different tests of proposed recursive timing relationships. Their comparisons are presented with the relevant physical mechanisms, conversion assumptions, and alternative explanations.

6.1 Solar and Stellar Magnetic Cycles

Solar Dynamo Physics

The Sun's magnetic activity is governed by a self-sustaining magnetohydrodynamic process known as the **solar dynamo**, which arises from interactions between plasma motion, rotation, and magnetic fields within the solar interior. Differential rotation—where the solar equator rotates faster than the poles—combined with convective turbulence generates and reorganizes magnetic fields over time (Charbonneau, 2020).

The most visible manifestation of this process is the approximately 11-year sunspot cycle, during which solar magnetic activity increases and decreases periodically. Importantly, every two sunspot cycles (approximately 22 years), the Sun's global magnetic polarity reverses, forming what is known as the **Hale magnetic cycle** (Hathaway, 2015). During reversal phases, magnetic field lines reorganize globally, accompanied by increased solar flares, coronal mass ejections, and complex magnetic reconnection events.

The solar dynamo is typically modeled through coupled nonlinear equations describing fluid motion and magnetic induction. While these models successfully reproduce many observed features, they remain computationally complex and sensitive to initial conditions. Consequently, simplified conceptual frameworks are often employed to identify higher-level organizational principles underlying magnetic behavior (Charbonneau, 2020).

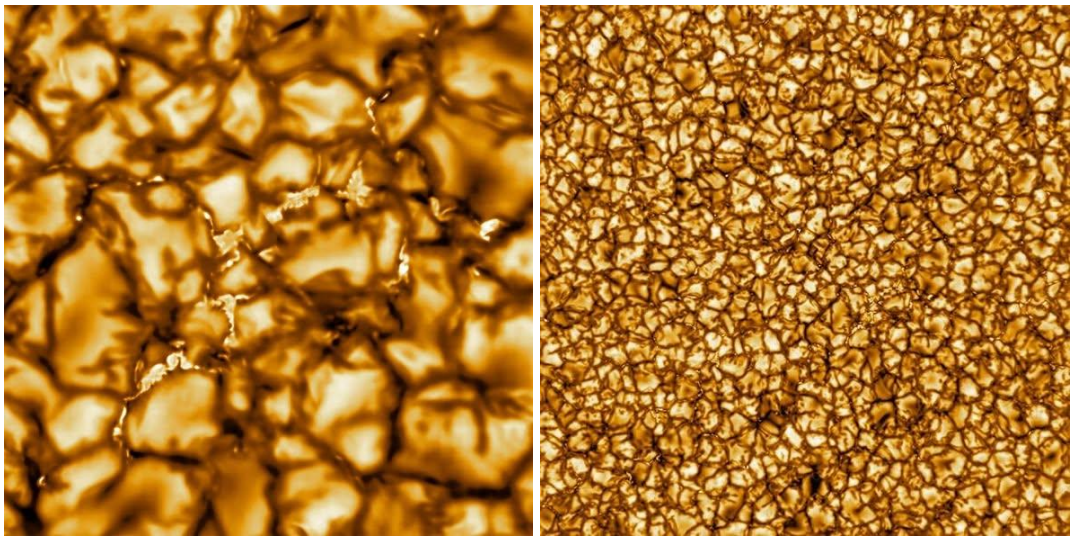

Figure 6.1 — Solar photospheric granulation. Images from the Daniel K. Inouye Solar Telescope show cellular patterns associated with convective plasma motion. The small- and large-field views illustrate distributed activity at the solar surface. Source: NSO/AURA/NSF.

One recurring empirical feature of the solar cycle is that magnetic activity is not distributed uniformly across latitude. Butterfly diagrams show sunspot emergence concentrated within belts that migrate equatorward over a cycle, with clustering commonly observed in the ~±15°–20° range near cycle maxima (Hathaway, 2015; McIntosh et al., 2015). While standard dynamo theory explains the broad migration pattern through differential rotation and meridional circulation, the persistence of preferred activity bands suggests that additional geometric or symmetry constraints may modulate where flux emergence becomes statistically favored (Charbonneau, 2020).

Binary State Modeling

In the case of solar magnetism, polarity reversal naturally lends itself to binary abstraction. At large scales, the Sun's magnetic field can be represented as occupying one of two global orientations. Although the underlying plasma physics remains continuous and multidimensional, polarity reversals themselves exhibit discrete, system-level transitions.

To clarify the level of abstraction employed, the binary representation used here can be understood as an extreme coarse-graining of solar magnetic dynamics. Rather than modeling continuous magnetic field strength or plasma motion, the system is reduced to a minimal distinction between persistence or cancellation of net magnetic coherence. In this sense, binary values represent whether local interactions produce a residual polarity or resolve through cancellation. This reduction is analogous to coarse-grained models in statistical physics, where complex systems are mapped onto simplified state variables in order to isolate structural transition behavior.

Parity Counts and Time Conversion

Binary persistence and cancellation provide a proposed coarse-grained comparison between polarity changes and Pascal mod-2 updating. This analogy does not model the magnetohydrodynamic mechanisms of the solar dynamo.

The sum of zero-based Pascal row n is 2^n, counting all binary paths of length n. Individual edge entries remain 1; the central entries count the greatest number of paths to a single endpoint. Reducing these counts modulo 2 retains parity, not the physical cancellation of opposing magnetic fields.

Table 6.1 preserves the parity-count series used in the proposed comparison with Bhindi and McMenamin (2010). Its entries require a distinction between counts within one row and cumulative counts through a row, clarified below.

The table's count columns are cumulative through the listed zero-based row index, rather than counts in that row alone.

Table 6.1 — Cumulative even and odd counts through Pascal row n

Pascal Row	Even	Odd	% Even
0	0	1	0.0000
1	0	3	0.0000
2	1	5	0.2000
3	1	9	0.1111
4	4	11	0.3636
5	6	15	0.4000
6	9	19	0.4737
7	9	27	0.3333
8	16	29	0.5517
9	22	33	0.6667
10	29	37	0.7838
11	33	45	0.7333
12	42	49	0.8571
13	48	57	0.8421
14	55	65	0.8462
15	55	81	0.6790
16	70	83	0.8434
17	84	87	0.9655
18	99	91	1.0879

Reading Table 6.1: “Even” and “Odd” are cumulative counts through row n. The column headed “% Even” numerically reports Even/Odd as a decimal ratio, not 100 × Even/(Even + Odd). The original entries and header are retained; the ratio crosses 1 when cumulative even counts exceed cumulative odd counts. This convention differs from the within-row entropy calculation in Table 3.2.

At zero-based row n = 18, the central coefficient is 48,620 and is even. This is a combinatorial path count. It does not establish a unique physical transition: central coefficients at many other rows are also even. In binomial notation, $\binom{18}{9} = 48{,}620$.

Table 6.2 presents the correspondence between Pascal row number, Fibonacci-derived intervals, and associated timescales.

Table 6.2 — Mapping Between Pascal Row Index and Fibonacci-Scaled Time Intervals

Years	Fibonacci Number (Days)	Pascal Row
0.00	1	0
0.00	1	1
0.01	2	2
0.01	3	3
0.01	5	4
0.02	8	5
0.04	13	6
0.06	21	7
0.09	34	8
0.15	55	9
0.24	89	10
0.39	144	11
0.64	233	12
1.03	377	13
1.67	610	14
2.70	987	15
4.38	1,597	16
7.08	2,584	17
11.45	4,181	18

Table 6.2 maps zero-based row n to F_{n+1} days and converts to years. At n = 18, 4,181 days gives approximately 11.45 years using 365.25 days per year. The proximity to an approximately 11-year solar activity cycle is a comparison under this chosen time unit, not a consequence of Pascal parity alone.

Proposed Polarity Mapping

The proposed analogy assigns binary values to persistence or cancellation and treats iteration depth as an ordering variable. To become a predictive solar model, it would need a defined observation operator, a calibrated time conversion, and tests against dynamo-based alternatives. The current tables provide descriptive comparisons.

Stellar Cycle Comparisons

If Fibonacci-like temporal scaling reflects a general property of recursive constraint dynamics rather than a peculiarity of the Sun alone, similar patterns should appear across stars exhibiting magnetic activity cycles. Stellar dynamos provide a natural comparative domain because stars with different rotational periods generate magnetic cycles through broadly similar magnetohydrodynamic mechanisms operating under varying energetic and rotational constraints.

Table 6.3 compares the stellar-cycle ranges attributed to Oláh et al. (2016) with Fibonacci-derived intervals. The examples use rotation periods near 40 and 18 days, with the Sun as a reference. They describe numerical proximity; the table does not report a statistical test of clustering against uniform spacing or a dynamo-based null.

Stars with longer rotational periods (~40 days) exhibit magnetic cycles ranging approximately from 7.8 to 11.6 years, with an average near 9.7 years (Oláh et al., 2016). These values lie between two Fibonacci-derived temporal intervals near 7.10 years and 11.50 years, suggesting that observed cycles occupy a bounded range comparable to proposed recursive scaling intervals.

Stars with shorter rotational periods (~18 days) display broader variability, with cycle lengths spanning approximately 2.7 to 12.5 years and averaging near 7.6 years (Oláh et al., 2016). The lower bound aligns numerically with a shorter Fibonacci-scaled interval (~2.70 years), while the mean value lies close to the ~7-year interval identified in solar-cycle comparisons. The upper bound approaches the longer ~11.5-year interval, indicating increased dispersion consistent with stronger nonlinear variability in faster-rotating stellar dynamos.

The Sun provides an intermediate reference case. Its approximately 11-year magnetic activity cycle lies near the longer Fibonacci-derived interval (~11.5 years), though substantial variability between cycles is well documented (Hathaway, 2015). This correspondence is therefore interpreted as approximate scaling proximity rather than precise numerical agreement.

These comparisons are summarized in Table 6.3.

Table 6.3 — Approximate Correspondence Between Stellar Magnetic Cycles and Fibonacci-Scaled Temporal Intervals

Rotation Period	Observed Cycle Length (Years)	Approximate Fibonacci Interval (Years)
~40 days	7.8–11.6 (avg 9.7)	7.10, 11.50
~18 days	2.7–12.5 (avg 7.6)	2.70, 7.10, 11.50
Sun (~27 days)	~11	~11.50

Importantly, these numerical proximities should not be interpreted as evidence that stellar magnetic cycles are governed by Fibonacci mathematics. Stellar activity cycles arise from nonlinear dynamo processes involving convection, rotation, and magnetic feedback. The present comparison instead evaluates whether recursive scaling provides a useful descriptive framework for organizing quasi-periodic variability observed across stellar systems.

The analysis presented here remains exploratory. Demonstrating genuine scaling structure would require statistical testing across large stellar samples, comparison with null dynamo models, and

evaluation of predictive performance. Nevertheless, extending the hypothesis beyond the Sun establishes a comparative framework in which recursive timing models can be empirically evaluated across astrophysical systems.

6.2 Geomagnetic Reversals and Planetary Change

The Structure and Origin of Earth's Geomagnetic Field

Earth is surrounded by a vast magnetic field generated deep within its interior. This geomagnetic field acts as a protective shield against charged particles from the Sun and cosmic radiation, shaping the near-Earth space environment and enabling long-term atmospheric stability. The field resembles that of a tilted dipole, with magnetic poles located near—but not identical to—the geographic poles.

The source of this magnetism lies approximately 3,000 km beneath the surface in Earth's liquid outer core. Composed primarily of molten iron and nickel, the outer core undergoes vigorous convection driven by heat escaping from the inner core and radioactive decay. Combined with Earth's rotation, these motions produce electrical currents that sustain a self-exciting magnetic dynamo, known as the **geodynamo** (Glatzmaier & Roberts, 1995).

In dynamo theory, moving conductive fluids generate magnetic fields, while the magnetic field in turn influences fluid motion. This feedback creates a nonlinear system capable of oscillation, instability, and long-term variability. Unlike a permanent magnet, Earth's field is therefore dynamic and continuously evolving.

The geomagnetic field extends outward into space, forming the **magnetosphere**, where solar wind particles are deflected around the planet. Without this magnetic barrier, atmospheric erosion and radiation exposure would increase substantially. Observations from satellites show that the field strength fluctuates on timescales ranging from decades to millions of years, reflecting the turbulent nature of core convection.

Importantly, the geomagnetic field is not fixed in orientation. Geological records preserved in volcanic rocks and ocean sediments reveal that Earth's magnetic polarity has reversed many times throughout its history. Magnetic minerals align with the ambient field as they cool or settle, preserving a permanent record of past field directions. These paleomagnetic archives allow scientists to reconstruct the chronology of geomagnetic behavior over hundreds of millions of years.

At least 183 magnetic reversals have occurred during the last 83 million years, implying an average interval of roughly 450,000 years, though the spacing is highly irregular. The present magnetic configuration, known as the Brunhes chron, began after the Brunhes–Matuyama reversal approximately 780,000 years ago.

Magnetic Reversals and Geomagnetic Excursions

Geomagnetic variability occurs in two principal forms: **full magnetic reversals** and **geomagnetic excursions**. Both reflect instabilities within the geodynamo but differ significantly in duration and outcome.

A **magnetic reversal** occurs when magnetic north and south permanently exchange positions. During such transitions, the global field weakens dramatically, often falling to a small fraction of its normal strength before reorganizing with opposite polarity. The process typically unfolds over thousands to tens of thousands of years.

Major reversals identified from geological records include:

- Brunhes–Matuyama (~773,000 years ago)
- Olduvai (~1.78 million years ago)
- Gauss-Matuyama (~2.58 million years ago)
- Gilbert-Gauss (~3.58 million years ago)

Ocean-floor magnetic stripes provide particularly strong evidence for these events, as symmetrical patterns of alternating polarity appear on either side of mid-ocean ridges.

In contrast, a **geomagnetic excursion** represents a temporary disruption rather than a permanent polarity change. During an excursion:

- Field strength weakens significantly.
- Magnetic poles wander far from normal positions.
- Multiple temporary poles may appear.
- The original polarity ultimately returns.

Excursions typically last hundreds to thousands of years—short compared with full reversals. The best-studied example is the **Laschamp Excursion** (~41,000 years ago), during which field intensity dropped to roughly 5–10% of modern levels before recovering.

Since the Brunhes–Matuyama reversal, approximately 10–12 excursions have been identified, including Mono Lake (~34 ka), Blake (~117 ka), and Iceland Basin (~189 ka). Using representative dates, the average spacing between excursions is about 71,000 years, though variability is large.

The distinction between reversals and excursions suggests that the geodynamo operates near a threshold of instability. Small perturbations may produce temporary reorganizations, while larger disruptions allow polarity to fully invert. Numerical simulations confirm that chaotic fluid flow within the outer core naturally produces such intermittent behavior (Glatzmaier & Roberts, 1995).

Rather than following a strict periodic cycle, reversals appear statistically irregular. Nonetheless, researchers continue exploring whether underlying dynamical rhythms or external influences modulate reversal probability over long timescales.

Proposed Scaling Comparisons

Table 6.4 examines proposed correspondences among magnetic timescales and Fibonacci-derived intervals. These are exploratory comparisons of heterogeneous phenomena, rather than a common periodic law.

Fibonacci ratios approach φ, while ratios between successive ratio estimates approach 1. The adopted temporal mapping supplies candidate intervals for comparison. Index labels in this section follow the zero-based convention used in Table 6.2.

Several examples illustrate these approximate correspondences:

- Solar magnetic polarity reversals occur on an average cycle of approximately 11 years, comparable to Fibonacci-derived scaling near row 18.
- Geomagnetic excursions cluster near ~66 kyr, consistent with higher Fibonacci indices around row 36.
- Long-term geomagnetic reversal spacing averages roughly ~280 kyr in some paleomagnetic datasets, aligning with indices near row 39.

Taken together, these relationships suggest a possible harmonic hierarchy linking magnetic variability across multiple dynamical scales, summarized in **Table 6.4**.

Table 6.4. Proposed correspondence between Fibonacci scaling and characteristic magnetic timescales.

Phenomenon	Characteristic Interval	Fibonacci Row	Fibonacci-Derived Time	Dynamical Role
Solar polarity cycle	~11 years	Row 18	11.45	Stable oscillator
Geomagnetic excursions	~66 kyr	Row 36	66,186	Instability regime
Geomagnetic reversals	~280 kyr	Row 39	280,368	Polarity switching

These correspondences remain speculative. Reversal intervals depend on the geological interval and event selection: the averages quoted in this section are not interchangeable. A valid comparison must specify the source catalog, date range, event definition, and uncertainty, then test the same mapping against suitable stochastic or dynamo-based alternatives.

A possible extension of this scaling framework to deep-time geomagnetic evolution is explored in the Ediacaran magnetic-weakening discussion in Section 6.2.

Implications for Planetary Dynamics and Future Magnetic Behavior

Understanding geomagnetic reversals has implications extending beyond Earth's interior physics. Because the magnetic field shields the planet from energetic particles, periods of reduced field strength influence atmospheric chemistry, radiation exposure, and technological systems.

During both reversals and excursions:

- The magnetosphere contracts.
- Increased cosmic radiation reaches the upper atmosphere.
- Auroral activity expands toward lower latitudes.
- Satellite and communication systems become more vulnerable.

Geological and ice-core records suggest that radiation increases during major excursions, though no evidence links reversals directly to mass extinctions. Life on Earth has persisted through hundreds of polarity changes, indicating that biological systems are resilient to magnetic variability.

From a dynamical perspective, geomagnetic behavior illustrates how planetary interiors operate as complex nonlinear systems. The geodynamo shares conceptual similarities with stellar magnetic cycles, reinforcing the continuity between planetary and stellar physics explored in broader celestial dynamics.

The apparent hierarchy of timescales—from solar cycles (~11 years) to excursions (~10^4–10^5 years) to reversals (~10^5–10^6 years)—may reflect nested dynamical regimes governed by energy transfer, rotational forces, and fluid turbulence. Whether these regimes obey deeper mathematical scaling laws remains an open question.

Presently, Earth's magnetic field is weakening at a modest rate, leading to speculation about an impending reversal. However, paleomagnetic evidence shows that field intensity fluctuations are common and do not necessarily precede polarity flips. A reversal, if it occurs, would likely unfold gradually over thousands of years rather than abruptly.

Future research combining satellite observations, paleomagnetism, numerical simulations, and statistical analysis may clarify whether geomagnetic behavior is purely chaotic or partially structured by underlying dynamical constraints.

Ediacaran Magnetic Weakening

Geomagnetic reversals and excursions demonstrate that Earth's magnetic field is inherently dynamic, but evidence from deep geological time suggests that long-term variations in magnetic intensity may also have influenced planetary environments and biological evolution. A notable example occurs during the Ediacaran Period (approximately 635–541 million years ago), when complex multicellular organisms first appeared in the fossil record. Recent paleomagnetic research indicates that a prolonged weakening of Earth's magnetic field may have contributed to environmental conditions associated with this evolutionary transition (Huang et al., 2024).

Geological measurements from ancient rocks show that around 591 million years ago the geomagnetic field declined dramatically, reaching strengths estimated to be up to thirty times weaker than today and remaining unusually weak for roughly 26 million years (Huang et al., 2024). Because the magnetic field shields Earth from charged solar particles, this reduction likely allowed increased interaction between solar radiation and the upper atmosphere. Enhanced atmospheric escape of lightweight gases, particularly hydrogen, would have gradually altered atmospheric composition.

One consequence of this process may have been a relative increase in atmospheric oxygen. Although oxygen had long been produced by photosynthesizing microorganisms, global oxygenation occurred in stages. The Ediacaran interval may represent a threshold period during which biological oxygen production and geophysical processes together stabilized higher oxygen levels, enabling energy-intensive multicellular metabolism (Huang et al., 2024).

This environmental transition coincides with the emergence of the Ediacaran biota, among the earliest known animals. Fossils such as *Dickinsonia*, a flattened organism preserved in ancient

marine sediments, display organized multicellular structure and possible metabolic complexity (Xiao & Laflamme, 2009). Increased oxygen availability would have supported larger body sizes, cellular specialization, and more complex ecological interactions. In this context, magnetic-field weakening is best interpreted as an indirect environmental catalyst rather than a primary biological driver.

The period of extreme magnetic instability appears to have ended around 565 million years ago, when renewed growth of Earth's inner core strengthened convection within the liquid outer core and reinvigorated the geodynamo (Huang et al., 2024). As magnetic intensity recovered, the magnetosphere expanded, stabilizing atmospheric protection and supporting long-term planetary habitability. The rise of complex life was therefore likely multifactorial, involving tectonic, chemical, climatic, and biological feedbacks, with geomagnetic evolution acting as one contributing component within a larger Earth-system transition.

Earth's magnetic behavior operates within a broader planetary framework linking core dynamics, mantle convection, and surface environments. Geological studies identify an approximately 36-million-year tectonic cycle associated with variations in seafloor spreading rates and global sea level, which influence marine biodiversity through the expansion and contraction of shallow continental-shelf habitats (Boulila et al., 2023). Although distinct from geomagnetic processes, such mantle-driven cycles regulate heat flow across the core-mantle boundary and may modulate the conditions under which the geodynamo operates. Geomagnetic variability can therefore be viewed as part of a hierarchy of coupled planetary rhythms spanning core, mantle, and biosphere evolution.

Table 6.5 extends the comparison from recurrent magnetic behavior to deep-time transitions. The Ediacaran episode is associated with row 55 in the proposed mapping, but an event's age before present is different from a cycle duration. Their juxtaposition does not establish a harmonic sequence.

The tectonic, magnetic, and biological examples motivate investigation of coupled planetary processes. Evaluating the proposed scaling requires separate treatment of periods, waiting times, and dates, with explicit time origins and selection rules.

Table 6.5. Near-harmonic cascade of magnetic dynamical regimes and coupled planetary timescales.

Phenomenon	Characteristic Interval	Fibonacci Row	Fibonacci-Derived Time	Dynamical Role
Solar polarity cycle	~11 years	Row 18	11.45	Stable oscillator
Geomagnetic excursions	~66 kyr	Row 36	66,186	Instability regime
Geomagnetic reversals	~280 kyr	Row 39	280,368	Polarity switching
Geomagnetic near-collapse (Ediacaran)	Singular transition (~591–565 Ma)	Row 55	618,771,051	Dynamo phase transition
Plate-tectonic biodiversity cycle	~36 Myr	Row 49	34,482,929	Mantle-biosphere modulation

6.3 Orbital Periods and Celestial Structure

Spiral Structure and Logarithmic Geometry

Spiral structures are among the most striking recurring patterns observed in natural systems, appearing in biological growth, atmospheric dynamics, and astrophysical formations. In astronomy, spiral galaxies, accretion disks, and rotating fluid systems frequently exhibit geometries approximated by logarithmic spirals, mathematical curves defined by constant angular growth relative to radial expansion (Binney & Tremaine, 2008).

This geometry possesses scale invariance: enlarging the spiral preserves its shape. Such invariance makes logarithmic spirals dynamically stable under processes involving rotation combined with outward transport of matter or energy.

A golden spiral is one particular logarithmic spiral. A galaxy image or spiral overlay does not establish its pitch angle or a Fibonacci relation. Such a claim requires a quantitative fit with uncertainty and comparison against other spiral models (Livio, 2002).

Spiral arms in galaxies form through density wave processes rather than rigid structures; stars move through these regions while gravitational interactions maintain large-scale patterns (Lin & Shu, 1964). The appearance of Fibonacci-like proportions therefore reflects underlying optimization and self-organization rather than discrete numerical enforcement.

Planetary Orbital Periods and Resonance Stability

Celestial mechanics reveals that planetary systems frequently organize into orbital resonances—relationships in which orbital periods approximate simple integer ratios. Well-known examples include the 2:1 resonance between Jupiter's moons Io and Europa and the 3:2 resonance between Neptune and Pluto (Murray & Dermott, 1999). Such resonances arise through gravitational interactions that stabilize orbital configurations by preventing repeated close encounters.

When orbital periods approach commensurate ratios, gravitational perturbations become phase-locked, allowing angular momentum exchange to average out over time. This process produces long-term dynamical stability. Systems not near stable resonances tend to evolve through migration, scattering, or ejection events until stable configurations emerge.

Some researchers have noted that chains of near-resonant ratios occasionally resemble successive Fibonacci fractions (e.g., 2/1, 3/2, 5/3). Importantly, these relationships arise indirectly from dynamical evolution rather than from explicit numerical constraints. Numerical simulations of planetary formation demonstrate that protoplanetary disks naturally generate resonance chains through migration and dissipative interactions with surrounding gas (Batygin & Morbidelli, 2013). Stable configurations minimize orbital energy exchange, and Fibonacci-like ratios may appear because successive rational approximations to irrational numbers—particularly those related to the golden ratio φ—often provide dynamically robust spacing relationships.

To explore whether Fibonacci relationships might nevertheless provide a useful descriptive approximation of orbital timing, we conducted an exploratory numerical comparison between observed orbital periods of major planets and selected dwarf planets and periods derived from Fibonacci numbers scaled to 24-hour temporal units. The results are summarized in **Table 6.6**, which lists Fibonacci indices, derived orbital periods, observed orbital periods, and percentage deviations between predicted and empirical values.

Table 6.6: Comparative Analysis of Orbital Periods and Fibonacci Sequence Approximations in the Solar System

Fibonacci Position	Fibonacci Number (Days)	Fibonacci Derived Years	Orbital Period (Years)	% Difference	Type	Name
F11	89	0.24	0.24	0.00%	Planet	Mercury
F13	233	0.62	0.63	-1.61%	Planet	Venus
F14	377	1	1.03	-3.00%	Planet	Earth
F15	610	1.88	1.67	11.17%	Planet	Mars
F17	1,597	4.6	4.37	5.00%	Dwarf Planet	Ceres
F19	4,181	11.86	11.45	3.46%	Planet	Jupiter
F21	10,946	29.46	29.98	-1.77%	Planet	Saturn
F23	28,657	84.02	78.51	6.56%	Planet	Uranus
F24	46,368	164.78	127.03	22.91%	Planet	Neptune
F25	75,025	248.4	205.54	17.25%	Dwarf Planet	Pluto
F26	121,393	282.1	332.58	-17.89%	Dwarf Planet	Haumea
F26	121,393	306.82	332.58	-8.40%	Dwarf Planet	Makemake
F27	196,418	562.55	538.13	4.34%	Dwarf Planet	Eris

Table 6.6 retains the original values and headings. Its two year columns are labeled in reverse relative to their contents: the column headed “Fibonacci Derived Years” contains the comparison orbital periods, while “Orbital Period (Years)” contains the converted Fibonacci values. For example, 610 days converts to approximately 1.67 years, shown in the fourth column. Deviations are not uniform across bodies, so this table is descriptive rather than an established predictive model.

Table 6.6 is a descriptive comparison under the stated 24-hour conversion. Numerical proximity alone does not identify an orbital mechanism or establish predictive value. The index-selection rule and comparison with other geometric sequences are essential to evaluating the apparent fit.

In this sense, Fibonacci alignment functions as a **descriptive heuristic rather than a causal mechanism**. The governing processes remain gravitational dynamics, angular momentum conservation, and dissipative evolution within protoplanetary disks (Murray & Dermott, 1999; Batygin & Morbidelli, 2013).

Validation and Alternative Models

Numerical correspondence becomes scientifically informative when it survives controls for selection and flexibility. The following tests apply to Table 6.6.

First, analyses must incorporate **measurement uncertainty**. Orbital periods, distances, and masses are estimated with finite precision. Apparent numerical matches must be assessed relative to error bounds rather than exact ratios.

Second, appropriate **null models** must be defined. Randomized or dynamically simulated planetary systems provide baselines against which observed patterns can be compared. If Fibonacci-like relationships occur no more frequently than expected under realistic formation models, the hypothesis lacks explanatory value.

Third, competing explanations must be evaluated. Alternative models include:

- gravitational resonance capture,
- migration-driven orbital rearrangement,
- disk-driven damping processes,
- chaotic diffusion within multi-body systems (Murray & Dermott, 1999).

A Fibonacci-based interpretation gains credibility only if it improves explanatory or predictive power beyond these established mechanisms.

Fourth, predictions must be prospective rather than retrospective. A valid framework should generate testable forecasts, such as expected resonance clustering in newly discovered exoplanet systems.

Finally, cross-system consistency is essential. If Fibonacci resonance represents a genuine emergent principle, similar statistical signatures should appear across independent planetary systems observed by missions such as *Kepler* and *TESS*.

Magnetic Structure

Spiral magnetic structures are widely observed across astrophysical environments, including galactic disks, stellar winds, and accretion flows. Standard explanations attribute these geometries to differential rotation and magnetohydrodynamic dynamo processes, which stretch and wind magnetic field lines into spiral configurations (Priest, 2014).

The magnetic-field maps in Figures 6.2–6.3 illustrate organized astrophysical structure (Beck, 2016; EHT Collaboration, 2024). They provide physical context but do not measure agreement with a golden spiral.

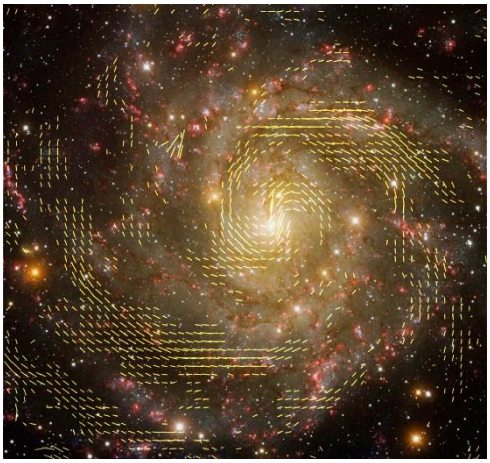

Figure 6.2 — Magnetic-field structure in IC 342. Composite observations from the VLA and Effelsberg telescope show the projected magnetic-field orientation across the galaxy. Source: Beck (2016).

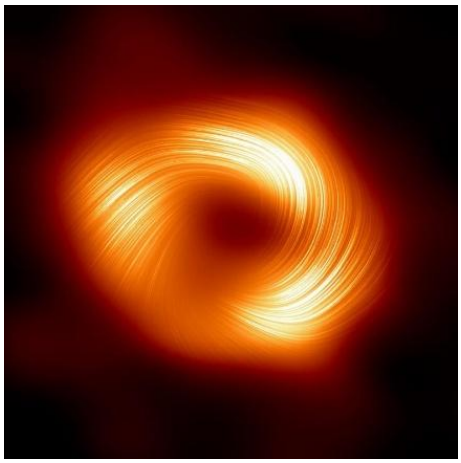

Figure 6.3 — Polarized view of Sagittarius A*. The overlaid orientation marks trace polarization related to magnetic-field organization around the black hole. Source: EHT Collaboration (2024).

These observations do not demonstrate φ-scaling as a governing physical law. Rather, they suggest that logarithmic spiral geometry may represent a recurring stability class arising across scales where rotation, flow, and constraint interact. Within this interpretation, φ-related spirals function as **statistical geometric attractors**, analogous to preferred resonance states in dynamical systems.

Future work would require quantitative testing comparing observed spiral pitch angles against null models derived from magnetohydrodynamic simulations. Only such analysis could determine whether φ-related geometry provides explanatory power beyond existing dynamical accounts.

Elemental Constraints and Biology

Stellar nucleosynthesis produces chemical elements through fusion pathways governed by nuclear binding energies and stability thresholds (Burbidge et al., 1957; Clayton, 1983). Element formation is not arbitrary; reactions proceed only along energetically permitted trajectories, generating the characteristic abundance patterns observed throughout the universe.

Living systems maintain order by sustaining electrochemical and redox gradients (Nicholls & Ferguson, 2013). These gradients depend directly on elemental properties rooted in atomic structure. Transition metals enable reversible electron transfer through multiple oxidation states, while alkali and alkaline-earth metals stabilize ionic potentials essential for signaling and membrane function. Such capacities arise from quantum mechanical constraints governing electronic configuration (Atkins & de Paula, 2014).

The periodic table organizes recurring electronic structures that determine bonding behavior and energetic stability (Scerri, 2007). In this sense, periodicity functions as a translation layer linking cosmological production with biological utility. Stellar evolution determines elemental availability, while quantum structure governs interaction possibilities. Biological evolution unfolds within this jointly constrained space, favoring chemistries compatible with stable energy transfer (Fraústo da Silva & Williams, 2001).

Stable metabolism requires incremental energy dissipation without structural breakdown. Discrete electronic states partition energetic transitions into controllable steps through redox reactions, ionic gradients, and catalytic processes (Alberts et al., 2022). Living systems maintain order by channeling energy through constrained pathways rather than uncontrolled dissipation (Schrödinger, 1944; Prigogine & Stengers, 1984).

Chapter 7 Cosmological Structure and Timelines

Cosmological structure formation provides a setting in which growth, organization, and temporal scale can be compared. We first establish the physical and mathematical distinctions, then evaluate the proposed milestone tables and their uncertainties.

7.1 Structure Formation in the Universe

Star Formation

The large-scale structure of the universe provides one of the clearest natural examples of emergence operating under physical constraints. Stars, galaxies, and cosmic networks arise not from centralized design but from local interactions governed primarily by gravity, thermodynamics, and energy dissipation. These processes demonstrate how ordered structures can emerge spontaneously from initially diffuse matter distributions.

Star formation begins within cold molecular clouds composed primarily of hydrogen gas and dust. Small density fluctuations within these clouds—produced by turbulence, shock waves, or gravitational instability—lead certain regions to collapse under their own gravitational attraction (McKee & Ostriker, 2007). As collapse proceeds, gravitational potential energy converts into thermal energy, increasing temperature and pressure until nuclear fusion ignites in the core, marking the birth of a star.

This process illustrates a fundamental emergent principle: global organization arises from local interactions constrained by physical laws. No external blueprint specifies star formation; rather, gravitational attraction amplifies small perturbations until stable structures emerge. Thermodynamic processes regulate collapse by balancing heating, radiation, and pressure, ensuring that structure formation occurs within constrained energetic regimes.

Importantly, star formation reflects a system operating far from thermodynamic equilibrium. According to nonequilibrium thermodynamics, ordered structures can arise when energy flows through a system and is dissipated efficiently (Prigogine & Stengers, 1984). Stars themselves function as dissipative structures, converting gravitational energy into radiation that drives further cosmic evolution.

Thus, stellar emergence exemplifies how gravity provides an organizing force while thermodynamics determines which configurations remain stable. Complexity arises not in opposition to entropy but through structured pathways of energy dissipation.

Galaxies and Clusters

Beyond individual stars, cosmic organization continues through hierarchical processes that assemble increasingly large structures. Galaxies form from the gravitational aggregation of matter within dark matter halos—regions where invisible mass dominates gravitational dynamics (Mo, van den Bosch, & White, 2010). Gas falling into these halos cools, condenses, and fragments into rotating disks or elliptical configurations depending on angular momentum and merger history.

Hierarchical emergence is evident in the nested structure of the cosmos:

- stars form within molecular clouds,
- stellar systems assemble into galaxies,
- galaxies organize into groups and clusters,
- clusters connect through filamentary networks known as the cosmic web.

Each level introduces new emergent properties not predictable solely from the previous scale. Galaxies exhibit spiral arms, bars, and star formation cycles arising from collective gravitational interactions (Binney & Tremaine, 2008). Galaxy clusters display large-scale dynamics influenced by dark matter distributions and hot intracluster gas. At even larger scales, gravitational attraction produces filamentary structures spanning hundreds of millions of light-years.

Computer simulations of cosmic evolution demonstrate that such hierarchical organization naturally emerges from simple initial conditions combined with gravitational physics (Springel et al., 2005). Small primordial fluctuations observed in the cosmic microwave background grow over billions of years through nonlinear amplification, illustrating how minor differences can generate vast structural diversity.

Hierarchical emergence reflects a recursive principle: structures formed at one scale become the constraints shaping formation at the next. This cascading organization aligns with broader theories of complexity in which higher-order systems arise from repeated aggregation and interaction across scales.

Self Organization and Scaling

Cosmic structures also exhibit statistical regularities and scaling laws suggesting underlying self-organizing principles. Self-organization refers to the spontaneous formation of ordered patterns through interactions among system components without centralized control (Haken, 1983).

One example is the distribution of galaxy sizes and luminosities, which follows power-law relationships characteristic of scale-invariant systems (Peebles, 1993). Similarly, clustering patterns of galaxies exhibit fractal-like behavior across certain spatial ranges, indicating repeating structural organization across scales (Mandelbrot, 1982).

Scaling laws arise because gravitational dynamics operate similarly regardless of spatial scale. The same inverse-square law governing planetary motion also shapes galaxy formation and cluster interactions. When combined with processes such as cooling, feedback from stellar radiation, and angular momentum conservation, these universal rules generate patterns that appear statistically self-similar.

The cosmic web—composed of filaments, nodes, and voids—is a particularly striking example of emergent self-organization. Numerical simulations show that matter naturally organizes into filamentary networks as gravitational collapse proceeds anisotropically along density gradients (Bond, Kofman, & Pogosyan, 1996). These structures resemble other emergent networks found in biological and ecological systems, suggesting shared principles of constrained growth.

Scaling behavior also appears in star formation rates, galactic rotation curves, and mass distributions, indicating that large-scale cosmic organization follows predictable statistical relationships rather than arbitrary arrangements (Mo et al., 2010).

From an emergence perspective, such scaling laws represent macroscopic signatures of underlying generative processes. They reveal that complex cosmic architecture results from iterative interactions governed by invariant physical constraints.

Entropy and Timing

Recent observations from the James Webb Space Telescope (JWST) further reinforce the emergent character of cosmic evolution. Evidence suggesting that massive galaxies formed earlier than previously expected indicates that structure formation may proceed through nonlinear transitions rather than smooth, uniform progression (Donnan et al., 2023). Such findings highlight the importance of feedback processes and evolving constraints in shaping cosmic history, consistent with emergence-driven perspectives.

Underlying these processes is the organizing role of entropy. In thermodynamic terms, the growth of structure does not contradict the Second Law of Thermodynamics; rather, ordered systems can arise locally when energy flows enable more efficient dissipation overall. Stars, galaxies, and planetary systems function as dissipative structures that transform concentrated energy into distributed radiation, increasing total entropy while temporarily sustaining organized configurations. Cosmic evolution can therefore be interpreted as a sequence of staged transitions in which new structures emerge as energetically favorable pathways for energy redistribution.

If emergence governs both the formation of structure and the thermodynamic direction of cosmic evolution, an open question follows: whether the *timing* of major cosmological transitions may also reflect underlying regularities associated with recursive growth. Mathematical sequences such as Fibonacci scaling provide one possible language for describing constrained expansion processes without implying deterministic causation. In this view, recursive relationships would serve not as governing laws but as descriptive patterns arising from repeated interactions under shared physical constraints.

These considerations motivate the exploration of whether recursive scaling relationships might provide a descriptive scaffold for cosmological epochs.

7.2 Expansion and Recursive Growth

Exponential Expansion

One of the most striking features of modern cosmology is the recognition that the universe underwent an early phase of extremely rapid expansion known as cosmic inflation. During this epoch, spacetime expanded exponentially, increasing in scale by many orders of magnitude within a fraction of a second after the Big Bang (Guth, 1981; Linde, 1983). Inflation explains several otherwise puzzling observations, including large-scale isotropy, spatial flatness, and the uniformity of the cosmic microwave background (Weinberg, 2008).

Exponential expansion represents a fundamental generative motif in physics: growth governed not by additive increments but by multiplicative recursion. In exponential systems, each state

produces the next through proportional scaling, meaning that structure emerges through repeated self-amplification rather than external design. Such dynamics are mathematically equivalent to iterative doubling processes, where each step depends directly on the previous one.

Recursive growth processes appear across many physical and biological systems, including population dynamics, chemical reactions, and gravitational clustering (West, Brown, & Enquist, 1997). Inflation therefore may be interpreted not merely as a unique cosmological event but as an instance of a broader class of recursive expansion phenomena governed by feedback between energy density and spacetime geometry.

Within the framework developed in this book, exponential expansion is treated as an archetypal example of **constraint-driven recursion**: growth proceeds rapidly until bounded by changing energetic or structural constraints. Inflation ended when field dynamics altered the energy landscape, transitioning the universe from exponential expansion to slower, matter-dominated evolution (Liddle & Lyth, 2000). This transition illustrates how recursive growth phases naturally generate discrete evolutionary epochs.

Period Doubling

Recursive growth frequently produces hierarchical structures through mechanisms known as **period-doubling cascades**. First identified in nonlinear dynamical systems, period doubling occurs when a system undergoing continuous parameter change transitions into oscillatory states whose periods successively double (Feigenbaum, 1978; Strogatz, 2015). These cascades represent universal routes to complexity and chaos.

The importance of period doubling lies in its universality: vastly different systems—from fluid turbulence to biological rhythms—exhibit identical scaling behavior near transition points. This universality suggests that complex structures may arise from generic mathematical principles rather than system-specific mechanisms.

Period-doubling processes generate scaling ratios approaching constant values, reflecting deep structural regularities in recursive systems. Such cascades produce hierarchical organization, where each level embeds previous levels while introducing new degrees of freedom. This mirrors earlier discussions of recursive emergence, in which later states preserve earlier informational structure while expanding complexity.

In cosmology, analogous processes may occur during structure formation. Gravitational clustering produces hierarchical aggregation: small overdensities collapse first, forming stars and galaxies that later assemble into clusters and superclusters (Peebles, 1993). Each scale emerges through repeated amplification of earlier fluctuations, resembling recursive doubling across spatial domains.

Thus, period doubling provides a conceptual bridge between nonlinear dynamics and cosmological evolution, illustrating how scaling laws can emerge naturally from iterative processes governed by simple rules.

Growth Summaries in Pascal Recursion

Pascal's triangle provides a discrete mathematical representation of recursive growth. Each row is generated through local additive rules:

$$\binom{n}{k} = \binom{n-1}{k-1} + \binom{n-1}{k}$$

The sum of entries in zero-based row n is 2^n, so local addition yields a doubling of the total count at each step (Graham, Knuth, & Patashnik, 1994).

This duality—local addition producing global doubling—is central to understanding how Fibonacci and golden-ratio (φ) relationships arise. Fibonacci numbers emerge naturally as diagonal sums within Pascal's triangle, revealing that Fibonacci scaling is not externally imposed but structurally embedded in binomial recursion.

Mathematically, Fibonacci growth approximates exponential expansion with base φ:

$$F_n \approx \frac{\phi^n}{\sqrt{5}}$$

Here φ ≈ 1.618 (Livio, 2002). Fibonacci growth and doubling are both exponential; they differ in rate and recurrence. A physical explanation must specify why one rule applies.

Within the broader framework of this book, Pascal recursion acts as a minimal generator linking three regimes:

1. **Doubling growth** (exponential expansion),
2. **Fibonacci scaling** (constrained recursive growth),
3. **Fractal structure** (modular filtering of recursive outputs).

The array therefore contains distinct growth summaries and filtered patterns. Their coexistence is a mathematical relationship, not proof that a physical system passes through them as successive stages.

Testing a Shared Growth Logic

The concept of a unified growth logic proposes that diverse phenomena—biological evolution, neural organization, stellar formation, and cosmic expansion—share underlying mathematical principles governing how complexity unfolds. Such a proposal does not claim identical mechanisms across domains; rather, it suggests shared **organizational dynamics** arising from recursion, constraint, and energy flow.

Scientifically, a unified growth logic would imply several testable expectations:

1. **Cross-scale scaling laws**
Similar mathematical relationships should appear across physical, biological, and informational systems.

2. **Predictable phase transitions**
Growth processes should exhibit identifiable transitions corresponding to constraint thresholds.

3. **Hierarchy formation through recursion**
Complex structures should arise through iterative aggregation rather than top-down design.

4. **Emergent optimality**
Observed patterns should reflect efficiency or stability under energetic and informational constraints.

Such principles align with theories of self-organization and far-from-equilibrium thermodynamics, in which ordered structures arise spontaneously through energy dissipation (Prigogine & Stengers, 1984). They also resonate with complexity science perspectives emphasizing feedback, nonlinearity, and hierarchical emergence (Holland, 1998).

However, scientific legitimacy requires clear boundaries. A unified growth logic must generate falsifiable predictions rather than post hoc pattern recognition. Competing explanations—such as stochastic processes, selection effects, or observational bias—must be rigorously evaluated. Only through comparative modeling and empirical testing can recursive growth frameworks be validated or rejected.

If supported, such a framework would reposition growth itself as a fundamental organizing principle of nature. Expansion, differentiation, and complexity would be understood not as isolated phenomena but as manifestations of a common recursive architecture governing systems across scales.

Limits of the Growth Analogy

This section examined expansion as a process of recursive doubling and hierarchical growth, linking cosmological inflation, nonlinear dynamics, and combinatorial recursion. Exponential expansion provides the generative template, period-doubling cascades illustrate universal scaling behavior, and Pascal recursion reveals how Fibonacci structures emerge intrinsically from constrained growth.

Together, these ideas suggest that complex structures—from galaxies to biological organisms—may arise through shared mathematical dynamics rooted in recursion and constraint. Whether this constitutes a genuine unified growth logic remains an empirical question, but the framework offers a coherent pathway for investigating how simple iterative rules generate the layered complexity observed throughout the universe.

7.3 Cosmological Milestones and Their Evaluation

Earlier chapters defined a formal entropy measure for recursive rows and identified phase-like regimes (uniform boundary states, alternating transitions, and differentiated high-entropy bands). The present section tests a separate hypothesis: whether epoch spacing in cosmology shows statistical proximity to Fibonacci-derived temporal scaffolds under a fixed, globally applied scaling.

The Proposal: Using Fibonacci Indexing as a Scaffold for Epochs

Modern cosmology describes the history of the universe as a sequence of distinct epochs characterized by changes in dominant physical processes, energy regimes, and structural organization. These include early inflationary expansion, nucleosynthesis, recombination, galaxy formation, stellar evolution, and long-term thermodynamic decline (Peebles, 1993; Weinberg, 2008). While standard cosmological models successfully explain many observational features,

they typically treat epoch boundaries as consequences of evolving physical parameters rather than as manifestations of deeper structural timing principles.

The present framework proposes that **Fibonacci indexing** may serve as a scaffolding heuristic for organizing cosmological epochs. The central hypothesis is not that Fibonacci numbers cause cosmic events, but that recursive growth under constraints can produce temporal spacing approximating Fibonacci intervals. In this view, Fibonacci indices function as **attractors**—preferred scaling relationships emerging from iterative processes governed by energy flow, gravitational aggregation, and entropy production.

Recursive systems frequently generate exponential or quasi-exponential scaling behaviors. Because Fibonacci growth approximates exponential expansion with ratio φ (the golden ratio), it provides a mathematically minimal model for describing staged expansion or phase transitions in evolving systems (Livio, 2002). If cosmic evolution unfolds through repeated constraint-driven transitions, then epoch spacing may statistically cluster near Fibonacci-derived temporal ratios.

Thus, Fibonacci indexing is introduced as a hypothesis about **temporal organization under recursive emergence**, not as numerological assignment. Its scientific value depends entirely on whether measurable correspondences exceed expectations derived from chance or alternative scaling models.

Methods

Evaluating whether recursive scaling provides a meaningful description of cosmological timing requires a transparent and reproducible comparison framework. The objective of this methodology is not to infer causation but to test whether independently defined cosmological epochs exhibit measurable correspondence with intervals derived from Fibonacci-based temporal scaling. To ensure interpretive clarity, all comparisons were constructed using predefined procedures applied uniformly across events.

Normalization of Cosmic Time

Cosmological events occur across an enormous temporal range spanning more than one hundred orders of magnitude, from fractions of a second after the Big Bang to speculative far-future eras. Direct comparison of such intervals requires a consistent temporal reference frame. All event times were therefore expressed as **elapsed time since the Big Bang**, adopting a present cosmic age of approximately 13.8 billion years as the standard normalization reference (Weinberg, 2008).

Normalization serves two purposes. First, it places observational and theoretical epochs within a common chronological coordinate system independent of local processes. Second, it allows proportional rather than absolute differences to be evaluated, which is essential when comparing early-universe particle epochs with long-term cosmological projections. Events defined in seconds or minutes during early cosmic evolution are retained for chronological completeness but are treated separately from later structure-formation epochs, where year-scale timing becomes physically meaningful.

Fibonacci Temporal Conversion

Predicted epochs were generated by mapping Fibonacci sequence indices onto cosmological time through a single global scaling transformation described in Appendix A. The Fibonacci sequence provides a discrete representation of recursive growth, where each term depends on the sum of the two preceding terms. Because Fibonacci growth approximates exponential expansion constrained by additive recursion, it serves as a candidate mathematical model for staged transitions in evolving systems (Livio, 2002).

The conversion procedure follows three steps:

1. **Sequence generation** — Fibonacci numbers were generated iteratively from initial conditions using standard recursion.

2. **Temporal scaling** — sequence values were converted into physical time units using a fixed multiplier derived independently of individual cosmological events.

3. **Epoch assignment** — Fibonacci-derived scaffold times were obtained by mapping scaled Fibonacci values onto elapsed cosmic time.

Importantly, the same transformation was applied uniformly to all epochs. No parameter adjustments were introduced for specific events or cosmological eras.

Event Selection and Observational Benchmarks

Reference dates for cosmological events were compiled from widely accepted astrophysical literature, including observational constraints derived from cosmic microwave background measurements, redshift surveys, stellar population modeling, and theoretical projections of long-term cosmic evolution (McKee & Ostriker, 2007; Mo, van den Bosch, & White, 2010; Donnan et al., 2023). These values represent approximate consensus estimates rather than precise singular timestamps, reflecting the inherent uncertainty and model dependence of cosmological reconstruction.

Events were grouped into developmental regimes—early universe physics, recombination and cooling, structure formation, stellar evolution, and far-future cosmology—to allow correspondence to be evaluated across distinct physical domains.

Quantifying Correspondence

Agreement is summarized by signed percentage difference: 100 × (predicted time − observed time) / observed time. This descriptive statistic must be interpreted with the uncertainty and time origin of each benchmark.

This metric provides a scale-independent measure suitable for comparisons spanning multiple orders of magnitude in time. Positive values indicate predicted epochs occurring later than consensus estimates, whereas negative values indicate earlier predictions.

The purpose of this metric is descriptive rather than inferential; no statistical significance testing is implied at this stage. Instead, deviations are interpreted qualitatively to identify domains of closer alignment or systematic divergence.

Treatment of Uncertainty

Cosmological epoch estimates carry substantial uncertainties arising from observational limitations, model assumptions, and evolving datasets. Early universe transitions may vary by orders of magnitude depending on particle physics models, while far-future projections rely on theoretical extrapolation rather than direct observation (Adams & Laughlin, 1997). Consequently, correspondence values should be interpreted as comparisons between approximate temporal ranges rather than exact event matches.

Where uncertainty ranges are large or poorly constrained, agreement or disagreement with Fibonacci-derived intervals is treated cautiously and discussed qualitatively rather than quantitatively.

Avoidance of Post-Hoc Fitting

The comparison is described as using one global scaling transformation without event-specific tuning. A reproducible assessment also needs the exact multiplier, time unit, direct or cumulative convention, index-assignment rule, and event-selection record. Applying one conversion does not by itself establish prospective specification.

This constraint ensures that any observed correspondence reflects properties of the scaling framework itself rather than retrospective calibration. The approach therefore allows the hypothesis to remain falsifiable: systematic divergence between predicted and observed epochs would indicate that recursive scaling does not provide an adequate descriptive model for cosmological timing.

The following section presents the resulting comparisons between normalized cosmological epochs and Fibonacci-derived temporal intervals.

Empirical Comparison of Cosmological Epochs

The cosmological benchmarks are compared with the reference intervals described in Section 7.3. This is a descriptive assessment of proposed temporal correspondence.

Cosmological benchmarks were organized into developmental phases reflecting dominant physical regimes of the universe, including early-universe processes, post-recombination cooling, structure formation, stellar evolution, and long-term cosmological projections. This phase-based organization allows correspondence to be assessed within physically meaningful contexts rather than across unrelated dynamical regimes.

Tables 7.1–7.6 preserve the phase-specific comparisons, and Table 7.7 consolidates selected entries. Early microphysical epochs are contextual; far-future epochs are theoretical projections. Neither should be pooled uncritically with observationally constrained structure-formation dates.

The reported comparisons use the stated global conversion. Their evidential interpretation depends on verification of the selection and assignment rules described above.

The tables follow the sequence from early-universe context through structure formation to future projections.

Together, these comparisons provide an empirical overview of how Fibonacci-derived temporal intervals align with, or diverge from, current cosmological timelines across more than one hundred orders of magnitude in cosmic time.

Note. Scientific consensus dates represent approximate values synthesized from observational and theoretical cosmology literature and may vary across models and datasets. Percentage differences are calculated as (Predicted−Observed)/Observed×100%.

Early-universe particle epochs are included for chronological continuity but are not expected to conform to large-scale temporal scaling due to differing governing physical regimes. Far-future events represent theoretical projections and should be interpreted as order-of-magnitude estimates rather than empirically constrained dates.

Table 7.1: Early Universe Events

Event	Scientific Consensus (Years After Big Bang)	Fibonacci-Derived Time	% Difference
Inflationary Epoch	1.00^{-32}	NA	NA
Quark-Gluon Plasma Formation	1.00^{-12}	NA	NA
Hadron Epoch	1.00^{-06}	NA	NA
Lepton Epoch	1 second	NA	NA
Neutrino Decoupling	2 seconds	NA	NA
Matter-Antimatter Annihilation	10 seconds	NA	NA
Photon Epoch	10 seconds	NA	NA
Nucleosynthesis	3 minutes	NA	NA

Table 7.2: Post-Big Bang Cooling and Dark Ages

Event	Scientific Consensus (Years After Big Bang)	Fibonacci-Derived Time	% Difference
Photon Decoupling	240,000	280,368	16.82%
Dark Ages	240,000	280,368	16.82%
Recombination	380,000	453,644	16.23%
Formation of First Atoms	380,000	453,644	16.23%
Cosmic Microwave Background	380,000	453,644	16.23%

Table 7.3: Reionization and Early Structure Formation

Event	Scientific Consensus (Years After Big Bang)	Fibonacci-Derived Time	% Difference
Reionization	150,000,000	146,072,031	-2.62%
First Starlight	150,000,000	146,072,031	-2.62%
Structure Formation Begins	150,000,000	146,072,031	-2.62%
Formation of First Galaxies	250,000,000	236,349,510	-5.78%
Formation of First Quasars	600,000,000	618,771,051	3.03%
Advanced Galaxy Formation	1,000,000,000	1,001,192,592	0.12%
Reionization and Galaxy Formation	1,000,000,000	1,001,192,592	0.12%
Population II Star Dominance	1,000,000,000	1,001,192,592	0.12%

Table 7.4: Large Scale Structure Formation

Event	Scientific Consensus (Years After Big Bang)	Fibonacci-Derived Time	% Difference
Formation of Galaxy Clusters	1,500,000,000	1,619,963,644	8.00%
Dark Matter Structure Maturation	1,500,000,000	1,619,963,644	8.00%
Peak of Star Formation	1,500,000,000	1,619,963,644	8.00%
Rich Galaxy Cluster Era	2,000,000,000	1,619,963,644	-19.00%
Supercluster Formations	2,500,000,000	2,621,156,236	4.85%
Intergalactic Stellar Populations	3,000,000,000	2,621,156,236	-12.63%
Decline in Star Formation	4,000,000,000	4,241,119,879	6.03%
Advanced Stellar Evolution	4,500,000,000	4,241,119,879	-5.75%
Increased Neutron Stars	5,000,000,000	4,241,119,879	-15.18%

Table 7.5: Solar System and Earth Formation

Event	Scientific Consensus (Years After Big Bang)	Fibonacci-Derived Time	% Difference
Formation of Solar System and Earth	9,000,000,000	11,103,395,994	23.37%
Cooling of White Dwarfs	10,000,000,000	11,103,395,994	11.03%
Evolution of Planetary Nebulae	10,000,000,000	11,103,395,994	11.03%
Solar White Dwarf	10,000,000,000	11,103,395,994	11.03%
Present Time	13,800,000,000	11,103,395,994	-19.54%

Table 7.6: Future Events

Event	Scientific Consensus (Years After Big Bang)	Fibonacci-Derived Time	% Difference
Galaxy Merging	55,000,000,000	47,034,740,213	-14.48%
Deep Future Galaxy Isolation	1.0000E+13	9.3601E+12	-6.40%
Stelliferous Era	1.0000E+14	1.0381E+14	3.81%
Last Generations of Stars	1.0000E+14	1.0381E+14	3.81%
End of Main Sequence Star Formation	1.0000E+14	1.0381E+14	3.81%
Black Hole Dominance	1.0000E+26	1.3725E+26	37.25%
Degenerate Era	1.0000E+27	1.5221E+27	52.21%
Proton Decay (Hypothetical)	1.0000E+37	1.0113E+37	1.13%
Evaporation of Black Holes	1.0000E+80	1.1385E+80	13.85%
Complete Black Hole Evaporation	1.0000E+80	1.1385E+80	13.85%
Heat Death Conditions Begin	1.0000E+100	1.3156E+100	31.56%
Dark Era Begins	1.0000E+100	1.3156E+100	31.56%
Big Freeze/Rip Speculations	1.0000E+110	1.4143E+110	41.43%
Final Energy Dispersal	1.0000E+110	1.4143E+110	41.43%
Goes Quiet	1.0000E+120	1.5203E+120	52.03%
Vacuum Energy Dominance	1.0000E+120	1.5203E+120	52.03%
Virtual Particle Fluctuations	1.0000E+120	1.5203E+120	52.03%

Correspondence and Divergence

The comparisons presented in Tables 7.1–6 reveal both regions of correspondence and systematic divergence between Fibonacci-derived temporal scaling and established cosmological

timelines. Interpretation therefore focuses on identifying domains in which recursive spacing appears consistent with observed transitions, as well as regimes where alignment is not expected based on underlying physical constraints.

To facilitate cross-era comparison, **Table 7.7** presents a consolidated summary of the cosmological events examined in Tables 7.1–6. Whereas the preceding tables preserve phase-specific physical context, the summary table aggregates representative epochs into a single chronological sequence, allowing overall patterns of correspondence and divergence to be viewed across the full temporal span of cosmic evolution. This consolidation serves as a comparative reference rather than an independent dataset.

Table 7.7: Consolidated Comparison of Cosmological Epochs

Event	Scientific Consensus (Years After Big Bang)	Fibonacci-Derived Time	Percent Deviation (%)
Dark Ages	240,000	280,368	+16.82%
First Starlight	150,000,000	146,072,031	−2.62%
Structure Formation Begins	150,000,000	146,072,031	−2.62%
Advanced Galaxy Formation	750,000,000	618,771,051	−17.50%
Reionization and Galaxy Formation	750,000,000	618,771,051	−17.50%
Population II Star Dominance	1,000,000,000	1,001,192,592	+0.12%
Formation of Galaxy Clusters	1,500,000,000	1,619,963,644	+8.00%
Rich Galaxy Cluster Era	2,000,000,000	1,619,963,644	−19.00%
Supercluster Formations	2,500,000,000	2,621,156,236	+4.85%
Intergalactic Stellar Populations	3,000,000,000	2,621,156,236	−12.63%
Dark Matter Structure Maturation	3,500,000,000	4,241,119,879	+21.17%
Peak of Star Formation	3,500,000,000	4,241,119,879	+21.17%
Decline in Star Formation	4,000,000,000	4,241,119,879	+6.03%
Advanced Stellar Evolution	4,500,000,000	4,241,119,879	−5.75%
Increased Neutron Stars	5,000,000,000	4,241,119,879	−15.18%
Formation of Solar System and Earth	9,000,000,000	11,103,395,994	+23.37%
Cooling of White Dwarfs	10,000,000,000	11,103,395,994	+11.03%
Evolution of Planetary Nebulae	10,000,000,000	11,103,395,994	+11.03%
Solar White Dwarf	10,000,000,000	11,103,395,994	+11.03%
Present Time*	13,800,000,000	11,103,395,994	−19.54%

Event	Scientific Consensus (Years After Big Bang)	Fibonacci-Derived Time	Percent Deviation (%)
Galaxy Merging	55,000,000,000	47,034,740,213	−14.48%
Deep Future Galaxy Isolation	1.0000E+13	9.3601E+12	−6.40%
Stelliferous Era	1.0000E+14	1.0381E+14	+3.81%
Last Generations of Stars	1.0000E+14	1.0381E+14	+3.81%
End of Main Sequence Star Formation	1.0000E+14	1.0381E+14	+3.81%
Black Hole Dominance	1.0000E+26	1.3725E+26	+37.25%
Degenerate Era	1.0000E+27	1.5221E+27	+52.21%
Proton Decay (Hypothetical)	1.0000E+37	1.0113E+37	+1.13%
Evaporation of Black Holes	1.0000E+80	1.1385E+80	+13.85%
Complete Black Hole Evaporation	1.0000E+80	1.1385E+80	+13.85%
Heat Death Conditions Begin	1.0000E+100	1.3156E+100	+31.56%
Dark Era Begins	1.0000E+100	1.3156E+100	+31.56%
Big Freeze/Rip Speculations	1.0000E+110	1.4143E+110	+41.43%
Final Energy Dispersal	1.0000E+110	1.4143E+110	+41.43%
Universe Goes Quiet	1.0000E+120	1.5203E+120	+52.03%
Vacuum Energy Dominance	1.0000E+120	1.5203E+120	+52.03%
Virtual Particle Fluctuations	1.0000E+120	1.5203E+120	+52.03%

Note: Percentage difference is calculated as *(Predicted − Scientific consensus) / Scientific consensus × 100*. Positive values indicate predicted epochs occurring later than consensus estimates, while negative values indicate earlier predicted timing. Scientific consensus cosmological age is taken as approximately 13.8 billion years based on ΛCDM measurements (Planck Collaboration). Some interpretations discussed in the text also consider alternative cosmological models proposing extended cosmic ages (e.g., Gupta, 2023; ~26.7 billion years). These alternatives are presented as comparative scaling frameworks rather than replacements for current consensus cosmology.

Preliminary comparisons indicate domain-specific correspondence between Fibonacci-scaled intervals and several broad cosmological transitions, particularly those associated with nonlinear structure formation. Notably, the onset of early galaxy formation and the peak epoch of star formation occur at temporal scales that approximate recursive growth spacing rather than uniform linear intervals (Madau & Dickinson, 2014).

Such correspondence may arise because cosmic evolution is governed by feedback-driven processes operating across multiple scales. Gravitational collapse accelerates structure formation,

stellar radiation regulates gas cooling, and supernova feedback redistributes matter and energy throughout galactic environments. These interacting mechanisms generate staged evolutionary transitions rather than continuous uniform change, making recursive temporal spacing a plausible emergent outcome rather than an imposed structure.

Figure 3.1 includes the uniform one-based row R = 64 (zero-based n = 63). Its H = 0 describes binary symbol frequencies. The proposed association with a cosmological origin in Gupta's (2023) alternative age framework is a separate interpretive mapping, not a derivation of the universe's age or gravitational entropy.

The discussion also associates preceding row labels with reionization, galaxy formation, and Cosmic Noon. Evaluating these assignments requires a consistent origin and direction of time. Moving backward through Pascal row labels is not forward recursion, and an increase in parity entropy is not a measured increase in cosmological thermodynamic entropy.

However, significant divergences are also evident. Early-universe particle epochs occur on extremely short timescales governed primarily by quantum field physics rather than large-scale gravitational dynamics. Because these phases operate under fundamentally different constraint regimes, correspondence with Fibonacci scaling is neither expected nor required.

Additional divergence appears in far-future projections, including proton decay and black-hole evaporation, whose estimated timescales remain highly uncertain theoretically (Adams & Laughlin, 1997). Apparent alignment at extreme temporal ranges must therefore be interpreted cautiously, as uncertainties spanning many orders of magnitude limit meaningful comparison.

Taken together, these results suggest an important boundary condition: if Fibonacci indexing provides useful descriptive insight, it is most likely to apply within domains dominated by recursive aggregation and entropy-driven energy redistribution, while remaining inapplicable in regimes governed primarily by quantum-scale or speculative long-term physics.

New Observations

A defining feature of a scientific framework is its ability to evolve in response to new evidence. Cosmology is currently undergoing rapid revision due to high-precision observations, particularly from the James Webb Space Telescope (JWST). Recent data indicate that massive galaxies formed earlier than predicted by standard hierarchical models, suggesting accelerated structure formation in the early universe (Donnan et al., 2023).

New observations provide independent tests only when earlier predictions and their tolerances remain recorded. Updating a fitted model and testing an unchanged prediction are different operations. Model revision may involve:

- recalibrating epoch scaling parameters,
- reassessing statistical significance of alignments,
- comparing Fibonacci indexing with alternative models (e.g., power-law or exponential scaling),
- testing predictive rather than retrospective accuracy.

A key strength of the attractor framework is falsifiability. If improved observational precision consistently shifts epoch timing away from Fibonacci-derived intervals beyond statistical tolerance, the hypothesis must be rejected or restricted in scope.

Conversely, if independent datasets repeatedly reveal clustering near recursive scaling ratios, Fibonacci indexing may function as an emergent descriptor of cosmological phase organization.

In this sense, cosmological timelines become an empirical testing ground for broader theories of emergence. The question is not whether the universe "follows Fibonacci numbers," but whether recursive constraint dynamics naturally generate temporal spacing approximating Fibonacci attractors.

Assessing Cosmological Correspondence

This section introduced Fibonacci attractors as a proposed scaffold for organizing cosmological epochs within an emergence-based framework. By interpreting Fibonacci indexing as a statistical consequence of recursive growth rather than a deterministic rule, the model reframes cosmic history as a sequence of constraint-driven phase transitions.

Methodological rigor—explicit comparison procedures, uncertainty analysis, and falsifiability criteria—is essential to distinguish scientific modeling from numerological interpretation. Current evidence suggests partial correspondence in domains governed by nonlinear structure formation, alongside clear limits in regimes dominated by different physical laws.

Future astronomical observations will ultimately determine whether Fibonacci indexing represents a meaningful descriptor of cosmological timing or merely an approximate heuristic. Regardless of outcome, the framework highlights a broader insight: large-scale cosmic evolution may reflect universal principles of emergence operating across scales, linking mathematical recursion, physical constraints, and the temporal unfolding of structure in the universe.

Part IV Life Development and Evolution

Chapter 8 Biological Rhythms and Organization

Biological organization combines rhythms, molecular constraints, tissue structure, and turnover across scales. The comparisons below distinguish observed organization from proposed Fibonacci interpretations and retain the evidence needed to assess each.

8.1 Biological Rhythms and Molecular Organization

Ultradian, Circadian, Circaseptan, and Infradian Rhythms

Biological oscillations coordinate metabolism, behavior, and development across several timescales. Their mechanisms include biochemical feedback and environmental synchronization (Goldbeter, 1996).

Ultradian rhythms are cycles shorter than twenty-four hours. Examples include heartbeat regulation, respiratory cycles, hormonal pulsatility, and stages of sleep such as rapid eye movement (REM) oscillations. These rhythms coordinate rapid physiological adjustments necessary for maintaining homeostasis. Their recurrence reflects internal feedback loops operating under energetic constraints, ensuring efficient allocation of metabolic resources.

Circadian rhythms, approximately twenty-four hours in duration, represent the most extensively studied biological oscillations. Governed by endogenous molecular clocks, circadian cycles regulate sleep–wake patterns, hormone secretion, body temperature, and gene expression. Although internally generated, these rhythms synchronize with environmental light–dark cycles through external cues known as zeitgebers (Dunlap et al., 2004). The circadian system therefore exemplifies how internal dynamics operate within external constraints.

Circaseptan rhythms, occurring on roughly seven-day cycles, have been observed in immune responses, cardiovascular regulation, and behavioral patterns (Halberg, 1983). While their origin remains debated, their persistence across cultures and species suggests intrinsic biological organization rather than purely social construction.

Infradian rhythms extend beyond twenty-four hours and include seasonal reproductive cycles, migration behaviors, and menstrual rhythms. These oscillations integrate environmental signals such as photoperiod and temperature, allowing organisms to align long-term biological processes with ecological conditions (Foster & Kreitzman, 2004).

Among ultradian rhythms, the vertebrate heart provides a particularly clear physical example of sustained biological oscillation. Cardiac activity arises from recurring electrical excitation waves that propagate through myocardial tissue, producing continuous cyclic blood flow rather than discrete mechanical pumping events. The pathways of inflow and outflow form coupled circulation loops linking pulmonary and systemic systems into a closed dynamical cycle. From a systems perspective, this organization resembles toroidal flow topology, in which motion is maintained through self-sustaining circulation rather than linear transfer. The heart therefore illustrates how biological structure and function co-evolve around stable oscillatory dynamics operating under energetic constraint.

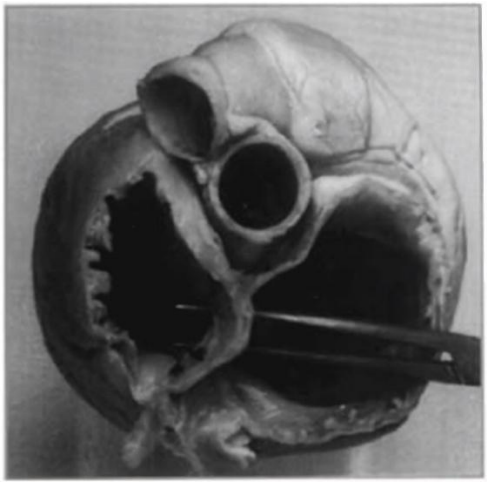

Figure 8.1 — Cardiac anatomy and flow context. The anatomical image supports discussion of recurring circulation. A toroidal analogy concerns flow topology; the photograph does not establish a toroidal dynamical attractor.

Environmental Entrainment as Constraint Coupling

Biological oscillators do not operate in isolation. Instead, they become synchronized with external cycles through a process known as **entrainment**, whereby environmental signals adjust internal timing mechanisms. Light exposure, temperature fluctuations, food availability, and social interaction function as regulatory inputs that stabilize biological rhythms (Pittendrigh, 1993).

Entrainment can be understood as **constraint coupling** between internal recursive dynamics and external periodic structures. Internal oscillators possess intrinsic frequencies determined by biochemical feedback loops, yet these frequencies remain plastic within limits. External constraints shift phase and amplitude without fundamentally altering the oscillator's generative rule.

The circadian clock provides a canonical example. Molecular feedback loops involving transcription and translation cycles generate near-24-hour oscillations even in isolation. However, exposure to light resets the clock daily, preventing drift from environmental time (Young & Kay, 2001). The organism thus maintains autonomy while remaining synchronized with planetary rotation.

Constraint coupling operates similarly across biological systems. Lunar cycles influence reproductive timing in marine organisms, while seasonal photoperiod changes regulate migration and breeding in terrestrial species (Naylor, 1999). These interactions illustrate how biological rhythms emerge from nested constraints rather than isolated mechanisms.

Testing Biological Timing

At the molecular level, biological clocks are constructed from feedback loops in which gene products inhibit or activate their own production. These loops generate repeating cycles analogous to iterative algorithms (Goldbeter, 1996). Each cycle depends on the previous one, preserving historical information while enabling adjustment through environmental signals.

This recursive character makes biological timing an effective testbed for theoretical models of constrained emergence. Unlike purely abstract mathematical systems, biological oscillators operate under measurable energetic and informational limits. They must maintain robustness against noise while remaining flexible enough to adapt to changing environments.

Because rhythmic phenomena are observable, quantifiable, and experimentally manipulable, they allow theoretical claims about recursion and constraint to be evaluated empirically. Predictions concerning phase stability, synchronization, and transition thresholds can be tested through physiological measurement and perturbation experiments.

The emergence of organized flow patterns in early cellular environments provides a direct physical illustration of this principle (Dutta et al., 2024; see also Figure 8.2).

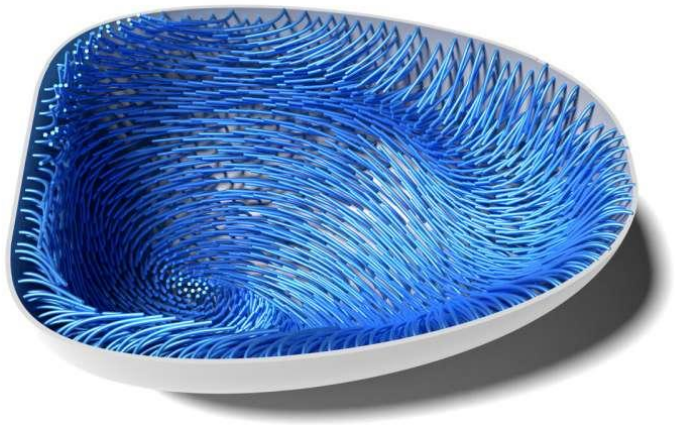

Figure 8.2 — Cytoplasmic flow in an egg cell. Organized motion illustrates the interaction of active flow with cellular boundaries. Source: Dutta et al. (2024).

Binary Regulatory Models

Gene regulatory networks (GRNs) provide a particularly clear illustration of biological recursion. Genes are activated or suppressed through regulatory interactions among DNA, RNA, proteins, and signaling molecules. At a simplified level, these interactions can be modeled as binary states—genes are either expressed ("on") or not expressed ("off") at a given moment (Kauffman, 1993).

Boolean network models represent GRNs as systems of interacting binary variables updated through logical rules. Despite their simplicity, such models generate complex temporal dynamics including oscillations, attractor states, and phase transitions. These behaviors arise from deterministic rule application rather than stochastic randomness.

Binary modeling connects biological regulation to combinatorial pattern spaces analogous to modular representations of Pascal's triangle. Each regulatory configuration corresponds to a position within a discrete state space, and successive updates trace trajectories through this space. Stable cellular identities can then be interpreted as attractors within regulatory dynamics (Huang, 2009).

Oscillatory gene expression—such as circadian clock genes—illustrates this principle directly. Feedback loops produce repeating on/off patterns that encode temporal information within

molecular systems (Young & Kay, 2001). The resulting dynamics resemble recursive binary sequences, where local update rules generate structured temporal patterns.

Importantly, binary abstraction does not deny biochemical complexity; rather, it captures essential informational structure underlying regulatory behavior. Biological timing thus becomes interpretable as movement through constrained pattern spaces governed by recursive update rules.

Molecular Fractals and Recursive Assembly

Recent experimental work provides evidence that recursive geometric organization may occur not only in biological timing and regulation but also at the molecular scale. Structural studies of the enzyme citrate synthase from the cyanobacterium *Synechococcus elongatus* have revealed protein assemblies forming Sierpiński-triangle–like architectures, representing one of the first documented examples of fractal organization in a functional biological enzyme (Sendker et al., 2024).

The citrate synthase assembly is a specific molecular example of recursively organized geometry. Its existence supports investigation of local assembly rules, while leaving the broader timing hypotheses to independent tests (Sendker et al., 2024).

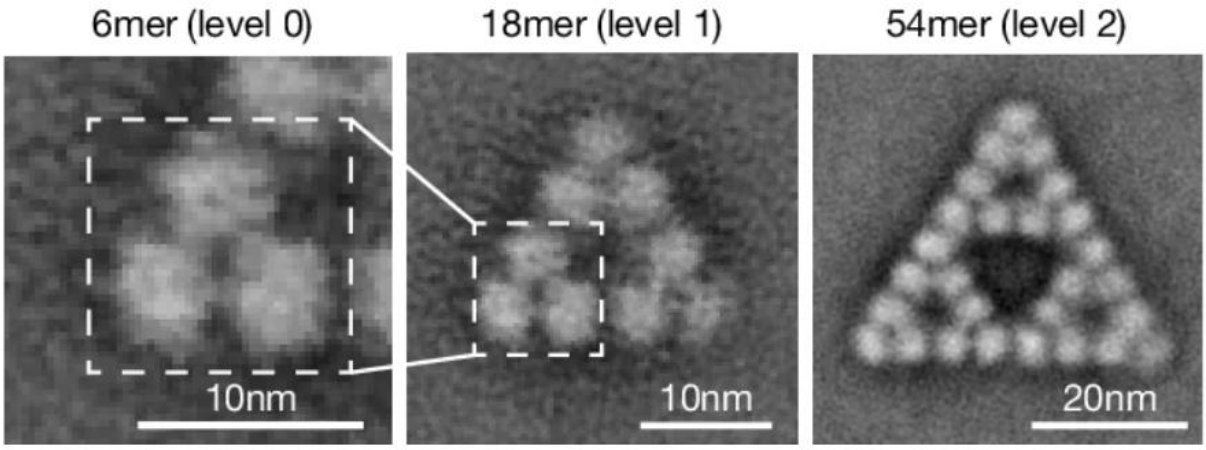

Figure 8.3 — Citrate synthase assembly. Molecular assemblies from Synechococcus elongatus display Sierpiński-like organization at successive scales. Source: Sendker et al. (2024).

Cellular Lattice Organization Under Mechanical Constraint

Recursive geometric organization is not limited to molecular assemblies but also appears at the cellular scale. The membrane of red blood cells contains a cytoskeletal network composed primarily of spectrin proteins arranged in a quasi-hexagonal lattice (Pan et al., 2018). This triangular meshwork distributes mechanical stress across the membrane, providing both elasticity and resilience as cells deform while passing through narrow capillaries.

The structure arises from local binding interactions among cytoskeletal proteins rather than from global geometric instruction. Mechanical constraints favor repeating triangular connections because triangular networks maximize stability while minimizing material use, a principle widely observed in engineering and physical lattice systems. The resulting geometry therefore reflects constraint optimization rather than symbolic mathematical design.

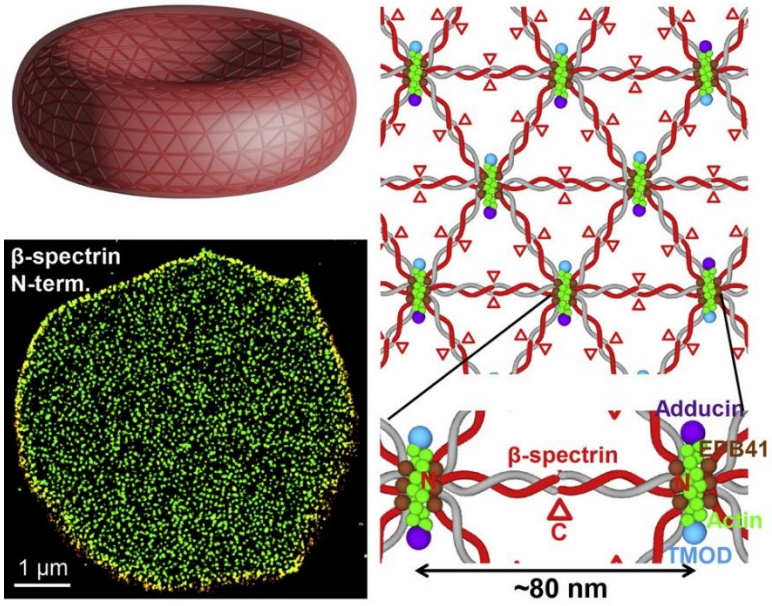

Figure 8.4 — Triangular cytoskeletal meshwork of the red blood cell membrane. Spectrin-based lattice organization providing mechanical resilience and flexibility during capillary transit (Pan et al., 2018).

8.2 Organism Structure Turnover and Lifespan Scaling

This section compares proposed Fibonacci-related patterns in morphology, cellular counts, lifespan, and developmental timing. The tables retain the source quantities and reference values. Their proximity is descriptive unless supported by a specified null model and independent prediction.

Spatial Fibonacci Organization in Living Systems

The Fibonacci sequence appears throughout biological morphology in ways that suggest underlying principles of efficiency rather than coincidence. Classic examples include phyllotaxis (leaf arrangement), spiral shells, branching architectures, and vascular networks. These structures frequently approximate Fibonacci ratios or the associated golden angle (~137.5°), which optimizes spatial distribution and resource access (Jean, 1994; Livio, 2002).

In plants, phyllotactic patterns minimize overlap between leaves, maximizing light exposure while reducing self-shading. Mathematical analyses demonstrate that angular arrangements approaching the golden angle produce near-optimal packing efficiency across successive growth stages (Vogel, 1979). Because growth occurs incrementally, each new element must occupy available space without disrupting prior structure. Fibonacci-like spacing therefore emerges naturally from iterative growth operating under geometric constraint.

Spiral shells provide a complementary example. Many approximate logarithmic spirals associated with Fibonacci scaling, maintaining proportional geometry as size increases and allowing continuous growth without functional redesign (Thompson, 1942). Such proportional expansion illustrates how constraint favors self-similar solutions.

Branching systems—including trees, lungs, and vascular networks—extend this principle into three dimensions. Fractal-like architectures distribute nutrients efficiently while minimizing energetic transport costs (West, Brown, & Enquist, 1997). These structures arise through repeated local growth decisions rather than centralized planning, closely paralleling recursive generative processes.

Some theoretical biologists have argued that evolutionary and developmental processes may reflect deeper physical principles associated with state transitions and informational constraints, drawing conceptual parallels between quantum mechanics and biological organization (Torday, 2018). From this perspective, biological form is not imposed by fixed blueprints but emerges through constrained transitions between dynamically stabilized states. Such views reinforce the interpretation advanced here: morphogenesis can be understood as a recursive process in which local interactions progressively stabilize higher-order organization under energetic and informational limits.

Morphogenesis as Recursive Organization

While Fibonacci organization is most visible in plant morphology, similar principles operate during animal development, where form emerges through coordinated tissue dynamics. Early embryogenesis begins with repeated cellular doubling, expanding combinatorially within confined space while maintaining mechanical stability. Development proceeds through folding, migration, and differential growth, transforming collective cellular motion into anatomical structure. Ordered biological form therefore arises from constrained dynamical interaction rather than geometric templates.

Branching morphogenesis—observed in neural development, vascular formation, and organogenesis—illustrates this recursive logic. As symmetry breaks, developmental pathways frequently organize into structured differentiation regimes, exemplified by germ-layer formation (Figure 8.5) and reflected more broadly in recurring anatomical triads across biological organization (see Appendix B: List of Threes in Anatomy). Hierarchical organization thus emerges through accumulated pathway constraints rather than centralized design.

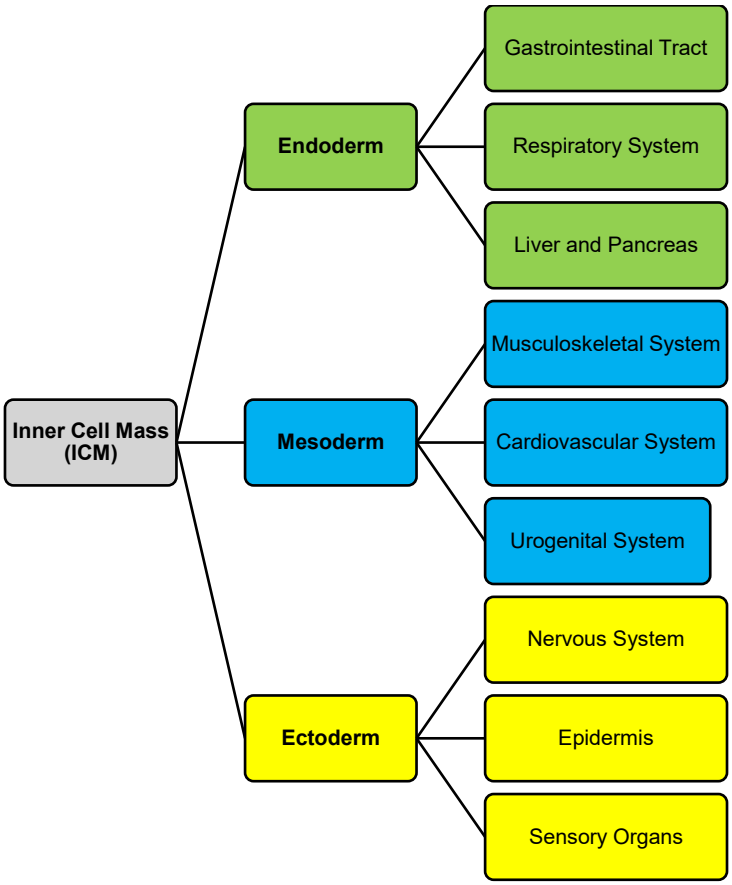

Figure 8.5 — Germ layers and selected cell types. A schematic organization of developmental outcomes, not a model of equal ternary divisions.

Recursive branching is a useful representation of developmental differentiation. Figure 8.5 groups cell types by germ layer; it should not be read as a literal genealogy of equal ternary divisions or a derivation of development from Sierpiński subdivision.

Anatomical Scaling Patterns in the Human Body

While Fibonacci organization is well documented in plant morphology and branching biological systems, comparable proportional tendencies have also been reported across multiple levels of human biological organization. These observations are not interpreted as evidence that living systems explicitly encode mathematical constants. Rather, structures shaped by growth dynamics, biomechanics, and energetic optimization may converge statistically toward proportional relationships predicted by constraint-based scaling models. Within this framework, the Golden Ratio ($\Phi \approx 1.618$) functions not as a design rule but as a statistical attractor emerging from recursive growth under spatial and functional constraint.

Empirical support varies across domains: some measurements approximate Φ closely, whereas others deviate substantially, indicating convergence toward efficient proportional regimes rather than strict geometric determinism. When considered collectively, however, these examples reveal a recurring pattern across biological scales.

At the molecular level, proportional relationships associated with Fibonacci numbers appear in the geometry of B-DNA. The canonical double helix exhibits dimensions near consecutive

Fibonacci values, measuring approximately 34 Å per helical turn and 21 Å in width (Larsen, 2021; Persaud-Sharma & O'Leary, 2015). The ratio between major and minor grooves similarly approaches Φ. These relationships are best understood as consequences of molecular packing constraints and electrostatic stability rather than numerical encoding. Molecular structure therefore provides an early example of how physical constraints can produce proportional regularities without predetermined mathematical intent.

At larger biological scales, proportional relationships emerge during developmental segmentation. Ratios between human finger phalanges have frequently been described as Fibonacci-like, with segment proportions approaching golden relationships (Persaud-Sharma & O'Leary, 2015). Such patterns likely reflect recursive growth processes operating during limb development, where successive tissue additions must maintain mechanical balance and functional continuity.

Proportional tendencies also appear within whole anatomical structures. Human facial proportions have historically been linked to the Golden Ratio, with classical analyses proposing approximate Φ relationships among facial height, width, and dental proportions (Persaud-Sharma & O'Leary, 2015). Contemporary morphometric studies, however, show no consistent association between facial attractiveness and strict golden-ratio adherence (Londono et al., 2022). Facial harmony instead appears to arise from interacting developmental and functional constraints—including respiration, mastication, and neural growth—suggesting convergence toward efficient proportional regimes rather than precise mathematical ratios.

Comparable geometric organization appears in spiral anatomical forms. The cochlea approximates logarithmic spiral scaling shaped primarily by spatial packing constraints (Pietsch et al., 2017), while scalp whorl patterns may emerge mechanically during rapid cranial expansion and tissue stretching (Paul, 2016). In both cases, spiral organization arises from growth dynamics rather than numerical prescription.

Branching biological networks extend these principles into functional transport systems. The bronchial tree balances airflow resistance with material efficiency, producing asymmetric bifurcation ratios approaching values near 1/Φ (West et al., 1986). Such architectures arise through repeated local growth decisions that collectively optimize distribution efficiency, illustrating how recursive processes generate large-scale organization without centralized planning.

Scaling tendencies are not limited to anatomical structure but also appear in physiological timing. Proposed golden-ratio relationships in cardiovascular dynamics suggest that the ratio between cardiac cycle duration and diastolic filling time averages approximately 1.63 in healthy adults (Bachani et al., 2025). This proportional balance may reflect optimization between energetic efficiency and circulatory stability rather than adherence to a fixed mathematical rule.

At the level of neural activity, ratios between dominant EEG frequency bands have been reported to approximate the golden proportion, potentially supporting flexible and desynchronized information processing in resting brain states (Pletzer et al., 2010). Here, proportional scaling emerges within dynamic regulation rather than static structure, extending the appearance of Fibonacci-like relationships into functional brain organization.

Organism-Scale Cellular Allocation

If proportional tendencies appear across molecular geometry, anatomy, physiology, and neural dynamics, a natural question is whether similar scaling persists when the organism is considered as an integrated whole. Rather than examining isolated structures, organism-wide cellular allocation reflects the cumulative outcome of developmental growth, energetic constraint, and functional specialization operating simultaneously across all tissues.

Quantitative organism-scale cellular censuses provide a means of evaluating this question independently of individual morphology. Estimates of human cellular composition derived from comprehensive reconstructions of the human body (Hatton et al., 2023) allow aggregation of cell populations by functional class, integrating contributions from multiple organs into a unified representation of biological allocation. When arranged by magnitude, these cellular populations span many orders of scale and cluster near successive exponential bands approximated by Fibonacci magnitudes (Table 8.1).

Table 8.1. Organism-Level Cellular Allocation and Fibonacci Scale Proximity

Cell Class	Male Cell Count (N)	Matched Fibonacci Number (F_n)	Fibonacci Scale (n)	Percent Deviation (%)
Myocytes	8.65×10^{10}	8.63×10^{10}	54	0.28
Neurons	8.87×10^{10}	8.63×10^{10}	54	2.87
Blood; Non-Nucleated	2.93×10^{13}	2.78×10^{13}	66	5.47
Blood; Nucleated	3.75×10^{12}	4.05×10^{12}	62	7.39
Osteoid Cells [Bone]	1.26×10^{11}	1.40×10^{11}	55	9.51
Epithelial Cells (EpC)	1.38×10^{12}	1.55×10^{12}	60	11.07
Germ Cells; Gametes	8.65×10^{9}	7.78×10^{9}	49	11.21
Fibroblasts	4.08×10^{11}	3.65×10^{11}	57	11.68
Perivascular / Pericytes	9.68×10^{10}	8.63×10^{10}	54	12.21
Blood; Nucleated; Glial	4.18×10^{9}	4.81×10^{9}	48	13.14
Epithelial (Non-Nucleated)	7.17×10^{10}	8.63×10^{10}	54	16.88
Neuroglia	7.04×10^{10}	8.63×10^{10}	54	18.42
Grand Total	3.65×10^{13}	4.49×10^{13}	67	18.82
Neuroglia Stem Cells	4.23×10^{6}	3.52×10^{6}	33	20.06
Stem Cells (SCs)	1.68×10^{11}	1.40×10^{11}	55	20.54
Adipocytes	1.68×10^{11}	1.40×10^{11}	55	20.71
Stem Cells; Epithelial	9.81×10^{9}	7.78×10^{9}	49	26.10
Endothelial Cells	7.55×10^{11}	5.91×10^{11}	58	27.63

Note. Cellular estimates adapted from Hatton et al. (2023). Fibonacci values serve as reference points within an exponential scaling lattice; proximity reflects statistical alignment rather than exact biological encoding.

Because total cellular estimates vary with body size, sex, and developmental stage, organism-scale magnitudes can also be compared across populations. Independent estimates for children, adult females, and adult males exhibit similar proximity to neighboring Fibonacci scale indices (Table 8.2).

Table 8.2. Cross-Population Human Cell Counts and Fibonacci Scale Proximity

Population	Total Cells	Closest Fibonacci	Fibonacci Index (Fn)	% Difference
Child	~17 T	$F_{63} \approx 17.17$ T	63	+0.99%
Adult Female	~28 T	$F_{64} \approx 27.78$ T	64	−0.79%
Adult Male	~36.5 T	$F_{65} \approx 44.95$ T	65	+18.8%

One interpretation is that energetic coordination and developmental history constrain organism-level allocation. Tables 8.1–8.2 test only proximity to selected Fibonacci magnitudes, however. Because any positive magnitude can be assigned a nearest point on a growing sequence, the strength of the match requires a baseline using alternative sequences and the uncertainty of the cellular estimates.

Biological Time Across Scales

Cellular Turnover as Micro-Temporal Structure

Biological time is heterogeneous at the cellular level. Different tissues regenerate at characteristic rates reflecting trade-offs between repair capacity and functional stability (Sender & Milo, 2021).

Table 8.3 — Representative Cellular Turnover Intervals Across Human Tissues

Cell Type	Approximate Turnover	Functional Role
Intestinal epithelium	3–5 days	environmental interface
Neutrophils	~7 days	immune response
Epidermal cells	~30 days	protective renewal
Red blood cells	~120 days	transport stability
T lymphocytes	~320 days	adaptive immunity
Endothelial cells	~6 years	vascular maintenance
Adipocytes	~11 years	metabolic storage
Myocytes	~49 years	structural persistence
Neurons	minimal turnover	information preservation

(Source: Sender & Milo, 2021)

The wide dispersion of cellular renewal intervals suggests that biological time is organized across multiple interacting scales rather than governed by a single internal clock. These heterogeneous rhythms raise a broader question: whether developmental and physiological timing might follow deeper organizational principles linking micro-temporal processes to organism-level life stages. The following chapters explore how such scaling relationships may emerge from constraint-driven growth dynamics.

Lifespan Scaling and Energetic Constraint

Across species, lifespan distributions exhibit systematic scaling relationships linked to metabolism, body size, and energetic efficiency. Allometric scaling laws demonstrate predictable relationships between energy consumption and lifespan duration, indicating that biological time is constrained by physical and metabolic principles rather than determined arbitrarily (West et al., 1997). Lifespan, therefore, may be understood as an emergent property of energy allocation, maintenance costs, and developmental timing operating across biological systems.

Within this framework, it becomes possible to examine whether characteristic lifespan averages align with mathematically structured temporal intervals. One candidate framework involves Fibonacci-derived age markers, which have been proposed as potential indicators of stable biological timing intervals. To explore this possibility, mean lifespans across representative vertebrate classes were compared with Fibonacci references ages, allowing evaluation of how closely empirical biological data approximate predicted temporal values (Torday & Sacco, 2024).

Table 8.4 — Lifespan Scaling Across Representative Species

Class	Mean Age	Fibonacci Age	% Difference	Sample Size
Reptilia	18.87	18.53	1.83%	240
Primates	30.83	29.99	2.80%	74
Teleostei	10.93	11.45	-4.54%	414
Mammalia	17.34	18.53	-6.42%	464
Amphibia	12.64	11.45	10.39%	75
Aves	15.68	18.53	-15.38%	646
All classes (overall)	15.57	18.53	-15.97%	1,808

Table 8.4 reports observed lifespan averages, reference ages, deviations, and sample sizes. Broad taxonomic averages should not be treated as individual predictions. Comparing this fit with other scaling families requires the same species selection, index-selection rule, and treatment of within-group variation.

Evidence supporting structured biological timing is also observable beyond vertebrates. Insects provide illustrative examples:

- **Queen ants** may live between **18–29 years** (Carey, 2001), approximating Fibonacci intervals near 18 and 30 years.
- **Periodical cicadas** exhibit life cycles lasting **12–18 years** (White & Lloyd, 1979), durations similarly close to Fibonacci-related age ranges.

Developmental Phase Transitions

Developmental milestones provide an illustrative example of structured biological timing across the human lifespan. Major transitions—including puberty, reproductive maturation, peak physiological performance, and aging-related changes—tend to occur within clustered intervals associated with large-scale physiological reorganization rather than appearing uniformly through time (Torday & Sacco, 2023). These observations suggest that biological development may proceed through staged transitions governed by underlying regulatory constraints.

Within this framework, two related temporal quantities can be distinguished:

- **Primary attractors**, representing stabilization points emerging from recursive developmental constraint.
- **Harmonic intervals**, describing transitional regimes generated through scaling relationships relative to these attractors, analogous to harmonics arising from a fundamental frequency in oscillatory systems.

Table 8.5 illustrates a *hypothesized* attractor structure beginning with the developmental transition near 11.5 years, corresponding to a pubertal priming boundary, followed by subsequent stabilization phases extending across the lifespan. The table represents a conceptual model intended to organize developmental phases rather than an empirical determination of fixed biological ages.

Table 8.5 — Developmental Attractors and Harmonic Intervals in Biological Timing

Temporal Role	Interval Window	Age (Years)	Classification	Developmental Interpretation
Phase I	0–11.5	11.5	Primary Attractor	Pubertal priming boundary
Phase II	11.5–23	18.5	Primary Attractor	Fertility establishment
Phase III	23–34.5	30	Primary Attractor	Reproductive stability
Phase IV	34.5–46	—	Harmonic transition	Transitional decline regime
Phase V	46–57.5	48.5	Primary Attractor	Menopausal transition
Phase VI	57.5+	—	Higher harmonic regime	Post-reproductive stabilization

The human reproductive lifespan provides a particularly clear biological context in which attractor-like developmental timing may be explored. Unlike many physiological processes that vary continuously, reproductive capacity is organized around discrete endocrine transitions governed by coordinated neuroendocrine regulation.

Independent demographic evidence offers a useful comparison point. The age at natural menopause varies globally between approximately 40 and 60 years, with a reported worldwide average of 48.8 years (Schoenaker et al., 2014). Within the present framework, this value lies close to the hypothesized developmental attractor near 48.5 years, suggesting that major endocrine transitions *may* preferentially occur near dynamically stabilized temporal regimes generated by constraint-mediated developmental processes.

These correspondences should be interpreted as statistical tendencies rather than biological laws. Individual variation remains substantial, and environmental, genetic, and sociocultural influences continue to shape developmental outcomes. The framework proposes only that developmental timing may exhibit clustering near dynamically favored regions generated by recursive constraint.

Disease Susceptibility as Harmonic Vulnerability Windows

Because neural development extends longer than most physiological systems and undergoes repeated large-scale reorganization, psychiatric disorders provide a particularly sensitive empirical domain for detecting temporal instability near developmental transitions.

If developmental timing reflects traversal through constraint-generated temporal attractors, an immediate empirical prediction follows: periods of physiological transition should correspond to increased systemic instability. In complex adaptive systems, transitions between stable regimes commonly produce heightened sensitivity to perturbation as regulatory networks reorganize before settling into new equilibria. Within biological organisms, such transitional intervals may therefore manifest as windows of increased vulnerability to disease onset.

The distinction parallels that between fundamental frequencies and harmonics in oscillatory systems: attractors define structural organization, whereas harmonics reflect resonance within that structure. Importantly, harmonics do not imply periodic biological clocks but describe uneven temporal spacing expected in history-dependent developmental systems.

Large-scale epidemiological evidence is consistent with this expectation. A global meta-analysis of 192 studies demonstrated that onset ages for many psychiatric disorders cluster within specific developmental intervals rather than distributing uniformly across the lifespan (Solmi et al., 2022). Peaks in neurodevelopmental, anxiety, obsessive–compulsive, and mood disorders occur primarily during late childhood, adolescence, and early adulthood—periods associated with major neurobiological reorganization.

The proposed onset-age comparison reports an average deviation below 5% (Table 8.6; Sacco, Beitman, & Marks-Tarlow, 2025). This is a descriptive error measure, not a significance test. Evaluation requires the underlying age distributions, uncertainty, selection rules, and comparison with other interval grids.

Table 8.6 — Alignment Between Mental Disorder Onset and Fibonacci Temporal Structure (≈7-Year Harmonic Scaling)

Disorder Category	Observed Peak Age (yrs)	Temporal Structure	Harmonic Order	Fibonacci Reference Age (yrs)	Percent Deviation
Neurodevelopmental disorders	12	**Primary attractor**	—	11.5	4.35%
Anxiety disorders	14.5	Harmonic resonance	2×	14.15	2.47%
General mental disorders (median)	18	**Primary attractor**	—	18.5	2.70%
Mood disorders	20.5	Harmonic resonance	3×	21.24	3.48%
Population second peak	30.5	**Primary attractor**	—	30	1.67%
Midlife vulnerability	44.5	Harmonic resonance	6×	42.48	4.76%
Late-life recurrence	49.5	Attractor–harmonic convergence	7×	48.5 / 49.56	0.12%

Table 8.6 does not establish individual risk windows. A developmental-vulnerability interpretation would require independent longitudinal evidence and prospective testing beyond agreement between selected summary ages.

Comparable clustering patterns appear across non-psychiatric disease categories. Data-driven analyses of electronic health records identify characteristic median onset ages for multiple age-related diseases—including metabolic disorders, cardiovascular disease, and neurodegeneration—that concentrate within specific lifespan intervals rather than appearing randomly (Kuan et al., 2021).

These onset distributions frequently align with later harmonic intervals associated with aging transitions, including midlife metabolic shifts (~35–56 years) and late-life systemic decline (~70–76 years). Such convergence suggests that disease emergence may reflect transitions between long-term physiological regimes shaped by energetic and regulatory constraints.

Table 8.7 — Disease Onset Ages and Harmonic Correspondence Across the Lifespan (≈7-Year Harmonic Scaling)

Disease Category	Typical Median Onset Age(s)	Temporal Structure	Harmonic Order	Fibonacci Reference	Interpretation
Psychiatric conditions	28 yrs	Harmonic resonance	4×	~28	Neural maturation window
Digestive diseases	35 yrs	Harmonic resonance	5×	~35	Early adult metabolic shift
Digestive diseases	42 yrs	Harmonic resonance	6×	~42	Metabolic recalibration phase
Digestive diseases	56 yrs	Harmonic resonance	8×	~56	Mid–late adulthood transition
Dementia spectrum	70 yrs	Higher harmonic regime	10x	~70	Neurodegenerative transition
Cardiovascular diseases	76 yrs	Higher harmonic regime	~11×	~77	Aging-system convergence
Certain cancers	76 yrs	Higher harmonic regime	~11×	~77	Shared aging susceptibility

The harmonic interpretation of Tables 8.6–8.7 is a hypothesis about uneven developmental timing. It does not show that Fibonacci scaling causes disease, and the comparisons are not clinical schedules. Different definitions of onset, diagnosis, cohort, and age summary must be accounted for before pooling their deviations.

Evaluating Alignment

Distinguishing meaningful structure from pattern-seeking bias requires rigorous evaluation.

Key approaches include:

- **Null models**, generating randomized datasets preserving biological constraints (Gotelli & Graves, 1996).
- **Effect-size analysis**, quantifying deviation from expected distributions.
- **Cross-domain replication**, identifying independent recurrence across systems.
- **Predictive testing**, generating forward hypotheses.
- **Robustness analysis**, testing sensitivity to measurement variation.

Chapter 9 Development Aging and Lifespan

Aging and development involve maintenance, changing function, and substantial variation among individuals. This chapter joins the biological mechanisms to the clinical example and milestone tables, including the time-origin limitations that affect their interpretation.

9.1 Aging Energy and Maintenance

Homeostasis as Biological Recursion

Homeostasis maintains function through ongoing regulation, repair, and replacement. Its recursive character lies in feedback: current conditions influence actions that alter subsequent conditions.

Classical physiology described homeostasis as the maintenance of stable internal variables such as temperature, pH, and glucose concentration (Cannon, 1932). Modern systems biology refines this view by emphasizing that organisms exist far from thermodynamic equilibrium and must constantly exchange matter and energy with their environment to sustain order (Prigogine & Stengers, 1984). Physiological variables fluctuate within constrained ranges; deviation is not failure but part of regulation. What defines life is the capacity to repeatedly restore coherence when perturbation occurs.

A central mechanism of this recursive stabilization is gradient maintenance across boundaries. Cellular membranes generate and preserve differences in concentration and electrical charge that store usable energy. Chemiosmotic proton gradients in mitochondria, for example, must be continually rebuilt to sustain ATP production. If reconstruction ceases, energetic collapse follows. Life depends not on equilibrium but on the repeated renewal of disequilibrium. This relationship is illustrated schematically in **Figure 9.1**, which depicts homeostasis as gradient preservation through boundary-driven feedback loops.

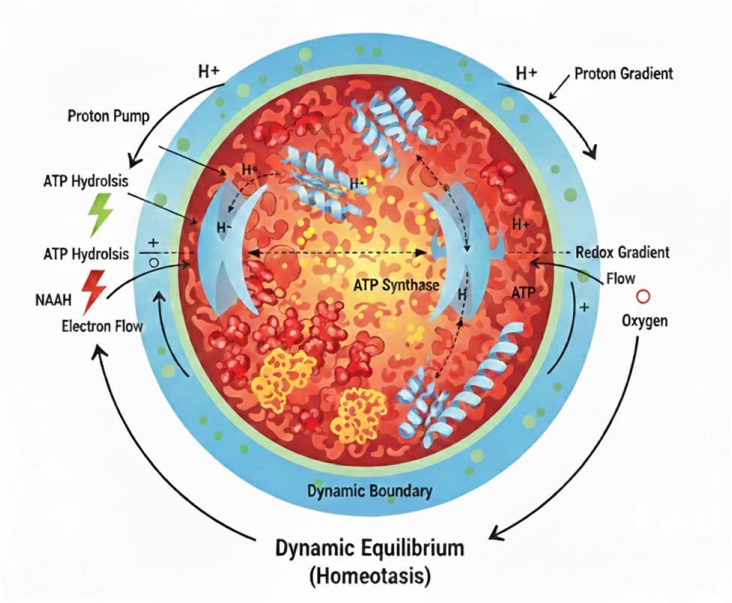

Figure 9.1. Homeostasis as Gradient Maintenance Across Boundaries. Schematic of a cell illustrating chemiosmotic gradients, redox flows, and membrane potentials as boundary-driven constraint systems maintaining dynamic equilibrium.

Because each regulatory cycle requires energy, homeostasis carries thermodynamic cost. Every act of repair dissipates energy and produces entropy (Schrödinger, 1944). Over time, the cumulative burden of maintaining recursive stability increases. Aging can thus be understood as the long-term energetic consequence of sustaining homeostatic recursion under irreversible constraint.

Homeostatic regulation does not operate only within narrow compensatory ranges. Biological systems also possess mechanisms for responding to disturbances that exceed ordinary regulatory capacity. When stress surpasses critical thresholds, systems may undergo qualitative reorganizations that alter their operating regime. Such shifts resemble phase transitions observed in complex physical systems, where gradual change culminates in structural reconfiguration (Scheffer et al., 2009).

At the cellular level, moderate stress activates repair pathways including protein refolding, antioxidant defenses, and metabolic adjustment (Kültz, 2005). If perturbation intensifies, inflammatory signaling coordinates tissue-level responses to restore integrity (Medzhitov, 2008). When damage becomes irreparable, programmed cell death (apoptosis) removes compromised cells to preserve organismal stability (Elmore, 2007). These processes function not as failures but as regulatory reset mechanisms that prevent runaway instability.

Aging as Energy Utilization and Entropy Accumulation

Aging can be understood as a thermodynamic process emerging from the continuous transformation of energy within living systems. Organisms maintain highly ordered internal states by exporting entropy to their environment through metabolism, growth, and repair processes. However, this maintenance is never perfectly efficient. Over time, molecular damage accumulates, regulatory systems degrade, and adaptive capacity declines, producing the observable phenomena associated with aging (Kirkwood, 2005; López-Otín et al., 2013).

Entropy accumulation manifests biologically through oxidative damage, protein misfolding, genomic instability, and declining cellular repair mechanisms. While organisms possess sophisticated maintenance pathways—such as DNA repair and autophagy—these systems themselves require energy and are subject to degradation over time (López-Otín et al., 2013). Aging emerges when maintenance capacity can no longer fully offset entropy production.

This perspective reframes aging as a dynamic balance between energy utilization and disorder accumulation. Longevity becomes a function of how effectively organisms allocate energy toward repair, reproduction, and survival within constrained energetic budgets. At the organismal level, this energetic balance is expressed through the preservation of coordinated activity across multiple biological scales—from molecular repair processes to systemic physiological regulation—forming what can be described as multi-scale coherence.

Replicative Limits and the Hayflick Boundary

Biological growth proceeds through recursive cellular division: existing structure generates future structure through repeated cycles of replication and differentiation. Unlike ideal mathematical recursion, however, biological replication is finite. Normal somatic cells can divide only a limited number of times before entering permanent growth arrest, a phenomenon known as the **Hayflick limit**.

First demonstrated by Hayflick and Moorhead (1961), cultured human fibroblasts undergo approximately **40–60 population doublings** before replication ceases. This discovery established that cellular aging is intrinsic rather than environmentally imposed. Cells stop dividing even under favorable laboratory conditions, indicating that limits arise from internal constraint accumulation rather than resource depletion alone.

The primary mechanism underlying this boundary is **telomere shortening**. Telomeres—protective DNA sequences at chromosome ends—shorten slightly during each replication cycle because DNA polymerase cannot fully copy terminal regions (Blackburn, 2000). When telomeres reach a critical length, DNA damage signaling triggers **cellular senescence**, preventing further division. Additional factors reinforce this transition, including accumulated DNA damage, oxidative stress, epigenetic drift, and metabolic burden (Campisi, 2013).

Replicative limits illustrate finite expansion under biological constraints. Their relation to the proposed recursive framework is conceptual: a cellular division limit does not by itself identify Fibonacci scaling or determine organismal lifespan.

Importantly, the limit constrains replication depth, not chronological time. Division rates vary widely among tissues—hours during embryogenesis, days or weeks in epithelial tissues, and rarely or never in neurons. Consequently, replicative exhaustion emerges at different temporal scales across the organism. Aging therefore reflects heterogeneous constraint accumulation rather than a universal biological clock.

From a systems perspective, cellular senescence marks a transition between dynamical regimes. Early life emphasizes expansion and differentiation, whereas later stages increasingly prioritize

maintenance and regulation. Replicative limits help stabilize multicellular organization by preventing uncontrolled proliferation and genomic instability, demonstrating that biological constraints can enhance long-term system coherence.

The "Energy Paradigm" Framing: Dissipation and Maintenance Costs

The energy paradigm of aging proposes that lifespan reflects trade-offs between metabolic expenditure and maintenance investment. Organisms must allocate limited energetic resources among competing demands, including growth, reproduction, immune function, and cellular repair (Kirkwood & Austad, 2000).

The **disposable soma theory** formalizes this idea by suggesting that evolution optimizes energy allocation for reproductive success rather than indefinite maintenance. Because perfect repair would require excessive energy investment, biological systems evolve maintenance strategies that are sufficient—but not optimal—for long-term preservation (Kirkwood, 2005).

Metabolic processes inherently produce entropy through heat dissipation and molecular turnover. Higher metabolic throughput can accelerate damage accumulation unless balanced by enhanced repair capacity. Comparative biology demonstrates correlations between metabolic scaling and lifespan, suggesting energetic constraints govern aging trajectories across species (West, Brown, & Enquist, 1997).

Proposed Life Stage Windows

If biological development unfolds through recursive growth under energetic constraints, life history transitions may occur in structured temporal phases rather than uniformly across time. The Fibonacci Life Chart hypothesis proposes that major developmental and aging transitions cluster near recursively scaled intervals reflecting nonlinear accumulation of biological complexity.

Within this framework, life stages correspond to **phase transitions** in energetic organization. Periods of stability alternate with vulnerability windows during which regulatory systems reorganize. Examples include adolescence, midlife physiological shifts, and late-life decline, each associated with hormonal, metabolic, and neurological restructuring (López-Otín et al., 2013).

The Fibonacci Life Chart proposes clustering of transitions near specified reference ages. The physiological explanation would need to connect measurable regulatory changes to those ages; an entropy threshold has not been established merely by placing milestones on the chart.

Fractal Networks

Biological organisms rely on fractal network architectures to distribute energy and information efficiently across scales. Vascular systems, respiratory structures, and neural networks exhibit branching geometries that maximize transport efficiency while minimizing energetic cost (West et al., 1997).

Fractal organization enables scalability. Such architectures maintain coherence across scales, allowing local processes and global regulation to remain dynamically coordinated despite increasing organismal size and complexity. As organisms grow, transport distances increase, yet

fractal branching preserves efficient resource delivery by maintaining proportional relationships between network levels. This architecture supports metabolic stability and resilience against localized damage.

However, aging introduces gradual degradation within these networks. Vascular stiffening, reduced neural connectivity, and impaired signaling efficiency reflect entropy accumulation within hierarchical structures. Because fractal systems depend on coordination across scales, small inefficiencies can propagate globally, contributing to systemic aging effects.

Despite vulnerability, fractal organization also enhances robustness. Redundant pathways allow partial compensation when local failures occur, delaying catastrophic collapse. Aging therefore reflects a tension between resilience provided by network architecture and entropy-driven degradation of connectivity.

Cross Species Tests

A viable theoretical framework must extend beyond human aging to generate cross-species predictions. The energy–entropy model proposes several generalizable expectations grounded in metabolic and structural constraints.

First, species with lower mass-specific metabolic rates should exhibit longer lifespans, consistent with allometric scaling laws (West et al., 1997). Reduced energy throughput slows entropy accumulation relative to repair capacity.

Second, organisms possessing more efficient transport networks or enhanced repair mechanisms should demonstrate delayed aging trajectories. Comparative studies of long-lived species—such as certain mammals and reptiles—support this prediction through improved cellular maintenance systems (Austad, 2010).

Third, life-history transitions should scale proportionally with lifespan. Developmental stages, reproductive timing, and aging phases should expand predictably across species rather than occurring at fixed chronological intervals.

Fourth, environmental energy availability should influence aging dynamics. Caloric restriction studies show lifespan extension across multiple species, suggesting that reduced metabolic load can slow entropy accumulation and enhance maintenance efficiency (Fontana & Partridge, 2015).

Finally, vulnerability windows associated with physiological transitions should appear across taxa, though shifted in scale according to lifespan and metabolic rate. Such predictions allow empirical testing of recursive aging models through comparative biology.

Many physiological signals and networks exhibit multi-scale structure, in which variability is distributed across multiple temporal and spatial scales rather than collapsing into a single dominant rhythm. Healthy systems tend to preserve this layered organization, supporting adaptability and efficient regulation. With aging, this structure often simplifies: scaling relationships flatten, long-range coordination weakens, and variability becomes either overly regular or excessively noisy. From an empirical standpoint, the relevance of Fibonacci or Φ-like scaling is therefore not that it dictates a universal developmental schedule, but that departures

from stable proportional scaling may serve as measurable indicators of declining multi-scale integration within aging systems.

9.2 Cockayne Syndrome as a Proposed Comparison

Cockayne syndrome is considered here as a possible example of disrupted developmental integration. The proposed interpretation concerns failure to sustain organization across scales; the established disease mechanisms and the hypothesized recursive description must remain distinct.

Cockayne syndrome (CS) is a rare autosomal recessive disorder primarily caused by mutations in the *ERCC6* (CSB) or *ERCC8* (CSA) genes, which encode proteins essential for transcription-coupled nucleotide excision repair (Karikkineth et al., 2017). These repair pathways maintain genomic integrity during active transcription, linking DNA maintenance directly to cellular metabolism and energy regulation. Defects in these systems lead to widespread mitochondrial dysfunction, impaired oxidative phosphorylation, chronic oxidative stress, and reduced ATP availability (Scheibye-Knudsen et al., 2014). Because mitochondria function as central regulators of cellular energy feedback, their disruption compromises the recursive bioenergetic loops that coordinate growth, repair, and developmental progression.

The clinical features discussed in the cited literature include growth retardation, neurodegeneration, sensory impairment, and features of accelerated aging (Wilson et al., 2016). These are compatible with impaired maintenance and development, but do not by themselves measure recursive depth or identify an entropy threshold.

The manuscript's proposed comparison relates reported clinical age groupings near 7, 12, and 30 years to Fibonacci-derived ages near 7, 11.5, and 30 years (Karikkineth et al., 2017; Wilson et al., 2016). Such a correspondence requires verification against the underlying cohorts, subtype definitions, survival distributions, and uncertainty. It is an exploratory hypothesis, not independent evidence that the disease follows a Fibonacci timetable.

9.3 Developmental Milestones and Their Evaluation

Developmental Comparisons

This section compares developmental milestones with Fibonacci-derived reference ages. The descriptive tables and the consolidated comparison are retained separately because they serve different purposes: one records stage content, the other juxtaposes benchmark and model ages.

Methods and Time Conventions

To examine developmental timing systematically, lifespan milestones were organized using a standardized comparison framework analogous to those used for cosmological timelines in Chapter 7 and evolutionary timelines in Chapter 10.

Normalization of Developmental Time

A valid developmental comparison requires a common time origin. Postnatal ages are conventionally measured from birth, while prenatal stages require their own stated origin. The source stage headings in Tables 9.1–9.16 retain model-derived values, including fertilization at 0.00 and birth at 0.24 years; these cannot simultaneously be interpreted as observed ages measured from birth. They are retained as model labels, not as a reconciled clinical chronology.

The time origin and conversion of the prenatal labels must be reconciled before those entries are included in a quantitative fit. Developmental processes also overlap, so even consistent empirical ages describe ranges rather than instantaneous events.

Fibonacci Temporal Conversion

Recursive temporal intervals were generated using Fibonacci sequence indexing converted into years through a fixed scaling transformation (Appendix A). The conversion procedure involved:

1. generation of Fibonacci numbers,
2. conversion into temporal intervals,
3. mapping intervals onto lifespan duration.

These values serve only as comparative reference points. They do not imply predictive biological scheduling.

Developmental Benchmarks

Consensus milestone ages were derived from established findings in developmental biology, neuroscience, endocrinology, and clinical medicine, including:

- prenatal embryology,
- cognitive development research,
- reproductive endocrinology,
- aging physiology (Casey et al., 2008; Kirkwood, 2005).

These benchmarks represent broadly observed developmental averages rather than individual trajectories.

Treatment of Uncertainty

Human development exhibits substantial variability influenced by genetics, environment, nutrition, and sociocultural context. Accordingly, comparisons emphasize approximate temporal correspondence rather than precise alignment.

Descriptive Rather Than Deterministic Interpretation

Recursive intervals are treated as descriptive temporal patterns that may reflect emergent structure in developmental timing. The analysis examines whether developmental transitions occur near temporal regions associated with constraint-driven growth dynamics. Development itself is governed by biological processes—including energy metabolism, cellular signaling, and

growth constraints—while the recursive framework serves as a lens for detecting statistically patterned temporal clustering.

Empirical Developmental Milestones

Developmental milestones are grouped into sequential life phases spanning prenatal development, infancy, childhood, adolescence, adulthood, and aging. Tables 9.1–9.16 summarize representative physiological and cognitive transitions across the lifespan.

The milestone descriptions and their model-derived stage labels should be distinguished. The labels are not individual developmental predictions.

Note. Tables 9.1–9.16 retain the proposed stage labels and accompanying descriptions. They combine approximate developmental content with a selected temporal grid; the headings should not be read as measured transition ages. Table 9.17 separately presents benchmark and Fibonacci-scaled values.

Table 9.1: Fertilization (0.00 years)

Milestone	Description
Fertilization	Fusion of sperm and egg resulting in the formation of a zygote
Cleavage	Rapid mitotic cell divisions of the zygote forming early embryonic cells

Table 9.2: Implantation (0.01 years)

Milestone	Description
Blastocyst formation	The blastocyst develops with an inner cell mass (future embryo) and an outer trophoblast layer
Implantation	The blastocyst attaches to and embeds within the uterine wall, initiating pregnancy

Table 9.3: Embryonic Period (0.06 years)

Milestone	Description
Neural tube formation	The neural tube forms, which will develop into the brain and spinal cord
Heartbeat initiation	The primitive heart begins beating and circulating blood
Organ rudiments	Early structures of major organs, including the digestive system, begin to form
Limb bud formation	Limb buds appear that will later develop into arms and legs
Sensitivity to teratogens	The embryo is highly vulnerable to substances that can cause congenital abnormalities

Table 9.4: Second Trimester (0.09 years)

Milestone	Description
Rapid growth	The fetus undergoes substantial increases in size and weight
Organ development	Continued maturation of organ systems, with increasing nervous system activity
Quickening	First noticeable fetal movements perceived by the mother
Increased fetal activity	Movements become stronger and more frequent as neuromuscular control improves
Fingerprint formation	Development of unique fingerprints on the fingers and toes

Table 9.5: Birth (0.24 years)

Milestone	Description
Labor and delivery	Transition from the prenatal environment to extrauterine life through childbirth
First breath	Expansion of the lungs and initiation of independent respiration
Physiological independence	Establishment of independent circulation and respiration, though the infant remains dependent on caregivers

Table 9.6: Infancy (1.03 years)

Milestone	Description
Rapid visual development	Improvements in depth perception and color vision
First steps	Ability to walk independently
First words	Emergence of early verbal communication
Fontanelle closure	Gradual closure of the soft spots in the skull
Increased oxygenation	Enhanced oxygen delivery to tissues supporting growth
Increased red blood cell count	Greater oxygen transport capacity
Maternal antibody transition	Gradual decline of maternal antibodies as the infant immune system develops

Table 9.7: Infancy (1.67 years)

Milestone	Description
Vestibular development	Improved balance and spatial orientation as the vestibular system matures
Rapid auditory development	Continued refinement of auditory processing and sound discrimination
Language development	Rapid vocabulary expansion and early word combinations
Self-recognition	Ability to recognize oneself in a mirror or photograph

Milestone	Description
Hand dominance	Emerging preference for using one hand over the other
Rapid digestive development	Enhanced digestive capacity with the introduction of solid foods
Immune system maturation	Increased antibody production and improved immune defense
Enhanced thermoregulation	Improved ability to regulate body temperature

Table 9.8: Toddlerhood (2.70 years)

Milestone	Description
Brain growth	Significant increases in synaptic connections and neural plasticity
Long-term memory formation	Increasing ability to form and retain lasting memories
Gender recognition	Identification of oneself and others as male or female
Neuromuscular coordination	Improved coordination between the nervous system and muscles
Increased muscle tone	Enhanced muscle strength and motor control
Kidney function development	Approaching near-adult function for waste excretion and fluid balance
Teething completed	Eruption of primary teeth completed

Table 9.9: Early Childhood (4.37 years)

Milestone	Description
Enhanced neural connectivity	Development of neural networks supporting increasingly complex cognitive functions
Critical cognitive development	Rapid expansion of reasoning, attention, and learning capacity
Autobiographical memory	Emergence of coherent narrative memories and personal experiences
Language complexity	Use of more complex sentences and expanding vocabulary
Emotional regulation	Increasing ability to regulate emotions and navigate social interactions
Enhanced enzyme production	Improved digestion and metabolism of a wider range of foods
Increased bone mineralization	Strengthening bones through increased mineral deposition

Table 9.10: Middle Childhood (7.08 years)

Milestone	Description
Improved glucose metabolism	More stable blood sugar regulation supporting sustained activity
Hemoglobin concentration increase	Higher hemoglobin levels supporting increased physical activity
Early androgen secretion	Initial stages of androgen hormone production
Balance control	Improved coordination and motor control
Visual perception	Enhanced visual processing and spatial interpretation
Auditory skills	Continued refinement of auditory processing abilities
First molar eruption	First permanent molars typically erupt

Table 9.11: Adolescence (11.45 years)

Milestone	Description
Puberty	Onset of major hormonal changes initiating sexual maturation
Increased androgen production	Supports muscle development and secondary sexual characteristics
Synaptogenesis	Continued growth of neural connections during early adolescence
Peak synaptic pruning	Refinement and strengthening of neural pathways
Executive function development	Growth in planning, decision-making, and impulse control
Abstract thinking	Increased ability for complex reasoning and hypothetical thought
Facial emotion recognition	Improved interpretation of facial expressions and social cues
Increased risk-taking behavior	Changes in reward-processing systems increase novelty seeking
Cardiovascular endurance	Improvements in heart and lung capacity with growth
Critical digestive development	Increased metabolic demand and digestive efficiency
Disrupted sleep patterns	Circadian rhythm shifts; adolescents require 8–10 hours of sleep
Second molar eruption	Emergence of permanent second molars during early adolescence

Table 9.12: Early Adulthood (18.53 years)

Milestone	Description
Completion of brain development	Full maturation of neural structures
Prefrontal cortex maturity	Executive function and decision-making reach full development
Peak cognitive performance	Memory, attention, and learning efficiency at their highest levels
Peak memory	Maximum capacity for memory formation and recall
Peak physical performance	Optimal strength, endurance, and coordination
Peak testosterone	Highest circulating levels in males
Start of optimal fertility	Peak reproductive potential begins
Strongest immune response	Maximum immune system activity and resilience
Peak visual acuity	Optimal clarity of vision
Peak sensitivity in hearing	Highest ability to detect a wide frequency range
Optimal sleep	Typical sleep duration stabilizes around 7–9 hours
Highest metabolic and energy expenditure	Maximum metabolic rate supporting physical performance
Peak entropy production	Highest biological energy throughput within the organism
Peak hematopoiesis	Optimal production of blood cells in bone marrow
Maximal renal function	Peak kidney filtration and regulatory efficiency
Optimal liver function	Maximum metabolic and detoxification capacity
Third molar eruption	Wisdom teeth typically emerge during late adolescence

Table 9.13: Middle Adulthood (29.99 years)

Milestone	Description
Peak bone mass	Maximum bone density reached in early adulthood
Peak muscle strength	Highest muscle mass and strength
Peak cardiovascular efficiency	Robust heart and circulatory system performance
Peak lung capacity	Optimal respiratory efficiency

Milestone	Description
Peak cognitive function	Highest levels of problem-solving and critical thinking
Peak facial recognition	Maximum efficiency in recognizing and remembering faces
Peak mental health	Psychological stability often strongest in late 20s to early 30s
Personality stability	Increased self-awareness and emotional maturity
End of optimal fertility	Fertility begins to gradually decline
Metabolic changes	Gradual decrease in basal metabolic rate
Onset of presbyopia	Early decline in the ability to focus on nearby objects

Table 9.14: Older Adulthood (48.52 years)

Milestone	Description
Metabolic reduction	Gradual slowing of metabolism contributing to increased weight gain
Hormonal changes (men)	Gradual reduction in testosterone levels
Menopause (women)	Significant hormonal transition marking the end of reproductive capacity
Cardiovascular health decline	Increasing risk of heart disease beginning in midlife
Kidney function decline	Gradual reduction in renal filtration beginning around age 50
Reduced renal function	Continued decline in kidney efficiency with age
Onset of chronic health conditions	Increased likelihood of hypertension, diabetes, and arthritis
Reduced muscle mass	Early stages of sarcopenia affecting strength and mobility
Decreased proprioception	Reduced ability to sense body position and balance
Presbyopia	Decline in near vision commonly beginning in the mid-40s
Changes in sleep patterns	Shift toward lighter and more fragmented sleep
Decreased thermoregulation	Reduced ability to regulate body temperature
Skin thinning	Gradual loss of skin thickness and elasticity
Facial wrinkles	Increased prominence due to declining collagen production
Hair graying	Progressive loss of pigment in hair follicles
Hair loss	Hair thinning associated with hormonal and genetic factors
Peak depression	Increased vulnerability to mood disorders during midlife transitions

Table 9.15: Old Age (78.51 years)

Milestone	Description
Average life expectancy	Approximate lifespan threshold used as a reference point for late-life biological decline within an entropy-based framework
Reduced cardiac output	Decreased heart efficiency and reduced circulatory performance
Reduced pulmonary function	Decreased lung capacity and respiratory efficiency
Reduced renal function	Declining kidney filtration and regulatory function
Reduced digestive efficiency	Slower digestion and reduced nutrient absorption
Decreased bone density	Increased risk of osteoporosis and fractures
Sarcopenia progression	Continued loss of muscle mass and strength
Significant physical decline	Increased frailty and susceptibility to injury
Decreased taste and smell	Reduced sensory sensitivity affecting appetite and perception
Cognitive decline	Increased risk of neurodegenerative disease
Dementia onset	Severe cognitive impairment affecting memory and daily functioning

Table 9.16: Theoretical Maximum Lifespan (127.0 years)

Milestone	Description
Average life expectancy reference	Late-life threshold from which extreme longevity scenarios are evaluated within an entropy-based biological framework
Reduced cardiac output	Progressive decline in cardiac pumping capacity and circulatory efficiency
Reduced pulmonary function	Reduced lung elasticity and gas-exchange efficiency
Reduced renal function	Impaired kidney filtration and homeostatic regulation

Correspondence and Divergence

Comparison of developmental milestones reveals several regions in which transitions appear temporally clustered rather than evenly distributed across lifespan duration.

Clustering Around Developmental Transitions

Early development displays dense clustering of milestones, including embryogenesis, neural formation, and rapid cognitive acquisition. This concentration reflects high metabolic throughput and rapid structural differentiation characteristic of growth-dominated phases.

A second region of clustering appears during adolescence, where endocrine activation, neural restructuring, and behavioral transformation occur concurrently. Puberty represents one of the

most pronounced systemic reorganizations in human biology, involving coordinated hormonal, cognitive, and social transitions (Blakemore & Mills, 2014).

Entropy Production and Peak Function

Early adulthood corresponds to peak physiological integration, including maximal physical performance, reproductive capacity, and cognitive efficiency. From a thermodynamic perspective, this stage may represent a balance between energy production and maintenance demands before entropy accumulation begins to dominate system dynamics.

Aging Acceleration

Later-life milestones increasingly reflect decline-related transitions—reduced metabolic efficiency, endocrine shifts, and increased susceptibility to chronic disease. These changes occur over expanding temporal intervals, consistent with reduced regenerative capacity and increased energetic cost of maintenance (Kirkwood, 2005).

Divergence and Individual Variability

Despite observable clustering, substantial divergence exists across individuals. Developmental timing depends on environmental, cultural, and genetic factors, limiting the applicability of any single temporal model. Particularly in late adulthood, variability increases significantly, reflecting stochastic influences and accumulated life-history effects.

Consolidated Comparison

To facilitate cross-stage comparison, Table 9.17 presents a consolidated summary of representative developmental milestones across the lifespan. Whereas earlier tables preserve physiological context, this summary aggregates milestones into a single chronological sequence, enabling visualization of overall temporal spacing.

Table 9.17 — Consolidated Lifespan Developmental Milestones

Developmental Stage	Consensus Age (Years)	Fibonacci-Scaled Age (Years)	Developmental Interpretation
Fertilization	0.00	0.00	Biological origin
Birth	0.24	0.24	Transition to independent metabolism
Early Infancy	~1	1.03	Motor and sensory integration
Toddlerhood	~2.5	2.70	Rapid cognitive expansion
Early Childhood	~4	4.37	Memory consolidation
Middle Childhood	~7	7.08	Cognitive stabilization
Adolescence	~12	11.45	Pubertal transition
Early Adulthood	18–20	18.53	Peak physiological integration
Mature Adulthood	~30	29.99	Physiological stability
Midlife Transition	~50	48.52	Endocrine reorganization

Developmental Stage	Consensus Age (Years)	Fibonacci-Scaled Age (Years)	Developmental Interpretation
Late Life	~80	78.51	Functional decline
Theoretical Lifespan Limit	~120	127.0	Systemic entropy limit

Note. Table 9.17 compares approximate developmental benchmarks with Fibonacci-scaled reference ages. The prenatal time-origin inconsistency identified in Section 9.3 remains relevant; the source values are preserved, and a quantitative assessment must reconcile that convention before interpreting deviations.

Chapter 10 Evolutionary Transitions and Timelines

10.1 Emergence and Scaling in Evolutionary Systems

Evolutionary transitions are unevenly distributed across geological time. This chapter compares selected milestones with Fibonacci-derived reference dates while retaining their paleontological context, dating uncertainty, and discrepancies.

Recent advances in molecular phylogenetics and geochemical analysis further motivate quantitative comparison. Evidence suggests that life may have emerged on Earth as early as 4.2 billion years ago, shortly after planetary stabilization, based on combined fossil, isotopic, and molecular clock analyses (Moody et al., 2024). Such findings indicate that biological emergence began rapidly once physical conditions permitted, reinforcing the possibility that evolutionary transitions reflect underlying constraint-driven dynamics.

10.2 Methods

To evaluate potential correspondence between evolutionary chronology and recursive temporal scaling, a standardized comparison framework was implemented. The methodology parallels that used for cosmological timelines, ensuring consistency across domains.

Normalization of Evolutionary Time

All evolutionary events were expressed using a **"years ago" temporal scale**, measured relative to the present. This normalization allows direct comparison across geological eras spanning billions of years while preserving chronological ordering independent of biological lineage.

Because evolutionary milestones vary widely in temporal precision, consensus dates were treated as approximate benchmarks rather than exact timestamps.

Fibonacci Temporal Conversion

Predicted evolutionary dates were generated using Fibonacci sequence indexing converted into temporal units through a fixed scaling transformation (Appendix A). The procedure involved:

1. Iterative generation of Fibonacci numbers.
2. Conversion of sequence values into days and subsequently into years.
3. Mapping scaled values onto geological time measured backward from the present.

A single global conversion parameter was applied uniformly across all evolutionary events.

Empirical Benchmarks: Fossil and Molecular Evidence

Scientific consensus dates were derived from multiple independent sources, including:

- fossil stratigraphy,
- radiometric dating,
- molecular clock analyses,
- comparative phylogenetics (Pagel, 1999).

These datasets provide convergent estimates for major evolutionary transitions such as multicellularity, vertebrate terrestrialization, hominid divergence, and cultural evolution.

Treatment of Uncertainty

Evolutionary timelines inherently contain uncertainty due to incomplete fossil preservation, dating resolution, and model dependence. Consequently, agreement between predicted and consensus dates is interpreted within approximate ranges rather than precise matches.

Avoidance of Post-Hoc Fitting

The comparison is described here as using one conversion without event-specific adjustments. Evaluating that claim requires the event-selection rule, index assignments, conversion constant, and dated analytical record; uniform arithmetic alone does not establish that choices were made before the benchmarks were inspected.

10.3 Empirical Comparison of Evolutionary Milestones

Tables 10.1–10.4 group the comparisons by geological era. Table 10.5 consolidates representative entries; it is not an independent replication.

These tables present observational comparisons only and do not imply causal relationships between mathematical sequences and biological processes.

Note. Scientific consensus dates represent approximate values synthesized from paleontological, geological, and molecular evidence. Percentage differences are calculated relative to consensus estimates. Evolutionary events may span extended intervals rather than discrete moments, and uncertainties increase toward both deep geological time and recent sociotechnological transitions.

Table 10.1: Precambrian to Paleozoic Era (4.2 Billion to 252 Million Years Ago)

Fibonacci-Derived Time	Scientific Consensus (Years Ago)	Event Title	Event Description
4,241,119,879	4.2 Billion	Origin of Life	Emergence of the earliest known life forms on Earth.
2,621,156,236	2.5 Billion	Great Oxygenation Event	Massive increase in Earth's oxygen levels due to photosynthetic cyanobacteria.
1,619,963,644	1.6 Billion	Multicellularity	Emergence of multicellular organisms, allowing for more complex life forms.
1,001,192,592	1.0 Billion	Sexual Reproduction	Likely appearance of the first sexual reproduction mechanisms in early life forms.
618,771,051	600 Million	Ediacaran Biota	Emergence of the Ediacaran biota, representing some of the earliest complex multicellular organisms.
382,421,541	375 Million	Water-Land Transition	The evolutionary transition of vertebrates from aquatic to terrestrial environments during the Devonian period.

Table 10.2: Mesozoic Era to Early Cenozoic (252 Million to 66 Million Years Ago)

Fibonacci-Derived Time	Scientific Consensus (Years Ago)	Event Title	Event Description
236,349,510	230 Million	Age of Dinosaurs	Dominance of dinosaurs across various ecosystems.
146,072,031	145-66 Million	Jurassic Period	Dominance of large dinosaurs and the appearance of the first birds during the Jurassic.
90,277,480	100-66 Million	Bird and Plant Diversification	Rapid diversification of early birds and flowering plants, forming new ecological niches.
55,794,551	55-50 Million	Post-Extinction Diversification	Early mammals diversify following the Cretaceous-Paleogene Extinction Event.

Table 10.3: Cenozoic Era (66 Million Years Ago to 10,000 Years Ago)

Fibonacci-Derived Time	Scientific Consensus (Years Ago)	Event Title	Event Description
34,482,929	30-35 Million	Primate Color Vision	Early primates develop refined color vision, crucial for foraging in forest canopies.
21,311,622	20 Million	Hominoid Ancestors	Earliest probable ancestors of hominoids adapt to diverse arboreal and terrestrial habitats.
13,171,307	12-15 Million	Climate Fluctuations	Major climate fluctuations begin, affecting hominoid evolutionary paths.
8,140,315	7-8 Million	First Hominids	Appearance of the first hominids, early primates that would eventually lead to humans.
5,030,992	5-6 Million	Divergence of Human-Pan Line	Divergence between the lineage leading to humans and the one leading to Pan (chimps and bonobos).
3,109,324	4-3 Million	Evolution of Bipedalism	Evolution of bipedalism in hominids, freeing hands for tool use and other functions.
1,921,668	1.76 Million	Acheulean Tools	Appearance and use of the Acheulean tool culture, characterized by the hand axe.
1,187,656	1.2 Million	Stone Tool Technology	Further refinement of stone tool technology and evidence of hunting large animals.
734,012	700,000-600,000	Homo Heidelbergensis	Evolution of Homo heidelbergensis, a crucial ancestor of both Neanderthals and modern humans.
453,644	400,000-300,000	Social and Hunting Strategies	More complex social structures and sophisticated hunting strategies in hominid groups.
280,368	400,000-300,000	Control of Fire	Early evidence of controlled use of fire by hominids, impacting diet and social organization.
173,277	200,000-100,000	Hominid Diversification	Further diversification of hominid populations and possible emergence of distinct subspecies.
107,091	100,000-50,000	Advanced Tool Use	Development of complex stone tools indicating advanced cognitive abilities and social structures.

Fibonacci-Derived Time	Scientific Consensus (Years Ago)	Event Title	Event Description
66,186	70,000-50,000	Human Out-of-Africa Migration	Significant migrations of Homo sapiens out of Africa, leading to global dispersal.
40,905	50,000-30,000	Modern Human Culture	Emergence of behaviorally modern humans, evidenced by art, advanced tools, and complex social practices.
25,281	26,500-19,000	Last Glacial Maximum	Peak of the last ice age, impacting species distribution and human migration patterns.
15,624	12,000-10,000	Early Human Settlements	Development of agriculture, domestication of animals, beginning of permanent settlements, and pottery.

Table 10.4: Modern Era (10,000 Years Ago to Present)

Fibonacci-Derived Time	Scientific Consensus (Years Ago)	Event Title	Event Description
9,656	9,800	Domestication of Wheat	Around 7,800 BC, wheat was domesticated, becoming a staple and changing human settlement patterns.
5,968	5,500	Development of Sumerian Civilization	The rise of Sumer, creating one of the first writing systems.
3,688	4,000	Middle Bronze Age Advancements	Advancements in urbanization, statecraft, and metallurgy fostering complex societal structures.
2,280	2,300-2,030	Hellenistic Cultural Expansion	Cultural diffusion of Greek science, philosophy, and art among Hellenistic states, circa 300-30 BC.
1,409	1,414	Rise of Islam	The early years of Islam under the Prophet Muhammad, laying the foundations for the rapid spread of Islam throughout the Arabian peninsula.
871	673-670	Black Death in Europe	The Black Death sweeps through Europe, drastically reducing the population and affecting society.
538	584	Invention of the Printing Press	The printing press revolutionizes book production, enhancing literacy and aiding the Renaissance and Reformation.

Fibonacci-Derived Time	Scientific Consensus (Years Ago)	Event Title	Event Description
333	374-324	Early Enlightenment	Intellectual and philosophical awakening marking the early stages of the Enlightenment.
206	264-184	Industrial Revolution Begins	The start of the Industrial Revolution in England, dramatically transforming manufacturing and society.
127	96	Discovery of Penicillin	In 1928, Alexander Fleming discovers penicillin, the first true antibiotic, revolutionizing medicine.
79	66	Invention of the Microchip	Invention of the integrated circuit or microchip, foundational for modern electronics.
49	55	First Human Moon Landing	In 1969, Apollo 11 mission successfully lands the first humans on the Moon.
30	33	World Wide Web Goes Public	The World Wide Web is made available to the public, initiating the modern Internet era.
19	20	Rise of Social Media	Expansion and impact of social media on communication, media, and politics globally.
11	16	Invention of Blockchain Technology	Creation of blockchain technology, enabling the development of cryptocurrencies and decentralized systems.
7	9	Paris Agreement on Climate Change	The Paris Agreement is signed, committing nations to limit global warming and reduce carbon emissions.
4	4	Global COVID-19 Pandemic Declared	WHO declares COVID-19 a global pandemic, leading to worldwide health crises and lockdowns.
3	3	Advances in CRISPR Technology	CRISPR gene-editing technology reaches new milestones in medical and agricultural applications.
2	2	Breakthroughs in Quantum Computing	Significant developments in Quantum computing, potentially revolutionizing computing and cryptography.
1	1	Rise of AI and Automation	Acceleration in artificial intelligence and automation technologies transforming industries.

Fibonacci-Derived Time	Scientific Consensus (Years Ago)	Event Title	Event Description
1	1	Advances in Space Exploration	Renewed interest and progress in space exploration, including missions to Mars and beyond.

10.4 Correspondence and Divergence

Comparison across evolutionary eras reveals both regions of correspondence and divergence between Fibonacci-derived intervals and established evolutionary timelines.

Several major transitions appear broadly consistent with recursive spacing, particularly those associated with increases in biological complexity. Events such as multicellularity, terrestrial adaptation, and hominid diversification occur at intervals resembling staged expansion rather than uniform linear progression. This pattern aligns with the theory of punctuated equilibrium, in which evolutionary history consists of extended stability interrupted by rapid transitions (Eldredge & Gould, 1972).

Recent research further contextualizes the earliest phase of biological emergence within this framework. A study published in *Nature Ecology and Evolution* found that life on Earth may have emerged as early as 4.2 billion years ago, shortly after the planet's formation (Moody et al., 2024). The study proposes that the first life form, known as LUCA (Last Universal Common Ancestor), was a simple single-celled organism possessing a genome of approximately 2.5 million base pairs. This early biological organization reflects the emergence of fundamental structural regularities in molecular assembly and replication, consistent with the recursive pattern formation explored in this model. Using genetic divergence analyses and molecular clocks calibrated with microbial fossils and isotope records, the research provides a more precise temporal estimate for life's origin, offering empirical support for applying fractal-based scaling approaches to deep evolutionary time.

Differentiated Pascal parity rows, illustrated in Figure 3.1, provide an analogy for heterogeneous organization. The correspondence between one-based row 58 and an evolutionary interval is an additional proposed mapping, not a result of the parity calculation.

However, divergence is also evident. Certain evolutionary events reflect strong contingency driven by environmental change, stochastic mutation, or ecological competition. Biological innovation depends not only on internal dynamics but also on unpredictable external conditions, limiting the extent to which any mathematical sequence can describe evolutionary timing universally.

Additional divergence appears in recent human technological history, where cultural acceleration compresses timescales dramatically relative to biological evolution. These deviations highlight

the growing influence of cognition and technological feedback loops, suggesting a transition toward new dynamical regimes explored in later parts of this work.

Likewise, one-based row 32 is an all-ones parity boundary. Associating that row with early societies requires the separate timing convention and event-selection rules. The visual analogy does not measure social or evolutionary entropy.

10.5 Consolidated Comparison

To enable cross-era evaluation, **Table 10.5** presents a consolidated comparison of representative evolutionary milestones drawn from Tables 10.1–4. While earlier tables preserve geological context, this summary aggregates events into a single chronological sequence, allowing overall correspondence patterns to be examined across the full evolutionary timeline.

This consolidated table serves as a comparative reference rather than an independent dataset.

Table 10.5: Consolidated Comparison of Evolutionary Epochs

Event	Scientific Consensus (Years Ago)	Fibonacci-Derived Time (Years Ago)	% Difference
Origin of Life	4,200,000,000	4,241,119,879	+0.98%
Great Oxygenation Event	2,500,000,000	2,621,156,236	+4.85%
Multicellularity	1,600,000,000	1,619,963,644	+1.25%
Sexual Reproduction	1,000,000,000	1,001,192,592	+0.12%
Ediacaran Biota	600,000,000	618,771,051	+3.13%
Water–Land Transition	375,000,000	382,421,541	+1.98%
Age of Dinosaurs (Triassic)	230,000,000	236,349,510	+2.76%
Jurassic Period	145,000,000	146,072,031	+0.74%
Bird & Plant Diversification	100,000,000	90,277,480	−9.72%
Post-Extinction Diversification	55,000,000	55,794,551	+1.45%
Primate Color Vision	32,500,000	34,482,929	+6.10%
Hominoid Ancestors	20,000,000	21,311,622	+6.56%
Climate Fluctuations	13,500,000	13,171,307	−2.43%
Human–Pan Divergence	5,500,000	8,140,315	+48.01%
Evolution of Bipedalism	3,500,000	5,030,992	+43.74%
Development of Stone Tools	2,600,000	3,109,324	+19.59%
Acheulean Tools	1,760,000	1,921,668	+9.18%
Homo heidelbergensis	650,000	734,012	+12.92%

Event	Scientific Consensus (Years Ago)	Fibonacci-Derived Time (Years Ago)	% Difference
Social & Hunting Strategies	350,000	453,644	+29.61%
Control of Fire	350,000	280,368	−19.90%
Hominid Diversification	150,000	173,277	+15.52%
Symbolic Behavior	125,000	107,091	−14.33%
Advanced Tool Use	75,000	107,091	+42.79%
Human Out-of-Africa Migration	60,000	66,186	+10.31%
Modern Human Culture	40,000	40,905	+2.26%
Last Glacial Maximum	22,750	25,281	+11.13%
Early Human Settlements	11,000	15,624	+42.04%

Note. Benchmark values are midpoint estimates from the ranges in Tables 10.1–10.4 and the cited literature. Percentage difference is 100 × (Fibonacci-derived years ago − benchmark years ago) / benchmark years ago. On a “years ago” axis, a positive difference means an older predicted date and a negative difference a more recent one. Events span intervals; the comparisons use approximate temporal centers.

Part V Mind Consciousness and Meaning

Chapter 11 Neural Organization and Consciousness

Learning, memory, and consciousness depend on interacting neural systems. This chapter connects the developmental comparisons to accounts of conscious integration while distinguishing established mechanisms from the proposed recursive analogies.

11.1 Learning Memory and Neural Networks

Learning and Memory as Emergent Plasticity

Synaptic Plasticity and Distributed Memory

Learning and memory represent foundational examples of emergence in biological systems. Rather than residing within individual neurons, cognitive capabilities arise from dynamic interactions among large populations of neural elements. At the cellular level, neurons communicate through synaptic connections whose strengths change over time, a process known as **synaptic plasticity** (Kandel et al., 2013). These local modifications collectively give rise to higher-order phenomena such as learning, memory consolidation, and adaptive behavior.

Plasticity operates through mechanisms including long-term potentiation (LTP) and long-term depression (LTD), which respectively strengthen or weaken synaptic efficacy in response to activity patterns (Bliss & Collingridge, 1993). Importantly, these processes depend not only on individual synapses but also on distributed activity across neural networks. Memory formation therefore emerges from coordinated patterns of activation rather than localized storage.

From an emergent systems perspective, learning reflects iterative updating within a constraint-based network. Neural systems continuously adjust connection weights to minimize prediction error while maintaining energetic and structural stability (Friston, 2010). The resulting cognitive states cannot be predicted solely from neuronal properties because they depend on collective dynamics unfolding across scales of organization.

This distributed nature explains why damage to specific neurons rarely eliminates memories entirely; instead, cognitive functions degrade gradually as network organization is disrupted. Memory is thus best understood as a property of **network configuration**, not neuronal components in isolation.

Emergent plasticity also demonstrates how complex behavior can arise from simple local rules. Individual neurons follow relatively straightforward electrochemical principles, yet recursive interaction among billions of such units produces flexible learning systems capable of abstraction and generalization. This exemplifies a core principle of emergence: global structure arises from repeated local interactions governed by constraints rather than centralized design.

Emergence Through Developmental Reorganization

Developmental neuroscience further demonstrates that neural organization evolves through staged transitions rather than continuous linear change. Across childhood and adulthood, identifiable shifts in brain structure, connectivity, and behavioral regulation occur at characteristic ages associated with large-scale network reorganization. These transitions reflect

changing balances between plasticity and stability, suggesting that cognitive emergence unfolds through temporally structured phases consistent with constraint-driven development.

Table 11.1 — Major Developmental Transitions in Brain Structure and Behavior

Age	Key Changes in Brain and Behavior	Supporting Evidence
7	Gray matter peaks before age 6	Bethlehem et al., 2022
11	Synaptic pruning and executive development	Sowell et al., 2004; Blakemore & Choudhury, 2006
18	Executive function maturity; peak neural entropy	Tervo-Clemmens et al., 2023; Carhart-Harris et al., 2014; Cieri et al., 2021
30	Personality stability and structural refinement	Terracciano et al., 2006
50	White matter decline; reduced neural entropy	Bethlehem et al., 2022; Cieri et al., 2021

Note. The listed ages summarize broad developmental transitions and vary across measures and populations. They do not establish discrete universal boundaries or measured entropy thresholds.

Recursive Stabilization as Conceptual Analogy

The staged developmental transitions summarized in Table 11.1 can be interpreted within a broader framework of recursive stabilization. Many iterative systems exhibit an early phase of variability followed by progressive convergence toward stable organization. In mathematical recursion, this behavior appears when successive ratios approach a limiting value.

Table 11.2 illustrates such convergence using Fibonacci ratios derived from Pascal recursion. Early iterations fluctuate substantially, but successive ratios rapidly stabilize toward unity when expressed as second-order ratios. This convergence reflects diminishing proportional change between successive states: each new step modifies the system less than the previous one.

Table 11.2 — Convergence of Recursive Ratios Toward Stability

Pascal Row	Fibonacci Number	First Ratios	Second Ratios	Sign	Years (Direct Conversion)	Years (Cumulative Days)
0	1	1.0000000	1.0000000	+	0.00	0.00
1	1	1.0000000	0.5000000	–	0.00	0.01
2	2	2.0000000	1.3333333	+	0.01	0.01
3	3	1.5000000	0.9000000	–	0.01	0.02
4	5	1.6666667	1.0416667	+	0.01	0.03
5	8	1.6000000	0.9846154	–	0.02	0.06
6	13	1.6250000	1.0059524	+	0.04	0.09
7	21	1.6153846	0.9977376	–	0.06	0.15
8	34	1.6190476	1.0008658	+	0.09	0.24
9	55	1.6176471	0.9996695	–	0.15	0.39
10	89	1.6181818	1.0001263	+	0.24	0.64
11	144	1.6179775	0.9999518	–	0.40	1.03
12	233	1.6180556	1.0000184	+	0.64	1.67
13	377	1.6180258	0.9999930	–	1.03	2.70
14	610	1.6180371	1.0000027	+	1.67	4.37
15	987	1.6180328	0.9999990	–	2.70	7.08
16	1597	1.6180344	1.0000004	+	4.38	11.45
17	2584	1.6180338	0.9999999	–	7.08	18.53
18	4181	1.6180341	1.0000001	+	11.46	29.99
19	6765	1.6180340	1.0000000	–	18.53	48.52

Pascal Row	Fibonacci Number	First Ratios	Second Ratios	Sign	Years (Direct Conversion)	Years (Cumulative Days)
20	10946	1.6180340	1.0000000	+	29.99	78.51
21	17711	1.6180340	1.0000000	–	48.52	127.03
22	28657	1.6180340	1.0000000	+	78.51	
23	46368	1.6180340	1.0000000	–	127.04	

Note. “First Ratios” are ratios of consecutive Fibonacci values and approach φ. “Second Ratios” compare consecutive first ratios and approach 1, with the sign indicating deviation about that limit. Ratios are displayed to seven decimal places and temporal conversions to two. The table uses a zero-based row label n with Fibonacci value F_{n+1}; direct and cumulative times follow Appendix A. This is a mathematical comparison, not a deterministic model of neural development.

This convergence provides a useful conceptual analogy for neural development. Early brain maturation is characterized by rapid structural change and high plasticity, analogous to large early ratio fluctuations. As development proceeds, successive reorganizations become proportionally smaller, reflecting increasing structural stability. Neural systems therefore transition from exploratory reconfiguration toward constrained optimization.

Importantly, the convergence toward unity does not represent cessation of change but stabilization around an attractor regime. Similarly, mature cognition retains plasticity while operating within increasingly stable network architectures.

Plasticity Windows and Language Acquisition

Developmental timing in cognition is particularly evident in language acquisition. Large-scale analyses demonstrate that the capacity to acquire grammatical structure in a new language remains highly efficient through late adolescence, with peak learning ability extending until approximately age 18, after which performance declines rapidly (Hartshorne, Tenenbaum, & Pinker, 2018). This transition corresponds to a shift in neural plasticity, during which synaptic remodeling and large-scale network flexibility give way to increased stabilization of cortical organization.

From an emergence perspective, this transition can be interpreted as a phase change in network dynamics rather than a discrete loss of capability. Early developmental stages favor exploration and structural reconfiguration, enabling rapid assimilation of linguistic rules. As neural systems mature, increased efficiency and specialization constrain plasticity, stabilizing learned structures while reducing sensitivity to novel grammatical patterns.

Interestingly, linguistic mastery continues to develop long after this plasticity peak. Studies suggest that full native-level command of language—including rhetorical nuance, cultural inference, and semantic flexibility—often requires several decades of cumulative experience, approaching maturation near age thirty (Hartshorne et al., 2018). This extended refinement phase reflects the gradual integration of distributed cognitive networks rather than continued structural rewiring.

Within the broader framework developed in this book, these milestones illustrate how cognitive development proceeds through temporally structured attractor transitions. Periods of heightened plasticity enable rapid structural formation, followed by phases of stabilization and refinement. Apparent clustering of developmental transitions near uneven temporal intervals should therefore be interpreted as consequences of recursive constraint-driven growth rather than evidence of predetermined numerical laws.

Autobiographical Memory and the Reminiscence Bump

A well-documented behavioral correlate of developmental neural transitions is the reminiscence bump, the tendency for adults to recall a disproportionate number of autobiographical memories from approximately ages 10-30 (Rubin, Rahhal, & Poon, 1998; Janssen et al., 2005). Rather than reflecting simple emotional preference, this pattern can be interpreted as an emergent consequence of heightened neural plasticity combined with large-scale network reorganization during adolescence and early adulthood. During this period, cognitive systems undergo rapid restructuring associated with identity formation, social learning, and abstract reasoning.

Memories encoded during periods of elevated plasticity and network instability may become more deeply integrated across distributed neural systems, increasing their long-term accessibility. As neural organization stabilizes in adulthood, encoding becomes more efficient but less globally transformative, producing fewer memories with comparable lifelong salience. The reminiscence bump therefore provides behavioral evidence that memory formation depends on system-level developmental dynamics rather than uniform encoding mechanisms across the lifespan.

Transformative Experiences and Identity-Level Encoding

The developmental interval associated with the reminiscence bump also corresponds to a documented clustering of spiritually interpreted or transformative experiences across cultures. Empirical studies report elevated rates of self-transcendent, existential, or anomalous experiences during late adolescence and emerging adulthood, frequently between ages eighteen and twenty-five. Within an emergent systems framework, this convergence may reflect heightened instability and reorganization of self-representational networks during identity formation. Periods of increased neural plasticity and social transition amplify the salience of experiences that challenge prior models of self and world, allowing certain events to function as attractor shifts in autobiographical organization. The lasting significance attributed to such experiences may therefore arise not solely from their intrinsic properties but from the developmental state of the cognitive system in which they are encoded.

The convergence of these phenomena becomes clearer when examined across multiple levels of cognitive organization. Although studied within different disciplines, autobiographical memory formation, identity development, and transformative experience exhibit parallel developmental timing and underlying mechanisms. This relationship can be summarized as follows:

Table 11.3 — Convergent Developmental Peaks Across Memory, Identity, and Transformative Experience

Domain	Observed Peak	Underlying Process
Autobiographical memory	10–30	heightened encoding during network reorganization
Identity formation	adolescence–20s	self-model restructuring
Spiritual/transformative experiences	~18–25	existential salience + cognitive reconfiguration

Note. Table 11.3 juxtaposes reported or proposed age windows across different psychological domains. Overlap does not establish a common neural mechanism. Definitions, sampling, and the evidence for each window must be evaluated separately; the table is not an independent test of Fibonacci timing.

The alignment of these developmental peaks supports the broader emergence framework advanced in this section: periods of increased neural plasticity and network instability not only enhance learning capacity but also increase the likelihood that experiences become structurally integrated into autobiographical identity.

Recursive Timing and Developmental Clustering

The developmental intervals summarized in Table 11.3 also exhibit an intriguing correspondence with the recursive timing patterns introduced earlier through the Pascal-Fibonacci analogy. When mapped onto lifespan development, several empirically observed transition periods—including early childhood reorganization, adolescent restructuring, early adult stabilization, and midlife decline—occur near unevenly spaced intervals resembling Fibonacci progression.

Within the framework developed in this section, this correspondence should not be interpreted as evidence that biological development follows an externally imposed numerical rule. Rather, Fibonacci spacing provides a mathematical illustration of how recursive systems undergoing iterative stabilization naturally generate temporally uneven transition points. Early stages exhibit rapid change separated by short intervals, whereas later reorganizations occur more gradually as the system approaches structural stability.

The proposed connection remains an analogy until the transition definitions, age distributions, timing conversion, and alternatives are specified and tested. Uneven developmental spacing alone does not establish Fibonacci scaling.

Neural Hierarchies

Neural systems exhibit hierarchical organization spanning multiple spatial and functional scales. At the lowest level, neurons form microcircuits composed of recurrent excitatory and inhibitory connections. These circuits aggregate into larger networks that coordinate perception, action, and cognition (Bassett & Sporns, 2017).

Hierarchical organization enables complexity by allowing emergent properties at one level to serve as building blocks for higher levels. Neural circuits generate oscillatory activity patterns, synchronization, and signal integration. Networks built from these circuits then support functions such as attention, memory, and decision-making.

For example, sensory processing follows hierarchical pathways in which early cortical regions encode basic features such as edges or frequencies, while higher regions integrate these signals into coherent perceptual representations (Felleman & Van Essen, 1991). Cognitive functions therefore emerge progressively as information is transformed across hierarchical layers.

Large-scale brain networks further illustrate this principle. Systems such as the default mode network (DMN), salience network, and frontoparietal control network coordinate activity across distant brain regions (Raichle, 2015). These networks exhibit dynamic coupling and decoupling depending on behavioral demands, demonstrating that cognition arises from flexible coordination rather than fixed localization.

Hierarchical organization also supports robustness and adaptability. Local disturbances can be compensated at higher levels through network reconfiguration, contributing to neural resilience following injury or environmental change. Such adaptability reflects the recursive integration of structure across scales—a defining feature of emergent systems.

Network Properties

A defining characteristic of emergence is the appearance of system-level properties that cannot be fully explained by analyzing individual components. In neural systems, several key phenomena illustrate this irreducibility.

First, **synchronization and oscillatory dynamics** emerge from interactions among neuronal populations. Brain rhythms such as alpha, beta, and gamma oscillations coordinate communication across regions and regulate information flow (Buzsáki, 2006). These rhythms do not exist at the level of single neurons but arise from collective timing relationships within networks.

Second, **functional connectivity** represents patterns of coordinated activity between distant brain regions. Neuroimaging studies demonstrate that cognition depends on network integration rather than localized processing (Bassett & Gazzaniga, 2011). Two neurons with identical properties may participate in entirely different functions depending on their network context, emphasizing relational rather than intrinsic organization.

Third, consciousness itself is widely interpreted as an emergent property of large-scale neural integration. Theories such as Integrated Information Theory propose that conscious experience corresponds to the degree of information integration across a system (Tononi, 2008). Similarly, Global Workspace Theory suggests consciousness emerges when information becomes globally accessible across distributed cognitive modules (Baars, 1997).

These theories share a common insight: cognitive phenomena arise from interactions among components rather than from any single neural structure.

Network-level emergence also aligns with principles observed in complex adaptive systems more broadly. Nonlinearity ensures that small changes in connectivity can produce large-scale behavioral shifts, while feedback loops stabilize or amplify neural dynamics (Mitchell, 2009). Consequently, understanding cognition requires studying patterns of interaction rather than isolated biological mechanisms.

From the perspective developed throughout this book, neural networks can be interpreted as constraint-driven recursive systems. Activity propagates through structured connectivity, generating increasingly abstract representations over time. Cognitive emergence thus reflects iterative transformation within a constrained possibility space shaped by energy, structure, and information flow.

Implications for Neural Organization

Neural cognition exemplifies emergence across multiple scales of organization. Learning and memory arise through distributed plasticity rather than localized storage, hierarchical organization enables complex cognitive functions to develop from simpler circuits, and network-level properties such as synchronization and consciousness cannot be reduced to individual neurons.

These findings reinforce a broader theoretical principle: complex intelligence emerges from recursive interaction under constraint. Neural systems demonstrate how simple local rules—

electrochemical signaling and synaptic adaptation—can generate adaptive, self-organizing cognition when embedded within large interconnected networks.

Understanding the brain therefore requires shifting explanatory emphasis from components to relationships, from mechanisms alone to patterns of interaction. In doing so, neural science provides one of the clearest empirical demonstrations of emergence as a unifying principle linking biological organization, information processing, and complex adaptive behavior.

11.2 Conscious Integration and Its Limits

Integration and Global Availability

Consciousness remains one of the most challenging problems in contemporary science because it involves subjective experience emerging from physical processes. Increasingly, researchers interpret consciousness not as a localized brain function but as an **emergent property of integrated neural activity**. Two influential theoretical frameworks—Integrated Information Theory (IIT) and Global Workspace Theory (GWT)—provide complementary approaches to understanding this emergence.

Integrated Information Theory proposes that consciousness corresponds to the degree to which a system integrates information into a unified whole (Tononi, 2008). According to IIT, conscious experience arises when a system's internal causal interactions generate irreducible informational structure. A highly integrated network possesses a high value of Φ (phi), representing the extent to which the system cannot be decomposed into independent parts without loss of informational content. In this framework, consciousness is fundamentally tied to network architecture and causal connectivity rather than specific biological substrates.

Global Workspace Theory, by contrast, emphasizes functional accessibility. GWT suggests that consciousness emerges when information becomes globally broadcast across distributed cognitive subsystems, enabling coordination among perception, memory, attention, and action (Baars, 1997; Dehaene & Naccache, 2001). Unconscious processing occurs locally, whereas conscious awareness corresponds to information entering a global workspace that integrates otherwise separate processes.

Despite differing emphases, both theories converge on a key principle: consciousness is not reducible to individual neurons or localized regions. Instead, it arises from large-scale integration across networks. IIT highlights structural integration, while GWT emphasizes functional communication. Together, they frame consciousness as an emergent property produced by coordinated neural interaction across hierarchical levels.

This convergence supports a broader emergence-based perspective in which cognitive unity arises from recursive integration within constrained neural systems.

Changes in Conscious State

Variations in conscious experience across waking, sleep, meditation, and pharmacologically altered states provide empirical evidence that consciousness depends on dynamic network organization. Rather than switching on or off, consciousness appears to vary continuously with patterns of neural connectivity and coordination.

During wakefulness, brain activity exhibits widespread integration across cortical and subcortical networks. Functional connectivity studies demonstrate strong interactions between attention, executive, and sensory networks (Raichle, 2015). In contrast, deep sleep involves reduced long-range connectivity and increased local synchronization, corresponding to diminished conscious awareness (Steriade, 2006).

Rapid eye movement (REM) sleep presents a distinct configuration in which internally generated imagery becomes prominent despite reduced sensory input, suggesting that conscious experience depends more on network dynamics than external stimulation (Hobson & Pace-Schott, 2002).

Meditative practices further illustrate network reconfiguration. Neuroimaging studies show altered interactions between the default mode network and attentional systems during focused attention and mindfulness meditation, often associated with reduced self-referential processing and increased present-centered awareness (Lutz et al., 2008). These findings suggest that conscious states correspond to specific configurations of large-scale neural coordination.

Similarly, psychedelic or pharmacologically altered states modify connectivity patterns, increasing communication between normally segregated brain regions (Carhart-Harris et al., 2014). The resulting experiences demonstrate that changes in integration structure directly influence subjective awareness.

Across these examples, consciousness appears as a dynamic emergent phenomenon shaped by evolving patterns of network organization rather than fixed anatomical structures.

Energy and State Stability

Underlying neural integration is the continuous flow and regulation of energy within the brain. Neural activity is metabolically expensive, and maintaining coherent conscious states requires tightly regulated energy allocation (Attwell & Laughlin, 2001). The brain consumes approximately 20% of the body's energy despite representing only a small fraction of its mass, underscoring the energetic demands of sustained integration.

From a systems perspective, consciousness may depend on maintaining neural activity within a regulated regime balancing stability and flexibility. Excessive synchronization can lead to pathological states such as seizures, whereas insufficient coordination results in reduced awareness or unconsciousness. Optimal conscious functioning therefore occurs within a constrained energetic window supporting coordinated but differentiated activity.

The free-energy principle proposes that biological systems minimize prediction error by maintaining stable internal models of their environments (Friston, 2010). Within this framework, consciousness reflects the brain's ongoing effort to regulate internal states through predictive integration of sensory information and prior expectations.

Energy flow thus provides the physical substrate enabling emergent integration. Neural systems must continuously dissipate energy while preserving organization, aligning with broader thermodynamic views of living systems as far-from-equilibrium structures sustained by energy exchange (Prigogine & Stengers, 1984).

Consequently, stable conscious states can be interpreted as dynamically maintained attractors within an energy-regulated network.

Contested Quantum Proposals

Some researchers have proposed that classical neural dynamics may be insufficient to explain consciousness, leading to theories involving quantum processes. The most prominent example is the Orchestrated Objective Reduction (Orch-OR) theory proposed by Penrose and Hameroff, which suggests that quantum computations within neuronal microtubules contribute to conscious experience (Hameroff & Penrose, 2014).

According to Orch-OR, quantum superposition states within microtubules undergo objective reduction events influenced by gravitational effects, producing discrete moments of conscious awareness. This proposal attempts to explain features such as unity of experience and rapid information integration that appear difficult to reconcile with purely classical models.

Quantum proposals are discussed because they address unresolved explanatory gaps, particularly the relationship between physical processes and subjective experience. However, they remain highly contested for several reasons.

First, maintaining quantum coherence in the warm, noisy environment of the brain appears physically challenging, as decoherence times are predicted to be extremely short (Tegmark, 2000). Second, empirical evidence directly supporting quantum computation in neural systems remains limited. Third, many cognitive phenomena can be modeled successfully using classical network dynamics without invoking quantum mechanisms.

Nevertheless, quantum approaches continue to stimulate interdisciplinary research by encouraging examination of fundamental assumptions about information processing and physical reality. Even if ultimately unsupported, they highlight the difficulty of explaining consciousness within existing frameworks.

From an emergence perspective, quantum theories represent attempts to locate deeper levels of integration underlying conscious experience. Whether necessary or not, their ongoing discussion reflects the complexity of bridging physical processes and phenomenological awareness.

Limits of Consciousness Models

Consciousness can be understood as an emergent integration arising from coordinated neural activity across multiple scales. Integrated Information Theory and Global Workspace Theory provide complementary accounts emphasizing structural and functional integration, respectively. Changes in conscious state correspond to dynamic reconfigurations of neural networks, demonstrating that awareness depends on patterns of interaction rather than isolated components.

Energy regulation forms the physical substrate enabling stable integration, positioning consciousness within broader thermodynamic principles governing living systems. Quantum proposals such as Orch-OR, while controversial, illustrate the continuing search for deeper explanatory frameworks.

Taken together, these perspectives support a unified view of consciousness as a dynamically maintained emergent phenomenon produced by recursive integration within constrained biological systems. Conscious awareness thus represents not a separate entity but a higher-order organizational state arising from complex interactions among neural processes.

Chapter 12 Synchronicity and Meaning

Reports of synchronicity—meaningful coincidences perceived as deeply significant despite lacking clear causal connection—have persisted across cultures and historical periods. Individuals frequently describe such events as temporally clustered, occurring during psychological transitions, and exhibiting an apparent structure or rhythm rather than random distribution. Classical interpretations, most prominently articulated by Carl Jung, framed synchronicity as an "acausal connecting principle," suggesting meaningful alignment beyond conventional causality (Jung, 1952).

Phenomenologically, reports of synchronicity consistently involve meaningful connection without identifiable causation, the recurrence of symbolic motifs across contexts, and convergence into moments experienced as unusually significant. These recurring features provide descriptive constraints that any explanatory framework must address. Yet such explanations remain philosophically and scientifically problematic because they appear to conflict with well-established physical laws.

Cognitive bias, selective recall, exposure frequency, and chance remain candidate explanations for reported coincidences. An account of their subjective significance must be distinguished from a claim that the events exhibit an objective excess of clustering.

This chapter explores synchronicity as a possible interaction between constrained event histories and an observer's interpretation. Pascal branching supplies a toy model of path multiplicity; history restrictions illustrate how accessible paths can change. Their application to lived experience is a hypothesis, not an established consequence of either construction.

12.1 Path Multiplicity

Every evolving system can be understood as traversing a branching space of possible futures. At its simplest, such branching may be modeled through binary decision processes. After n steps, the number of possible trajectories grows exponentially according to 2^n. Pascal's triangle provides a canonical representation of this expansion, where each row enumerates the number of distinct paths leading to particular outcomes.

Under independent, equally probable binary choices, more paths end near the center of the binomial distribution than at its extremes. This demonstrates nonuniform endpoint probabilities in that model; the probability law for real experiences must be established separately.

Different histories can lead to similar outcomes. A coincidence model must specify those histories, the definition of a match, and the sampling process before it can quantify whether an observed convergence is unusual.

The proposed interpretation treats internal development and external events as processes that may reach compatible states. Whether their intersections exceed chance expectations is an empirical question; shared context or common causes must also be considered.

The relevant distinction is between the meaningfulness of an experience and evidence that its occurrence has a special probability structure.

12.2 History Constraints

The binary-choice model can be extended with restrictions depending on earlier choices. Markovian updating refers to dependence on the current state, not independence between successive states. An expanded state can include remembered information.

As shown in Section 4.2, forbidding consecutive 1s yields Fibonacci path counts. Other restrictions yield other recurrences. Memory therefore supplies a modeling possibility, not a general derivation of Fibonacci timing for psychological events.

Constraints can alter the distribution of event times when incorporated into a specified dynamical model. They do not automatically produce quasiperiodicity or coordinated transitions.

“Meaning peaks” names the proposed concentration of subjectively significant experiences around transitions. This requires measurement of reporting rates and opportunities for coincidence, including periods in which no meaningful event is reported.

Repeated motifs in dreams, thoughts, and encounters are phenomenological observations. Testing a temporal model requires recording motifs prospectively and using comparison criteria that are fixed before the later event occurs.

The contrast between expanding possibilities and persistent constraints is a conceptual aid. Neither Pascal counts nor Fibonacci sequences directly measure thermodynamic entropy in a person’s experience.

12.3 Cognitive Interpretation

Predictive accounts of cognition offer one possible account of how unexpected events become significant: they may alter an observer’s model of the environment (Friston, 2010; Clark, 2016). The existence of objective convergence regions in experiential space remains to be established.

Informational compression can serve as a model of explanatory coherence, but Shannon entropy does not itself measure personal meaning (Shannon, 1948). A compelling interpretation may reduce subjective uncertainty without improving prediction.

The proposed account combines two features:

1. **Prediction error increase** — the coincidence is unexpected.
2. **Coherence increase** — the coincidence fits an emerging narrative or interpretation.

Together, surprise and perceived coherence may encourage a strong interpretive update. Whether that update improves the model or reflects overinterpretation must be evaluated separately.

An experience of unity or significance can be described without inferring an acausal influence. The proposed mechanism of model reorganization is one hypothesis about that experience.

Not every coincidence becomes personally meaningful. Context, attention, memory, and prior concerns can influence which events are noticed and retained.

The compression account therefore concerns interpretation as well as event structure. It can be tested by asking whether the resulting model predicts independent observations better than chance-based and cognitive alternatives.

12.4 Criteria for a Real Pattern

Philosopher Daniel Dennett argues that higher-level phenomena are real when they constitute "real patterns"—structures that enable reliable prediction and compression even if they are not fundamental physical entities (Dennett, 1991). Examples include centers of mass, economic markets, or traffic waves: patterns invisible at the microphysical level yet objectively explanatory.

To qualify as a "real pattern" in this stronger sense, the proposed structure would have to improve reproducible prediction or compression beyond flexible retrospective storytelling. Subjective salience alone does not establish that criterion.

The experience of meaning can be real while the proposed external regularity remains unverified. Keeping these claims separate preserves both the phenomenology and the empirical question.

A constraint-based account would model how histories, contexts, and interpretations converge. Its variables and probability structure must be specified before "coherence" can function as an explanatory measure.

The road-intersection analogy illustrates how paths can meet without a coordinating intention; it does not show that a particular coincidence was unusually likely or objectively directed.

Meaning therefore arises without teleology. Selection occurs without a selector, and coherence emerges without metaphysical grounding.

Meaning and Evidence

Synchronicity has long occupied an ambiguous position between psychology, philosophy, and mysticism. Traditional explanations either invoke acausal principles or dismiss meaningful coincidence as cognitive error. The framework developed here offers an alternative grounded in combinatorics and complexity science.

The proposal connects path multiplicity, history-dependent restriction, and cognitive interpretation. Its testable burden is to show whether it explains observations beyond chance, common causes, selective attention, and memory effects.

Meaningful coincidence need not violate natural law. A recursive account remains useful only insofar as it yields clearer definitions and better predictions than the alternatives.

Within this interpretation, perceived synchronicity can arise when trajectories converge and an observer assigns significance to the coincidence. Establishing a shared generative mechanism requires evidence beyond the experience of meaning itself.

Part VI Synthesis and Scientific Evaluation

Chapter 13 A Unified Framework and Its Scientific Tests

The cross-domain comparisons motivate a possible common framework, but its scientific value depends on explicit models and discriminating tests. The synthesis is followed by operational definitions, controls, independent benchmarks, and criteria for failure.

13.1 Constraint and Organization Across Scales

Nonlinearity Feedback and Hierarchy

Nonlinearity describes systems in which outputs are not proportional to inputs. Small perturbations may produce large-scale consequences, while large interventions sometimes yield minimal change. Nonlinear dynamics are fundamental to complex systems because they allow for bifurcations, attractors, and phase transitions—mechanisms through which new patterns arise (Strogatz, 2015). Biological evolution, neural activity, and gravitational clustering all exhibit nonlinear behavior, indicating that emergence depends on interaction structure rather than component complexity alone.

Feedback regulates system stability and transformation. Positive feedback amplifies deviations, enabling rapid structural change, whereas negative feedback stabilizes systems by counteracting fluctuations. Ecological population dynamics, metabolic regulation, and climate systems all rely on interacting feedback loops to maintain dynamic equilibrium (Levin, 1998). Emergent properties often appear when feedback loops operate across multiple scales simultaneously, producing self-organized order without centralized control.

Hierarchy organizes emergent complexity into nested levels. Structures produced at one scale become building blocks for higher levels of organization. In biology, molecules form cells, cells form tissues, tissues form organisms, and organisms form ecosystems. Similarly, cosmological structures develop hierarchically, from density fluctuations to galaxies and galaxy clusters (Mo, van den Bosch, & White, 2010). Hierarchical organization allows complexity to accumulate while preserving stability, enabling systems to evolve without losing coherence.

Symbiogenesis and Physical Coupling

One of the most powerful biological examples of emergence is **symbiogenesis**, the process by which new biological structures arise through cooperative integration between previously independent organisms. The origin of eukaryotic cells—resulting from symbiotic incorporation of mitochondria and chloroplasts—demonstrates how evolutionary innovation can occur through integration rather than competition alone (Margulis, 1970; Torday, 2019).

Symbiogenesis illustrates how integration can produce a new level of organization. The resulting functions depend on cooperation among the integrated components and their shared regulation (Margulis, 1970; Torday, 2019).

Beyond biology, symbiogenesis provides a conceptual metaphor for **coupling processes in physics**. Physical systems frequently exhibit emergent behavior when previously independent subsystems become dynamically linked. Examples include phase synchronization in oscillators,

gravitational coupling in stellar systems, and coherence phenomena in condensed matter physics (Pikovsky, Rosenblum, & Kurths, 2001).

A Constraint First Perspective

The proposed framework asks which transformations a system permits and how repeated transformations produce organization. Pascal recursion is a minimal example with explicit rules. Physical applications also require substrate-specific mechanisms; shared mathematics does not make those mechanisms dispensable.

Finite Recursion and Transition Regimes

The cross-domain hypothesis is that growth, constraint accumulation, and reorganization can share measurable structure. Cellular replicative limits, developmental changes, and magnetic transitions provide candidate comparisons. These examples do not yet establish one universality class: that would require an explicit mapping and common invariants demonstrated across the systems.

Open Ended Yet Constrained

“Open-ended yet constrained” summarizes the book’s proposal: iterative processes generate new possibilities, while physical and informational limits restrict what persists. The mathematical constructions demonstrate particular instances of this relationship. The empirical tables ask how far their timing and scaling signatures extend; they do not settle that question by resemblance alone.

Across the domains examined throughout this book, one recurring organizational pattern appears when cyclic processes stabilize under feedback and constraint: systems frequently organize around closed circulation pathways that sustain continuous transformation rather than linear progression. Such dynamics give rise to vortex-like or toroidal flow topologies observable in mathematical attractors, biological circulation, fluid systems, and astrophysical magnetic structures. Although the physical mechanisms differ in each case, the convergence toward cyclic organization reflects shared dynamical principles rather than shared material composition.

13.2 Methods Validation and a Research Program

From Construction to Empirical Model

A Pascal-based empirical model must specify the mathematical generator, observation rule, time conversion, and predicted outcome. Its contribution is measured against alternatives of comparable flexibility. The procedures below distinguish exploratory correspondence from confirmatory testing and define a reproducible research program.

Operational Definitions

For a theoretical framework to move beyond analogy, its concepts must be operationalized. The Pascal model therefore requires explicit definitions and measurable procedures.

Operational Definitions

- Recursive depth is the discrete iteration index; any correspondence with an empirical developmental stage must be defined separately.
- **Constraint space:** the set of energetically and structurally permissible system states.
- Entropy phase is a specified pattern regime classified using an identified entropy measure and, where needed, arrangement-sensitive metrics.
- **Modular filter:** algebraic or observational transformation revealing structural regularities (e.g., modulo reduction or coarse-graining).
- Fibonacci index selects a term in a defined sequence. Its conversion to a physical scale is an explicit modeling assumption.

Test Procedures

Evaluation of the model follows three methodological steps:

1. **Model generation**
Predict structural or temporal features using recursion-derived rules before examining empirical data.

2. **Independent dataset comparison**
Compare predictions against observational or experimental measurements not used in model construction.

3. **Statistical validation**
Assess whether correspondences exceed expectations under null models (random timing, power-law scaling, or alternative dynamics).

Prediction Classes

Phase Transition Points (Entropy Thresholds)

Phase-transition predictions specify a measurable state change and an independently chosen threshold. In Pascal parity, entropy is calculated from symbol frequencies; in an empirical system, the observed variables and their probability model must be defined before using the same term.

Empirical confirmation requires detecting statistically significant clustering of transitions near predicted entropy thresholds.

Timing Windows (Fibonacci Indexing)

Timing-window predictions specify reference times, widths, and uncertainty before testing. The diagonal identity motivates the candidate sequence; empirical clustering remains a separate hypothesis.

Crucially, predictions concern probabilistic alignment rather than deterministic exactness.

Structural Invariants (Modular/Fractal Signatures)

Structural predictions identify measurable features such as correlations, modular organization, or scaling dimensions. Modular filtering generates exact mathematical patterns; resemblance in an empirical image is insufficient to infer the same generator (Mandelbrot, 1983).

Support requires these features to discriminate the proposed model from plausible alternatives on independent observations.

Evidence Standards

A major challenge for pattern-based theories is distinguishing meaningful structure from coincidence. The Pascal framework therefore establishes explicit evidentiary criteria.

Strong Evidence

Evidence supporting the model would include:

1. **Prospective prediction success**
Accurate prediction of previously unknown transition points or timing windows.

2. **Cross-domain convergence**
Independent confirmation in biology, physics, and cognition using different datasets.

3. **Statistical robustness**
Observed alignments significantly exceeding null-model expectations.

4. **Mechanistic compatibility**
Demonstration that recursive constraint dynamics plausibly generate observed patterns.

5. **Parameter stability**
Predictions remaining valid without continuous adjustment of scaling parameters.

Weak Evidence (Coincidence Indicators)

Evidence should be considered weak if:

- matches are identified only retrospectively,
- multiple alternative scalings fit equally well,
- predictions require arbitrary parameter tuning,
- correspondence disappears with improved measurement precision,
- patterns depend on selective data inclusion.

Preregistered Evaluation

Numerology arises when patterns are identified **post hoc**, after inspecting data, without independent predictive criteria. Scientific methodology addresses this risk through **preregistration logic**, in which hypotheses, analytic procedures, and evaluation criteria are specified before examining the target dataset (Nosek et al., 2018). Although preregistration originated in psychology and clinical research, its principles apply broadly to pattern-based theoretical claims.

Within the Pascal framework, preregistration entails defining in advance:

1. the mathematical rule generating predictions (e.g., Fibonacci indexing or entropy thresholds),

2. acceptable parameter ranges,

3. datasets to be tested,

4. statistical criteria for success or failure.

Predictions must therefore precede confirmation attempts. For example, if Fibonacci indices are proposed as timing windows, their numerical values must be specified prior to comparison with empirical timelines. Adjusting parameters after observing data transforms hypothesis testing into curve fitting, undermining falsifiability (Popper, 1959).

Null Models and Controls

Validation of emergent-pattern models requires comparison against appropriate **null models**, which represent outcomes expected in the absence of the proposed mechanism. Without null comparisons, apparent structure may simply reflect statistical regularities common to complex datasets, such as power-law scaling or clustering.

A null model preserves certain properties of the original data while removing the hypothesized organizing principle (Gotelli & Graves, 1996). Several null strategies are particularly relevant to Pascal-based predictions:

Randomized timelines. Choose a null that changes the event-time structure relevant to the hypothesis while preserving justified constraints. Merely permuting event labels leaves an unlabeled set of event times unchanged and cannot test its proximity to a numerical grid.

Surrogate data generation.
Synthetic datasets matching statistical features—mean, variance, autocorrelation, or spectral density—allow evaluation of whether observed patterns exceed expectations from generic stochastic processes (Theiler et al., 1992).

Alternative scaling controls.
Comparisons against logarithmic, exponential, or power-law models help determine whether Fibonacci-based scaling provides superior explanatory power.

Robustness Across Datasets

Robust validation therefore requires testing across:

- **multiple biological systems** (developmental timing, physiological rhythms, evolutionary transitions),
- **physical systems** (solar cycles, cosmological timelines, dynamical phase transitions),
- **measurement scales** (micro-, meso-, and macro-level phenomena).

Robustness also involves parameter stability. If predictions require continuous recalibration for each dataset, explanatory power diminishes. A foundational model should operate with minimal adjustable parameters, demonstrating transferability across contexts (Gelman & Carlin, 2014).

Replication across independent research groups provides an additional robustness criterion. Findings reproduced using different methodologies or datasets significantly strengthen claims of underlying generative structure.

Measurement Error and Bias

Scientific hygiene requires explicit attention to cognitive and methodological biases that can distort interpretation.

Measurement Error

Empirical timelines and structural measurements contain uncertainty arising from observational limits, sampling variation, and model assumptions. Cosmological dates, biological milestones, and physiological rhythms often include substantial error margins. Analyses must therefore incorporate uncertainty estimates rather than treating values as exact points (Jaynes, 2003).

Prediction evaluation should consider confidence intervals or probabilistic windows rather than precise numerical matches. Apparent alignment falling within measurement uncertainty may not constitute meaningful support.

Cherry-Picking

Selective inclusion of favorable data creates false confirmation. To prevent this, inclusion criteria must be defined before analysis. All eligible observations should be reported, including those inconsistent with predictions. Transparent reporting standards reduce the risk of biased inference (Ioannidis, 2005).

Confirmation Bias

Researchers naturally favor evidence supporting their hypotheses (Nickerson, 1998). Countermeasures include:

- blind analysis procedures,
- independent replication,
- adversarial collaboration between proponents and skeptics,
- publication of negative results.

Statistical corrections for multiple comparisons are also essential when testing numerous potential pattern alignments, as repeated testing increases the likelihood of spurious correlations (Benjamini & Hochberg, 1995).

A Minimal Computational Toolkit

A reproducible toolkit should expose the generators, transformations, and metrics used in each comparison. It should reproduce table values from documented inputs and retain a record of excluded observations and failed predictions.

At its core, the toolkit treats Pascal recursion as a generative engine capable of producing structured pattern spaces through iterative local rules. Computationally, Pascal recursion can be expressed through discrete convolution or local additive updating:

$$C(n,k) = C(n-1,k-1) + C(n-1,k)$$

which defines a minimal recursive generator (Graham, Knuth, & Patashnik, 1994). When combined with modular reduction (e.g., mod n filtering), this generator produces families of deterministic patterns whose statistical properties can be analyzed quantitatively.

A minimal toolkit would include:

1. Recursive generation algorithms

- Pascal triangle and multinomial extensions (Pascal pyramids)
- Modular filtering operators
- Iterative depth expansion functions

2. Structural metrics

- Shannon entropy for row complexity (Shannon, 1948)
- symmetry indices
- periodicity and alternation detection
- fractal dimension estimation (Mandelbrot, 1982)

3. Temporal indexing tools

- Fibonacci projection functions
- cumulative versus direct indexing schemes
- attractor detection across iteration depth

4. Cross-scale comparison measures

- scaling-law fits
- recurrence quantification analysis
- pattern similarity metrics across datasets

The goal is not to impose structure onto empirical data but to test whether independently observed systems exhibit statistical signatures predicted by recursive constraint generators. By formalizing algorithms and metrics, the framework transitions from conceptual analogy toward computational methodology.

Independent Benchmarks

Benchmarks should test the same stated hypothesis across independently sourced datasets. Cross-domain breadth is informative only when measurement and selection rules are comparable.

Benchmark datasets should include representative systems spanning multiple scales:

Biological benchmarks

- developmental timing datasets
- lifespan and maturation intervals across species
- gene regulatory oscillation data
- physiological rhythm datasets

Physical benchmarks

- solar cycle polarity records

- stellar activity cycles
- cosmological structure formation timelines

Cognitive benchmarks

- neural activity dynamics
- network connectivity evolution
- learning-curve scaling in artificial neural networks

Synthetic benchmarks

- cellular automata
- agent-based simulations
- randomized recursive models (controls)

Each dataset would be analyzed using identical metrics derived from the Pascal Emergence Toolkit. This standardized approach reduces interpretive bias and allows meaningful comparisons between domains.

Benchmarking aligns with broader scientific practices in machine learning and complex systems research, where shared evaluation frameworks accelerate theory testing and refinement (Goodfellow et al., 2016). Importantly, benchmark failure is as informative as success; absence of predicted structure in well-chosen datasets would directly challenge the framework's generality.

Decisive Tests

The strongest tests can reject a proposed mapping. They should separate mathematical reproducibility, empirical correspondence, and added predictive value.

Several classes of decisive tests emerge:

(a) Entropy Phase Predictions

If recursive depth predicts entropy transitions, empirical systems modeled as binary or modular sequences should display identifiable phase thresholds. Failure to detect statistically significant entropy transitions where predicted would weaken the theory.

(b) Fibonacci Timing Predictions

The framework proposes that Fibonacci indexing functions as a coarse-grained temporal scaffold in constrained systems. Strong tests include:

- preregistered predictions of timing windows,
- comparison against randomized timelines,
- effect-size evaluation against null models.

If Fibonacci alignment performs no better than chance under rigorous controls, the hypothesis would be falsified.

(c) Structural Invariance Tests

Recursive generators predict recurring modular or fractal signatures across scales. Independent datasets should exhibit measurable invariants if the framework is correct. Lack of reproducibility across domains would undermine claims of universality.

(d) Predictive Novelty

Perhaps the strongest test involves forward prediction rather than retrospective fitting. Examples include:

- forecasting solar-cycle transitions,
- predicting developmental risk windows,
- identifying structural phase boundaries in simulations.

Scientific history shows that predictive success distinguishes genuine theory from post hoc explanation (Popper, 1959). Accordingly, predictions must be specified prior to data analysis and evaluated transparently.

Chapter 14 Implications and Research Directions

14.1 Development and Regeneration

Regeneration and cellular turnover provide a particularly promising domain for prediction. Many tissues exhibit characteristic renewal cycles governed by stem-cell dynamics and metabolic constraints (Blanpain & Fuchs, 2009). For example, epithelial tissues renew rapidly, whereas neural tissues exhibit slower or limited regeneration. Under a constraint-based model, turnover rates reflect optimal solutions balancing repair efficiency against energetic cost and error accumulation.

The Pascal framework suggests that regeneration intervals may cluster within constrained timing windows determined by recursive scaling relationships. Rather than implying rigid numerical determinism, the model predicts probabilistic bands within which regeneration events are most stable. Empirical testing could involve comparing observed tissue turnover intervals against null distributions derived from randomized timing models.

14.2 Aging and Longitudinal Tests

A research hypothesis is that changes in physiological resilience may cluster around measurable transitions. The proposed Fibonacci mapping has not established intervention windows. Any application to treatment timing would require independent longitudinal validation followed by appropriate clinical evaluation.

Testing these predictions requires longitudinal datasets tracking biomarkers, functional capacity, and disease onset across populations. Strong support would involve reproducible clustering of transitions across independent cohorts exceeding expectations under random aging models.

14.3 Systems Biology

Systems biology seeks to understand organisms as integrated networks rather than collections of independent molecular components. This shift reflects recognition that biological behavior arises from interactions among genes, proteins, cells, and environments (Kitano, 2002). Constraint-based modeling represents one of the most successful strategies within this paradigm.

Constraint-based approaches, such as flux balance analysis (FBA), model metabolic networks by defining allowable states under thermodynamic and stoichiometric limits rather than simulating every molecular interaction explicitly (Orth, Thiele, & Palsson, 2010). Remarkably, such models can accurately predict cellular growth behavior using only constraints and optimization principles.

14.4 Solar Cycle Forecasting

The proposed contribution to solar forecasting is a probability model for transitions, evaluated against established dynamo and statistical baselines. A timing grid is useful only if it improves forecasts on cycles not used to construct it.

Forecasting limitations arise from several sources:

1. **Nonlinearity of the dynamo system**, where small perturbations produce large long-term effects.

2. **Incomplete observational data**, particularly regarding subsurface magnetic fields.

3. **Multiscale coupling**, linking convection, rotation, and magnetic flux emergence.

Recent prediction methods combine dynamo theory with data assimilation techniques, improving short-term forecasts but still struggling with multi-cycle prediction horizons (Bhowmik & Nandy, 2018). A recursive constraint perspective suggests that forecasting success depends less on predicting exact trajectories and more on identifying phase transitions within bounded dynamical spaces.

14.5 Stellar Comparisons

Solar variability is not unique; many stars exhibit magnetic activity cycles analogous to the solar cycle. Observations of stellar chromospheric activity reveal correlations between stellar rotation rate, magnetic field strength, and cycle duration (Brun & Browning, 2017). Faster-rotating stars generally display stronger magnetic activity and shorter cycles, while slower rotators exhibit weaker, longer-period variability.

Observational surveys have revealed clustering of stellar cycles into discrete branches within rotation–activity diagrams, sometimes referred to as “active” and “inactive” sequences (Böhm-Vitense, 2007). These clusters imply that stellar activity does not vary continuously but instead occupies preferred dynamical states.

Testing this interpretation requires comparative stellar datasets examining whether cycle transitions align with predicted dynamical thresholds rather than random variation. Large surveys from missions such as *Kepler* and *TESS* increasingly enable such cross-scale comparisons (Mathur et al., 2014).

14.6 Cosmological Milestones

The observations discussed in Chapter 7 illustrate how new data can revise earlier reconstructions (Donnan et al., 2023). A recursive timing model must retain its original predictions when evaluated against such revisions; recalibration belongs to a new model version.

Future cosmological modeling may therefore benefit from integrating constraint-based approaches emphasizing phase transitions and hierarchical emergence. Such frameworks do not replace ΛCDM cosmology but may complement it by providing organizational principles explaining why structure formation proceeds in punctuated stages.

14.7 Intelligent Systems

Candidate design principles for intelligent systems include:

1. Local learning rules whose interactions support coherent global behavior.

2. Architectural and resource constraints that regulate instability and overfitting.

3. Updating mechanisms that integrate new information while retaining useful prior structure.

14.8 Network Integration and Stability

Network science reveals that brains exhibit **small-world** and **modular** architectures—structures combining local clustering with long-range connectivity (Bassett & Sporns, 2017). These architectures optimize efficiency by minimizing wiring costs while maximizing information transfer. Similar design principles increasingly appear in artificial neural networks, where hierarchical layers support abstraction and generalization.

Emergence theory reframes integration as a constraint optimization problem. Networks must satisfy competing demands:

- **integration**, enabling global coordination;
- **segregation**, preserving specialized processing;
- **stability**, preventing runaway activity;
- **plasticity**, allowing learning and adaptation.

Biological systems solve this problem through feedback regulation and energy constraints. Neural activity consumes substantial metabolic resources, imposing limits on sustained activation patterns (Attwell & Laughlin, 2001). These energetic costs function as stabilizing constraints preventing uncontrolled excitation.

In AI systems, analogous constraints appear through regularization methods, learning-rate schedules, and architectural bottlenecks. Without such constraints, networks may exhibit catastrophic forgetting, overfitting, or unstable training dynamics (Goodfellow, Bengio, & Courville, 2016).

14.9 Consciousness and Explanatory Limits

However, emergence also has limits. While it explains *how* complex organization arises, it does not fully resolve the philosophical "hard problem" of consciousness—why physical processes are accompanied by subjective experience (Chalmers, 1996). Emergent explanations describe functional organization but do not yet bridge the explanatory gap between objective mechanisms and phenomenological experience.

Conclusion

Pascal Time offers a set of explicit mathematical constructions and exploratory comparisons, together with a program for testing their empirical relevance. The next step is to reproduce the tables, reconcile their conventions, and evaluate a small number of fixed predictions against strong alternatives. A successful framework must explain where its mappings work, where they fail, and what predictive information they add.

Back Matter

Glossary of Key Terms

This glossary defines the core conceptual and technical terminology used throughout the book. The definitions integrate established scientific meanings with the specific operational usage adopted within the Pascal-based emergence framework. Where applicable, terms are grounded in existing literature from mathematics, physics, biology, and complexity science.

Attractor

An attractor is a set toward which trajectories of a specified dynamical system approach from a surrounding set of initial conditions (Strogatz, 2015). Calling a recurring pattern an attractor requires a defined state space and update rule; visual recurrence alone does not establish dynamical attraction.

Binary Sequence

A sequence composed of two possible values (typically 0 and 1). Binary sequences arise naturally when Pascal's triangle is reduced under modulo 2 arithmetic, enabling information-theoretic analysis using entropy measures (Shannon, 1948).

Constraint Space

The set of all configurations permitted under governing physical, informational, or structural limits. Rather than assuming unrestricted possibility, systems evolve within constraint spaces defined by conservation laws, geometry, or interaction rules (Prigogine & Stengers, 1984). Constraint space forms a central concept of the book's emergence framework.

Deterministic Recursion

A generative process in which each new state is produced through fixed rules applied to prior states. Deterministic recursion produces complex outcomes without randomness, demonstrating how structured complexity can arise from simple local operations (Wolfram, 2002).

Emergence

The appearance of system-level properties that cannot be fully predicted from the behavior of individual components alone (Anderson, 1972). Emergence results from interactions, feedback, and organization across scales. In this work, emergence is interpreted as the exploration of constraint space through recursive generation.

Entropy (Information-Theoretic)

A measure of uncertainty in a specified probability distribution (Shannon, 1948). For the binary rows analyzed here, Shannon entropy measures the balance of zeros and ones. It does not by itself distinguish different arrangements with the same frequencies or measure thermodynamic entropy.

Entropy Ladder

A descriptive comparison of uniform and differentiated recursive rows using symbol-frequency entropy. The term does not imply a monotonic increase with recursion depth: uniform rows recur, and an alternating row can have entropy close to one bit.

Feedback Loop

A process in which system outputs influence future inputs. Positive feedback amplifies change, while negative feedback stabilizes behavior (Nicolis & Prigogine, 1989). Feedback loops are essential mechanisms enabling emergent organization.

Fibonacci Attractors

Proposed structural or temporal regularities aligned with Fibonacci indices. Their interpretation as physical attractors requires a dynamical model and evidence of attraction; numerical alignment alone is insufficient.

Fibonacci Indexing

A method of assigning Fibonacci indices to selected milestones. The index, unit, time origin, direct or cumulative mapping, and event-selection rule are model choices that must be reported and tested independently.

Fractal

A structure exhibiting self-similarity across scales, meaning patterns repeat at different levels of magnification (Mandelbrot, 1982). Fractals arise naturally from recursive processes and nonlinear dynamics.

Fractal Time

A proposed representation of temporal organization through nested recursive scales. Self-similarity in a mathematical construction does not by itself establish that physical time has the same structure.

Hierarchical Emergence

The process by which structures formed at one level become building blocks for higher-order organization. Examples include cells forming tissues and galaxies forming clusters (Noble, 2008).

Local Additivity

A rule in which new system states arise from combining neighboring values. Pascal's triangle exemplifies local additivity through binomial recursion, demonstrating how global structure emerges from local interactions (Graham et al., 1994).

Modular Filtering (Modulo Operation)

An algebraic transformation that reduces numerical values according to a modulus (e.g., mod 2). Modular filtering reveals hidden structural patterns within recursive systems, such as the Sierpiński triangle emerging from Pascal's triangle modulo 2.

Nonlinearity

A property of a system whose input-output relationship or evolution equations do not satisfy linear superposition (Strogatz, 2015). Nonlinear dynamics can produce behavior that depends strongly on initial conditions and interactions.

Pascal Space

The abstract generative space defined by binomial recursion and its higher-dimensional extensions. Pascal space represents the set of all structures obtainable through recursive additive rules and their modular projections.

Pascal Recursion

The iterative rule defining Pascal's triangle:

$$C(n,k) = C(n-1,k-1) + C(n-1,k)$$

This rule serves as a minimal generator capable of producing combinatorial, fractal, and scaling structures (Graham et al., 1994).

Phase Transition (Structural)

A qualitative change in organization as a control parameter varies. The pattern classes used in this book are descriptive; identifying a physical phase transition requires a specified system, control parameter, and observable.

Recursive Depth

The number of iterations applied in a recursive process. Greater depth can reveal additional structure but does not imply a monotonic increase in entropy or complexity.

Scaling Law

A mathematical relationship describing how system properties change predictably with size or scale. Power-law scaling commonly appears in biological and cosmic systems (West, Brown, & Enquist, 1997).

Self-Organization

The spontaneous emergence of ordered structure without centralized control, driven by local interactions among system components (Haken, 1983).

Symmetry Breaking

A loss of invariance under a specified transformation. In physical applications, the relevant symmetry and mechanism must be stated; visible differentiation alone is not a complete symmetry-breaking model (Nicolis & Prigogine, 1989).

Unified Growth Logic

The hypothesis that diverse natural systems share common generative principles rooted in recursive growth, constraint dynamics, and scaling relationships.

Appendix A Fibonacci Time Tables and Indexing

This appendix tabulates direct and cumulative Fibonacci mappings. With $F_1 = F_2 = 1$, a zero-based Pascal label n corresponds here to F_{n+1}. Direct times treat that value as days; cumulative times use the sum through that term. The displayed year values are consistent with division by 365.25. These are chosen conversion conventions, not physical consequences of the sequence. The sum through F_m equals $F_{m+2} - 1$, so cumulative and direct mappings have a related but distinct index assignment (Figure A1). The convention must be fixed before comparison.

$Pascal_0$ labels begin at n = 0 and $Pascal_1$ labels at R = 1, with R = n + 1. Chapter 3 and its entropy table use the one-based labels R; the timing tables in Chapters 6 and 11 use zero-based labels n. This appendix displays both. A match between labels is meaningful only after the convention, Fibonacci index, time origin, and direct or cumulative mapping are specified.

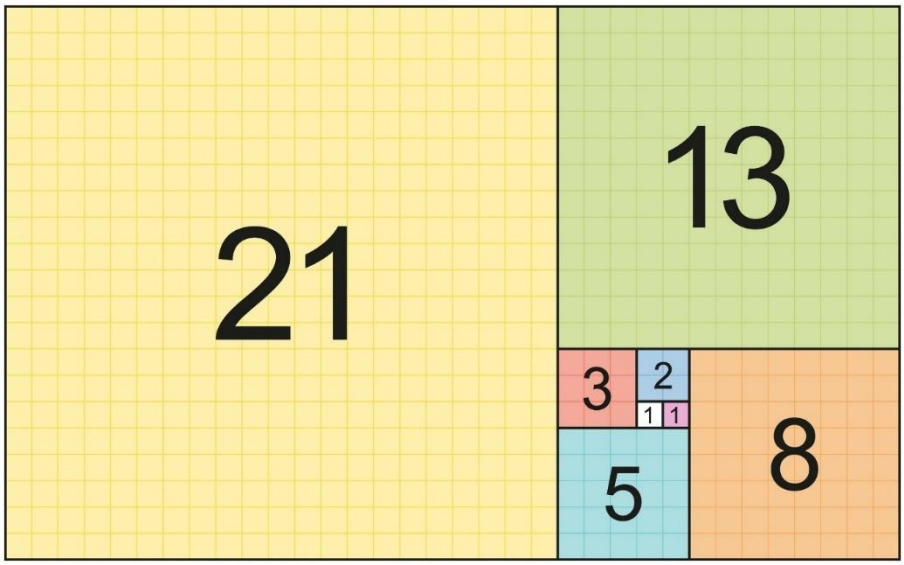

Figure A1. Geometric illustration of the Fibonacci summation identity showing that the cumulative sum of preceding terms equals the Fibonacci value two indices ahead minus one. For example, the sum of the first four terms (1 + 1 + 2 + 3 = 7) equals F6 − 1, since F6 = 8.

Table A1: Direct Fibonacci Values

Pascal Row (0-indexed)	Pascal Row (1-indexed)	Direct Fibonacci FnF_nFn	Years (Direct)
0	1	1	0.00
1	2	1	0.00
2	3	2	0.01
3	4	3	0.01
4	5	5	0.01
5	6	8	0.02

Pascal Row (0-indexed)	Pascal Row (1-indexed)	Direct Fibonacci F_nFn	Years (Direct)
6	7	13	0.04
7	8	21	0.06
8	9	34	0.09
9	10	55	0.15
10	11	89	0.24
11	12	144	0.39
12	13	233	0.64
13	14	377	1.03
14	15	610	1.67
15	16	987	2.70
16	17	1,597	4.38
17	18	2,584	7.08
18	19	4,181	11.45
19	20	6,765	18.53
20	21	10,946	29.99
21	22	17,711	48.52
22	23	28,657	78.51
23	24	46,368	127.04
24	25	75,025	205.5
25	26	121,393	332.6
26	27	196,418	538.1
27	28	317,811	870.7
28	29	514,229	1,409
29	30	832,040	2,280
30	31	1,346,269	3,688
31	32	2,178,309	5,968
32	33	3,524,578	9,656
33	34	5,702,887	15,624
34	35	9,227,465	25,281

Pascal Row (0-indexed)	Pascal Row (1-indexed)	Direct Fibonacci F_nFn	Years (Direct)
35	36	14,930,352	40,905
36	37	24,157,817	66,186
37	38	39,088,169	107,091
38	39	63,245,986	173,277
39	40	102,334,155	280,368
40	41	165,580,141	453,644
41	42	267,914,296	734,012
42	43	433,494,437	1,187,656
43	44	701,408,733	1,921,668
44	45	1,134,903,170	3,109,324
45	46	1,836,311,903	5,030,992
46	47	2,971,215,073	8,140,315
47	48	4,807,526,976	13,171,307
48	49	7,778,742,049	21,311,622
49	50	12,586,269,025	34,482,929
50	51	20,365,011,074	55,794,551
51	52	32,951,280,099	90,277,480
52	53	53,316,291,173	146,072,031
53	54	86,267,571,272	236,349,510
54	55	139,583,862,445	382,421,541
55	56	225,851,433,717	618,771,051
56	57	365,435,296,162	1,001,192,592
57	58	591,286,729,879	1,619,963,644
58	59	956,722,026,041	2,621,156,236
59	60	1,548,008,755,920	4,241,119,879
60	61	2,504,730,781,961	6,862,276,115
61	62	4,052,739,537,881	11,103,395,994
62	63	6,557,470,319,842	17,965,672,109
63	64	10,610,209,857,723	29,069,068,103

Pascal Row (0-indexed)	Pascal Row (1-indexed)	Direct Fibonacci F_nFn	Years (Direct)
64	65	17,167,680,177,565	47,034,740,213
65	66	27,777,890,035,288	76,103,808,316
66	67	44,945,570,212,853	123,138,548,528

Note. Fibonacci values are presented directly, where each row corresponds to a single Fibonacci number.

Table A2: Cumulative Fibonacci Values

Pascal Row (0-indexed)	Pascal Row (1-indexed)	Cumulative Fibonacci ΣFn	Years (Cumulative)
0	1	1	0.00
1	2	2	0.01
2	3	4	0.01
3	4	7	0.02
4	5	12	0.03
5	6	20	0.05
6	7	33	0.09
7	8	54	0.15
8	9	88	0.24
9	10	143	0.39
10	11	232	0.64
11	12	376	1.03
12	13	609	1.67
13	14	986	2.70
14	15	1,596	4.37
15	16	2,583	7.08
16	17	4,180	11.45
17	18	6,764	18.53
18	19	10,945	29.99
19	20	17,710	48.52
20	21	28,656	78.51
21	22	46,367	127.03

Pascal Row (0-indexed)	Pascal Row (1-indexed)	Cumulative Fibonacci ΣFn	Years (Cumulative)
22	23	75,024	205.5
23	24	121,392	332.6
24	25	196,417	538.1
25	26	317,810	870.7
26	27	514,228	1,409
27	28	832,039	2,280
28	29	1,346,268	3,688
29	30	2,178,308	5,968
30	31	3,524,577	9,656
31	32	5,702,886	15,624
32	33	9,227,464	25,281
33	34	14,930,351	40,905
34	35	24,157,816	66,186
35	36	39,088,168	107,091
36	37	63,245,985	173,277
37	38	102,334,154	280,368
38	39	165,580,140	453,644
39	40	267,914,295	734,012
40	41	433,494,436	1,187,656
41	42	701,408,732	1,921,668
42	43	1,134,903,169	3,109,324
43	44	1,836,311,902	5,030,992
44	45	2,971,215,072	8,140,315
45	46	4,807,526,975	13,171,307
46	47	7,778,742,048	21,311,622
47	48	12,586,269,024	34,482,929
48	49	20,365,011,073	55,794,551
49	50	32,951,280,098	90,277,480
50	51	53,316,291,172	146,072,031

Pascal Row (0-indexed)	Pascal Row (1-indexed)	Cumulative Fibonacci ΣFn	Years (Cumulative)
51	52	86,267,571,271	236,349,510
52	53	139,583,862,444	382,421,541
53	54	225,851,433,716	618,771,051
54	55	365,435,296,161	1,001,192,592
55	56	591,286,729,878	1,619,963,644
56	57	956,722,026,040	2,621,156,236
57	58	1,548,008,755,919	4,241,119,879
58	59	2,504,730,781,960	6,862,276,115
59	60	4,052,739,537,880	11,103,395,994
60	61	6,557,470,319,841	17,965,672,109
61	62	10,610,209,857,722	29,069,068,103
62	63	17,167,680,177,564	47,034,740,213
63	64	27,777,890,035,287	76,103,808,316
64	65	44,945,570,212,852	123,138,548,528
65	66	72,723,460,248,140	199,242,356,844
66	67	117,669,030,460,993	322,380,905,373

Note. Cumulative Fibonacci values represent the running total obtained by summing all Fibonacci numbers up to the given row.

Appendix B Anatomical and Developmental Patterns

This appendix provides detailed tables outlining various aspects of human anatomy and developmental biology. The tables summarize the organization and branching patterns observed in different anatomical structures, highlighting the role of ternary branching in the efficient organization and function of complex biological systems. These detailed categorizations illustrate the deep interconnectedness between cell-cell communication, genetic regulatory networks, and the emergence of structured biological patterns. The tables serve as a reference to support the concepts discussed in the main text, demonstrating the application of geometric principles in understanding biological complexity.

The compilation of these tables has been significantly informed by the work of Prof. John A. McNulty, Ph.D., of Loyola University of Chicago's School of Medicine, particularly his "List of Three's in Anatomy" (www.meddean.luc.edu/lumen/MedEd/GrossAnatomy/Threes.html).

Table B.1: General Anatomy

Category	Details
Body Planes	1. Frontal 2. Sagittal 3. Transverse
Layers of Skin	1. Epidermis 2. Dermis 3. Hypodermis
General Venous Circulations	1. Systemic 2. Pulmonary 3. Portal
Types of Muscle Tissue	1. Skeletal, 2. Cardiac, 3. Smooth
Main Types of Blood Cells	1. Red Blood Cells 2. White Blood Cells 3. Platelets

Table B.2: Embryology

Category	Details
Germ Layers	1. Endoderm 2. Mesoderm 3. Ectoderm
Divisions of Somites	1. Sclerotome 2. Dermatome 3. Myotome
Definitive Kidneys	1. Pronephros 2. Mesonephros 3. Metanephros
Derivatives of Skull	1. Desmo/Dermatocranium 2. Splanchno/Viscerocranium 3. Chondrocranium
Embryonic Divisions of the Brain	1. Prosencephalon 2. Mesencephalon 3. Rhombencephalon
Primary Vesicles of the Neural Tube	1. Forebrain (Prosencephalon), 2. Midbrain (Mesencephalon), 3. Hindbrain (Rhombencephalon)

Table B.3: Back

Category	Details
Erector Spinae Muscles	1. Iliocostalis 2. Longissimus 3. Spinalis
Transversospinalis Muscles	1. Semispinalis 2. Multifidus 3. Rotator
Coverings of the Spinal Cord	1. Dura Mater 2. Arachnoid 3. Pia
Spaces Surrounding Spinal Cord	1. Epidural 2. Subdural 3. Subarachnoid
Borders of the Scapula	1. Medial, 2. Lateral, 3. Superior
Angles of the Scapula	1. Superior, 2. Lateral, 3. Inferior

Table B.4: Neck and Head

Category	Details
Brachial Plexus	Trunks: 1. Upper 2. Middle 3. Lower
Branches off the Thyrocervical Trunk	1. Transverse Cervical 2. Suprascapular 3. Inferior Thyroid
Veins Draining the Thyroid Gland	1. Superior 2. Middle 3. Inferior
Scalene Muscles	1. Anterior 2. Middle 3. Posterior
Parts of the Pharynx	1. Nasopharynx 2. Oropharynx 3. Laryngeopharynx
Structures Inside Carotid Sheath	1. Common Carotid Artery 2. Internal Jugular Vein 3. Vagus Nerve
Divisions of the Trigeminal Nerve	V1 - Ophthalmic V2 - Maxillary V3 - Mandibular
Cranial Fossae	1. Anterior 2. Middle 3. Posterior
Nasal Conchae	1. Superior 2. Middle 3. Inferior
Salivary Glands	1. Parotid 2. Submaxillary 3. Sublingual
Middle Ear Bones	1. Incus 2. Malleus 3. Stapes
Parts of the Ear	1. Outer 2. Middle 3. Inner
Semicircular Canals	1. Anterior 2. Posterior 3. Lateral
Intrinsic Muscles of the Tongue	1. Longitudinal 2. Vertical 3. Transverse
Cerebral Arteries	1. Anterior 2. Middle 3. Posterior

Table B.5: Thoracic and Abdominal Anatomy

Category	Details
Thoracic Compartments	1. Mediastinum 2. Left Pleural Cavity 3. Right Pleural Cavity
Branches off the Aortic Arch	1. Brachiocephalic A. 2. Left Common Carotid A. 3. Left Subclavian A.
Principal Surfaces of the Pleura	1. Costal 2. Diaphragmatic 3. Mediastinal
Lobes of the Right Lung	1. Superior 2. Middle 3. Inferior
Parts of the Stomach	1. Fundus 2. Body 3. Pylorus
Layers of the Stomach	1. Oblique 2. Longitudinal 3. Circular
Divisions of the Mediastinum	1. Superior 2. Anterior 3. Posterior

Table B.6: Limb Anatomy (Upper and Lower Limbs)

Category	Details
Muscles of the Arm	Anterior: 1. Biceps Brachii, 2. Coracobrachialis, 3. Brachialis Triceps Brachii: 1. Long, 2. Lateral, 3. Medial
Forearm Muscles	1. Flexor Digitorum Profundus 2. Flexor Pollicis Longus 3. Pronator Quadratus
Hand Muscles	Thenar: 1. Opponens Pollicis, 2. Flexor Pollicis Brevis, 3. Abductor Pollicis Brevis Hypothenar: 1. Flexor Digiti Minimi, 2. Abductor Digiti Minimi, 3. Opponens Digiti Minimi
Thigh Muscles	1. Anterior 2. Medial 3. Posterior
Leg Muscles	Anterior: 1. Tibialis Anterior, 2. Extensor Digitorum, 3. Extensor Hallucis Deep Posterior: 1. Tibialis Posterioris, 2. Flexor Hallucis Longus, 3. Flexor Digitorum Longus
Major Arm Veins	1. Cephalic, 2. Basilic, 3. Brachial

Table B.7: Pelvis and Perineum

Category	Details
Bones in Os Coxae	1. Pubis, 2. Ilium, 3. Ischium
Foramina in the Pelvis	1. Obturator Foramen, 2. Greater Ischiadic Foramen, 3. Lesser Ischiadic Foramen
Gluteus Muscles	1. Gluteus Maximus, 2. Gluteus Medius, 3. Gluteus Minimus
Rectal Arteries	1. Superior Rectal (from Inferior Mesenteric A.), 2. Middle Rectal (from Internal Iliac A.), 3. Inferior Rectal (from Internal Pudendal A.)
Branches of the Posterior Division of Internal Iliac Artery	1. Iliolumbar, 2. Lateral Sacral, 3. Superior Gluteal
Openings in the Urinary Bladder	1. Left Ureter, 2. Right Ureter, 3. Urethra
Parts of the Uterus	1. Fundus, 2. Body, 3. Cervix

Category	Details
Erectile Compartments of the Penis	1. Corpus Spongiosum, 2. Left Corpus Cavernosum, 3. Right Corpus Cavernosum
Muscles in Superficial Perineal Pouch	1. Bulbospongiosus, 2. Ischiocavernosus, 3. Superficial Transverse Perineus
Arteries Supplying the Rectum	1. Superior Rectal (from Inferior Mesenteric), 2. Middle Rectal (from Internal Iliac), 3. Inferior Rectal (from Internal Pudendal)

Table B.8: Gluteus

Category	Details
Gluteal Muscles	1. Gluteus Maximus, 2. Gluteus Medius, 3. Gluteus Minimus
Muscles Innervated by Superior Gluteal Nerve	1. Gluteus Medius, 2. Gluteus Minimus, 3. Tensor Fascia Lata

Table B.9: Thigh

Category	Details
Hamstring Muscles	1. Biceps Femoris, 2. Semitendinosus, 3. Semimembranosus
Muscular Compartments of the Thigh	1. Anterior, 2. Medial, 3. Posterior
Muscles Contributing to the Pes Anserinus	1. Sartorius, 2. Semitendinosus, 3. Gracilis

Table B.10: Leg

Category	Details
Compartments in the Leg	1. Anterior, 2. Posterior, 3. Lateral
Muscles in Anterior Compartment	1. Tibialis Anterior, 2. Extensor Digitorum, 3. Extensor Hallucis
Peroneal Muscles	1. Peroneus Longus, 2. Peroneus Brevis, 3. Peroneus Tertius
Muscles in Deep Posterior Compartment	1. Tibialis Posterioris, 2. Flexor Hallucis Longus, 3. Flexor Digitorum Longus

Table B.11: Foot

Category	Details
Cuneiform Bones	1. Medial, 2. Intermediate, 3. Lateral
Plantar Interossei	1. First, 2. Second, 3. Third
Described Arches	1. Medial, 2. Lateral, 3. Transverse

Appendix C Formal Foundations

This appendix summarizes the formal mathematical relations supporting the conceptual framework developed throughout the book. The purpose is not to introduce advanced mathematics but to provide precise reference definitions demonstrating that the emergence framework rests on established combinatorial and information-theoretic principles. Mathematical expressions are included as structural anchors for readers seeking formal grounding.

C.1 Pascal Recursion

Pascal's triangle is generated by the binomial coefficient

$$\binom{n}{k} = \frac{n!}{k!\,(n-k)!}, \qquad \binom{k}{n} = \frac{k!}{n!\,(k-n)!}$$

where *n* denotes recursion depth (row index) and *k* denotes position within the row (Graham, Knuth, & Patashnik, 1994).

The defining recursive identity is

$$\binom{n}{k} = \binom{n-1}{k-1} + \binom{n-1}{k}, \qquad \binom{k}{n} = \binom{k-1}{n-1} + \binom{k}{n-1}$$

with boundary conditions

$$\binom{n}{0} = \binom{n}{n} = 1, \qquad \binom{0}{n} = \binom{n}{n} = 1$$

This relation follows from combinatorial decomposition: selecting *k* elements from *n* either includes or excludes a chosen element. Global combinatorial structure therefore emerges from strictly local additive rules.

C.2 Multinomial Extension

Higher-dimensional generalizations arise through multinomial coefficients:

$$\binom{n}{k_1, k_2, \ldots, k_m} = \frac{n!}{k_1!\,k_2!\cdots k_m!}, \qquad \binom{k_1, k_2, \ldots, k_m}{n} = \frac{k_1!\,k_2!\cdots k_m!}{n!}$$

subject to

$$\sum_{i=1}^{m} k_i = n$$

This extension produces Pascal's pyramid and higher-dimensional analogues. The generative rule remains local addition, demonstrating that recursion is independent of geometric embedding while expanding configuration space dimensionality.

C.3 Modular Filtering

Given entries $\binom{n}{k}$, modular reduction applies

$$\binom{n}{k} \backslash bmodm, \qquad \binom{k}{n} \backslash bmodm$$

Modular arithmetic partitions values into equivalence classes that act as observational filters on recursive structure.

For prime modulus *p*, Lucas's theorem states:

$$\binom{n}{k} \equiv \prod_i \binom{n_i}{k_i} \backslash pmodp, \qquad \binom{k}{n} \equiv \prod_i \binom{k_i}{n_i} \backslash pmodp$$

where n_i and k_i are digits in base *p*. Under modulus 2, coefficients are odd only when binary digits of *k* do not exceed those of *n*, producing the Sierpiński triangle (Mandelbrot, 1982).

Fractal structure therefore emerges from deterministic arithmetic rather than stochastic processes.

C.4 Entropy Measure

The balance of symbols in a recursive row is quantified using Shannon entropy:

$$\mathrm{H} = -\sum_{i=1}^{m} p_i \log_2(p_i)$$

where p_i denotes symbol probabilities (Shannon, 1948).

Within Pascal systems evaluated under modular filtering:

- uniform rows yield $\mathrm{H} = 0$ (maximal symmetry),
- balanced symbol distributions yield higher entropy,
- entropy measures configurational diversity rather than randomness.

This entropy distinguishes symbol balances, not spatial arrangements. Structural comparisons therefore also require pattern descriptions or measures sensitive to correlations (Cover & Thomas, 2006).

C.5 Fibonacci Relations

Fibonacci numbers arise intrinsically within Pascal's triangle through diagonal summation identities:

$$F_n = \sum_k \binom{n-k}{k}$$

Defined recursively as

$$F_{n+1} = F_n + F_{n-1}, \quad F_0 = 0,\ F_1 = 1$$

the sequence represents an internal combinatorial property rather than an externally imposed structure (Benjamin & Quinn, 2003).

Within the present framework, Fibonacci indexing is proposed as a marker of recursive scaling. Table C1 illustrates the mathematical diagonal correspondence; the empirical timing interpretation requires the separate conversion convention.

Table C1 — Fibonacci numbers from shallow diagonal sums in Pascal's triangle

Fibonacci number	Pascal 1-indexed										
1	1	1									
1	2	1	1								
2	3	1	2	1							
3	4	1	3	3	1						
5	5	1	4	6	4	1					
8	6	1	5	10	10	5	1				
13	7	1	6	15	20	15	6	1			
21	8	1	7	21	35	35	21	7	1		
34	9	1	8	28	56	70	56	28	8	1	
55	10	1	9	36	84	126	126	84	36	9	1

C.6 Structural Interpretation

Together these relations establish four formal principles underlying the book's framework:

1. **Recursive generation** — local additive rules produce expanding configuration spaces.
2. **Constraint filtering** — modular representations reveal latent structural regimes.
3. Entropy measurement — symbol-frequency uncertainty complements, but does not replace, analysis of arrangement and correlations.
4. **Intrinsic scaling** — Fibonacci relations emerge naturally from recursive combinatorics.

Complex organization can therefore arise from deterministic recursion operating within constrained mathematical spaces, without requiring stochastic forcing or externally imposed design.

References

Adami, C. (2016). What is information? *Philosophical Transactions of the Royal Society A, 374*(2063), 20150230. https://doi.org/10.1098/rsta.2015.0230

Adams, F. C., & Laughlin, G. (1997). A dying universe: The long-term fate and evolution of astrophysical objects. *Reviews of Modern Physics, 69*(2), 337–372. https://doi.org/10.1103/RevModPhys.69.337

Alberts, B., Johnson, A., Lewis, J., Morgan, D., Raff, M., Roberts, K., & Walter, P. (2015). *Molecular biology of the cell* (6th ed.). Garland Science.

Alfvén, H. (1942). Existence of electromagnetic-hydrodynamic waves. *Nature*, 150, 405–406.

Alon, U. (2007). *An introduction to systems biology: Design principles of biological circuits*. Chapman & Hall/CRC.

Arnold, V. I. (1989). *Mathematical Methods of Classical Mechanics*. Springer.

Anderson, P. W. (1972). More is different. *Science, 177*(4047), 393–396. https://doi.org/10.1126/science.177.4047.393

Aschoff, J. (1981). *Biological rhythms*. Springer.

Asencio, K., Acevedo, M., Zuriguel, I., & Maza, D. (2017). Experimental study of ordering of hard cubes by shearing. *Physical Review Letters, 119*(22), 228002. https://doi.org/10.1103/PhysRevLett.119.228002

Atkins, P., & de Paula, J. (2014). *Physical chemistry* (10th ed.). Oxford University Press.

Attwell, D., & Laughlin, S. B. (2001). An energy budget for signaling in the grey matter of the brain. *Journal of Cerebral Blood Flow & Metabolism, 21*(10), 1133–1145. https://doi.org/10.1097/00004647-200110000-00001

Austad, S. N. (2010). Methuselah's zoo: How nature provides us with clues for extending human health span. *Journal of Comparative Pathology, 142*(Suppl. 1), S10–S21.

Baars, B. J. (1997). *In the theater of consciousness: The workspace of the mind*. Oxford University Press.

Bachani, N., Vijay, S., Vyas, A., Jadwani, J., Panicker, G., & Lokhandwala, Y. (2025). The cardiac cycle and diastolic duration in healthy adults: Verifying golden ratio? *Indian Heart Journal, 77*(2), 164–168.

Bak, P. (1996). *How nature works: The science of self-organized criticality*. Springer.

Bak, P., Tang, C., & Wiesenfeld, K. (1987). Self-organized criticality: An explanation of 1/f noise. *Physical Review Letters, 59*(4), 381–384. https://doi.org/10.1103/PhysRevLett.59.381

Ball, P. (2009). *Nature's patterns: A tapestry in three parts*. Oxford University Press.

Bannink, T. and Buhrman, H., 2017. Quantum Pascal's Triangle and Sierpinski's carpet. arXiv preprint arXiv:1708.07429.

Bassett, D. S., & Gazzaniga, M. S. (2011). Understanding complexity in the human brain. *Trends in Cognitive Sciences, 15*(5), 200–209. https://doi.org/10.1016/j.tics.2011.03.006

Bassett, D. S., & Sporns, O. (2017). Network neuroscience. *Nature Neuroscience, 20*(3), 353–364. https://doi.org/10.1038/nn.4502

Batygin, K., & Morbidelli, A. (2013). Resonant transport of exoplanets. *Astronomy & Astrophysics, 556*, A28. https://doi.org/10.1051/0004-6361/201321260

Beck, R. (2016). Magnetic fields in spiral galaxies. *Astronomy and Astrophysics Review*, 24(4).

Belohlavek, M., MacLellan-Tobert, S. G., Seward, J. B., & Greenleaf, J. F. (1997). Toroidal geometry: Novel three-dimensional intracardiac imaging with a phased-array transducer. *Journal of the American Society of Echocardiography, 10*(5), 493–498. https://doi.org/10.1016/S0894-7317(97)70001-4

Benjamini, Y., & Hochberg, Y. (1995). Controlling the false discovery rate: A practical and powerful approach to multiple testing. *Journal of the Royal Statistical Society: Series B, 57*(1), 289–300.

Benjamin, A. T., & Quinn, J. J. (2003). *Proofs that really count: The art of combinatorial proof*. Mathematical Association of America.

Bhindi, N., & McMenamin, J. (2010). PASCAL'S TRIANGLE: 100% of the numbers are even!. Australian Mathematics Teacher, 66(1).

Bhowmik, P., & Nandy, D. (2018). Prediction of the strength and timing of sunspot cycle 25 reveal decadal-scale space environmental conditions. *Nature Communications, 9*, 5209. https://doi.org/10.1038/s41467-018-07690-0

Binney, J., & Tremaine, S. (2008). *Galactic dynamics* (2nd ed.). Princeton University Press.

Blackburn, E. H. (2000). Telomere states and cell fates. *Nature*, 408, 53–56.

Blakemore, S.-J., & Mills, K. L. (2014). Is adolescence a sensitive period for sociocultural processing? *Annual Review of Psychology, 65*, 187–207.

Blanpain, C., & Fuchs, E. (2009). Epidermal homeostasis: A balancing act of stem cells in the skin. *Nature Reviews Molecular Cell Biology, 10*(3), 207–217. https://doi.org/10.1038/nrm2636

Bliss, T. V. P., & Collingridge, G. L. (1993). A synaptic model of memory: Long-term potentiation in the hippocampus. *Nature, 361*, 31–39. https://doi.org/10.1038/361031a0

Boltzmann, L. (1877). Über die Beziehung zwischen dem zweiten Hauptsatze der mechanischen Wärmetheorie und der Wahrscheinlichkeitsrechnung. *Wiener Berichte*, 76, 373–435.

Bond, J. R., Kofman, L., & Pogosyan, D. (1996). How filaments of galaxies are woven into the cosmic web. *Nature, 380*, 603–606. https://doi.org/10.1038/380603a0

Böhm-Vitense, E. (2007). Chromospheric activity in G and K main-sequence stars, and what it tells us about stellar dynamos. *The Astrophysical Journal, 657*(1), 486–493. https://doi.org/10.1086/510482

Bonner, J. T. (2000). *First signals: The evolution of multicellular development*. Princeton University Press.

Boulila, S., Peters, S. E., Müller, R. D., & Hara, N. (2023). Earth's interior dynamics drive marine fossil diversity cycles of tens of millions of years. *Proceedings of the National Academy of Sciences of the United States of America, 120*(29), e2221149120. https://doi.org/10.1073/pnas.2221149120

Brun, A. S., & Browning, M. K. (2017). Magnetism, dynamo action and the solar–stellar connection. *Living Reviews in Solar Physics, 14*(1), 4. https://doi.org/10.1007/s41116-017-0007-8

Buonomano, D. V., & Rovelli, C. (2021). Bridging the neuroscience and physics of time. *Nature Reviews Neuroscience, 22*(10), 585–599. https://doi.org/10.1038/s41583-021-00478-0

Burbidge, E. M., Burbidge, G. R., Fowler, W. A., & Hoyle, F. (1957). Synthesis of the elements in stars. *Reviews of Modern Physics, 29*(4), 547–650. https://doi.org/10.1103/RevModPhys.29.547

Buzsáki, G. (2006). *Rhythms of the brain*. Oxford University Press.

Callen, H. B. (1985). *Thermodynamics and an introduction to thermostatistics* (2nd ed.). Wiley.

Camazine, S., Deneubourg, J. L., Franks, N. R., Sneyd, J., Theraulaz, G., & Bonabeau, E. (2001). *Self-organization in biological systems*. Princeton University Press.

Campisi, J. (2013). Aging, cellular senescence, and cancer. *Annual Review of Physiology*, 75, 685–705.

Cannon, W. B. (1932). *The wisdom of the body*. W. W. Norton.

Carey, J. R. (2001). Demographic mechanisms for the evolution of long life in social insects. *Experimental Gerontology, 36*(4–6), 713–722.

Casey, B. J., Jones, R. M., & Hare, T. A. (2008). The adolescent brain. *Annals of the New York Academy of Sciences, 1124*, 111–126.

Carney, D., & Varcoe, B., 2022. Universal Statistical Simulator. arXiv preprint

arXiv:2202.01735. Available at: https://doi.org/10.48550/arXiv.2202.01735

Carhart-Harris, R. L., Leech, R., Williams, T. M., Erritzoe, D., Abbasi, N., Bargiotas, T., … Nutt, D. J. (2014). Implications for psychedelic-assisted psychotherapy: Functional connectivity changes. *Frontiers in Human Neuroscience, 8*, 20. https://doi.org/10.3389/fnhum.2014.00020

Carroll, S. (2010). *From eternity to here: The quest for the ultimate theory of time*. Dutton.

Carroll, S. (2016). *The big picture: On the origins of life, meaning, and the universe itself*. Dutton.

Chaitin, G. J. (2004). *Meta math! The quest for Omega*. Pantheon Books.

Chalmers, D. J. (1996). *The conscious mind: In search of a fundamental theory*. Oxford University Press.

Charbonneau, P. (2020). Dynamo models of the solar cycle. *Living Reviews in Solar Physics, 17*(1), 4. https://doi.org/10.1007/s41116-020-00025-6

Chomsky, N. (1956). Three models for the description of language. *IRE Transactions on Information Theory, 2*(3), 113–124.

Clark, A. (2013). *Surfing uncertainty: Prediction, action, and the embodied mind*. Oxford University Press.

Clayton, D. D. (1983). *Principles of stellar evolution and nucleosynthesis*. University of Chicago Press.

Cohee, D. (2012). *Begonia leaf* [Photograph]. Wikimedia Commons. https://commons.wikimedia.org/wiki/File:Nautilus_leaf_begonia_Surreybrooke_farm_2012-07-1.jpg

Cover, T. M., & Thomas, J. A. (2006). *Elements of information theory* (2nd ed.). Wiley.

Crombach, A. (2021). Evolutionary systems biology: Integrating gene regulation and evolutionary dynamics. *BioSystems, 208*, 104482.

Darwin, C. (2009). *On the origin of species* (Original work published 1859). Oxford University Press.

Dehaene, S., Lau, H., & Kouider, S. (2017). What is consciousness, and could machines have it? *Science, 358*(6362), 486–492. https://doi.org/10.1126/science.aan8871

Dehaene, S., & Naccache, L. (2001). Towards a cognitive neuroscience of consciousness. *Cognition, 79*(1–2), 1–37. https://doi.org/10.1016/S0010-0277(00)00123-2

Dennett, D. C. (1991). *Real Patterns*. Journal of Philosophy, 88(1), 27–51.

Donnan, C. T., McLeod, D. J., Dunlop, J. S., McLure, R. J., Carnall, A. C., Begley, R., et al. (2023). The evolution of the galaxy UV luminosity function at redshifts z ≃ 8–15 from deep JWST imaging. *Monthly Notices of the Royal Astronomical Society, 518*(4), 6011–6040. https://doi.org/10.1093/mnras/stac3472

Dunlap, J. C., Loros, J. J., & DeCoursey, P. J. (2004). *Chronobiology: Biological timekeeping*. Sinauer Associates.

Dutta, S., Farhadifar, R., Lu, W., Kabacaoğlu, G., Blackwell, R., Stein, D. B., Lakonishok, M., Gelfand, V. I., Shvartsman, S. Y., & Shelley, M. J. (2024). Self-organized intracellular twisters. *Nature Physics, 20*, 666–674. https://doi.org/10.1038/s41567-023-02342-9

Edwards, A. W. F. (2002). *Pascal's arithmetical triangle: The story of a mathematical idea*. Johns Hopkins University Press.

Eldredge, N., & Gould, S. J. (1972). Punctuated equilibria: An alternative to phyletic gradualism. In T. Schopf (Ed.), *Models in paleobiology* (pp. 82–115). Freeman Cooper.

Elmore, S. (2007). Apoptosis: A review of programmed cell death. *Toxicologic Pathology, 35*(4), 495–516. https://doi.org/10.1080/01926230701320337

Falconer, K. (2003). *Fractal geometry: Mathematical foundations and applications* (2nd ed.). Wiley.

Fathauer, R. (2013). *Poinsettia leaf* [Photograph]. http://robertfathauer.com/PoinsettiaLeaf1.html

Feigenbaum, M. J. (1978). Quantitative universality for a class of nonlinear transformations. *Journal of Statistical Physics, 19*(1), 25–52. https://doi.org/10.1007/BF01020332

Felleman, D. J., & Van Essen, D. C. (1991). Distributed hierarchical processing in the primate cerebral cortex. *Cerebral Cortex, 1*(1), 1–47. https://doi.org/10.1093/cercor/1.1.1

Feller, W. (1968). *An introduction to probability theory and its applications* (3rd ed., Vol. 1). Wiley.

Fine, N. J. (1947). Binomial coefficients modulo a prime. *American Mathematical Monthly, 54*(10), 589–592.

Fontana, L., & Partridge, L. (2015). Promoting health and longevity through diet: From model organisms to humans. *Cell, 161*(1), 106–118.

Foster, R. G., & Kreitzman, L. (2004). *Rhythms of life: The biological clocks that control the daily lives of every living thing*. Yale University Press.

Fraústo da Silva, J. J. R., & Williams, R. J. P. (2001). *The biological chemistry of the elements* (2nd ed.). Oxford University Press.

Friston, K. (2010). The free-energy principle: A unified brain theory? *Nature Reviews Neuroscience, 11*(2), 127–138. https://doi.org/10.1038/nrn2787

Gelman, A., & Carlin, J. (2014). Beyond power calculations: Assessing Type S and Type M errors. *Perspectives on Psychological Science, 9*(6), 641–651. https://doi.org/10.1177/1745691614551642

Glatzmaier, G. A., & Roberts, P. H. (1995). A three-dimensional self-consistent computer simulation of a geomagnetic field reversal. *Nature*, 377, 203–209.

Gleick, J. (1987). *Chaos: Making a New Science*. Viking.

Goldbeter, A. (1996). *Biochemical oscillations and cellular rhythms*. Cambridge University Press.

Goodfellow, I., Bengio, Y., & Courville, A. (2016). *Deep learning*. MIT Press.

Gotelli, N. J., & Graves, G. R. (1996). *Null models in ecology*. Smithsonian Institution Press.

Gould, S. J. (2002). *The structure of evolutionary theory*. Harvard University Press.

Graham, R. L., Knuth, D. E., & Patashnik, O. (1994). *Concrete mathematics* (2nd ed.). Addison-Wesley.

Grant, B. L. (2021). *Shriveled poinsettia leaves*. Gardening Know How. https://www.gardeningknowhow.com/ornamental/flowers/poinsettia/shriveled-poinsettia-leaves.htm

Granville, A. (1997). Arithmetic properties of binomial coefficients. In Y. Motohashi (Ed.), *Organic mathematics* (pp. 253–276). American Mathematical Society.

Griffiths, D. J. (2018). *Introduction to quantum mechanics* (3rd ed.). Cambridge University Press.

Guckenheimer, J., & Holmes, P. (1983). *Nonlinear Oscillations, Dynamical Systems, and Bifurcations of Vector Fields*. Springer.

Gupta, R. P. (2023). JWST early Universe observations and ΛCDM cosmology. Monthly Notices of the Royal Astronomical Society, 524(3), 3385-3395.

Guth, A. H. (1981). Inflationary universe: A possible solution to the horizon and flatness problems. *Physical Review D, 23*(2), 347–356. https://doi.org/10.1103/PhysRevD.23.347

Haken, H. (1983). *Synergetics: An introduction* (3rd ed.). Springer.

Halberg, F. (1983). Chronobiology. *Annual Review of Physiology, 45*, 615–627.

Hameroff, S., & Penrose, R. (2014). Consciousness in the universe: A review of the Orch OR theory. *Physics of Life Reviews, 11*(1), 39–78. https://doi.org/10.1016/j.plrev.2013.08.002

Hathaway, D. H. (2015). The solar cycle. *Living Reviews in Solar Physics, 12*(1), 4. https://doi.org/10.1007/lrsp-2015-4

Hatton, I.A., Galbraith, E.D., Merleau, N.S., Miettinen, T.P., Smith, B.M. and Shander, J.A.,

2023. The human cell count and size distribution. Proceedings of the National Academy of Sciences, 120(39), p.e2303077120.

Hayflick, L., & Moorhead, P. S. (1961). The serial cultivation of human diploid cell strains. *Experimental Cell Research*, 25, 585–621.

Hayflick, L. (2007). Biological aging is no longer an unsolved problem. *Annals of the New York Academy of Sciences, 1100*(1), 1–13. https://doi.org/10.1196/annals.1395.001

Ho, M. W., El Naschie, M., & Vitiello, G. (2015). Is spacetime fractal and quantum coherent in

the golden mean? Global Journal of Science Frontier Research A, XV(I), 61-80.

Hobson, J. A., & Pace-Schott, E. F. (2002). The cognitive neuroscience of sleep. *Nature Reviews Neuroscience, 3*(9), 679–693. https://doi.org/10.1038/nrn915

Holland, J. H. (1998). *Emergence: From chaos to order*. Perseus Books.

Huang, S. (2009). Reprogramming cell fates: Reconciling rarity with robustness. *BioEssays, 31*(5), 546–560.

Huang, W., Tarduno, J. A., Zhou, T., Ibañez-Mejia, M., Dal Olmo-Barbosa, L., Koester, E., Blackman, E. G., Smirnov, A. V., Ahrendt, G., Cottrell, R. D., Kodama, K. P., Bono, R. K., Sibeck, D. G., Li, Y.-X., Nimmo, F., Xiao, S., & Watkeys, M. K. (2024). Near-collapse of the geomagnetic field may have contributed to atmospheric oxygenation and animal radiation in the Ediacaran Period. *Communications Earth & Environment, 5*, Article 207. https://doi.org/10.1038/s43247-024-01360-4

Ioannidis, J. P. A. (2005). Why most published research findings are false. *PLoS Medicine, 2*(8), e124. https://doi.org/10.1371/journal.pmed.0020124

Jaynes, E. T. (2003). *Probability theory: The logic of science*. Cambridge University Press.

Jean, R. V. (1994). *Phyllotaxis: A systemic study in plant morphogenesis*. Cambridge University Press.

Jung, C. G. (1952). *Synchronicity: An Acausal Connecting Principle*. Princeton University Press.

Kadanoff, L. P. (2000). *Statistical physics: Statics, dynamics and renormalization*. World Scientific.

Kandel, E. R., Schwartz, J. H., Jessell, T. M., Siegelbaum, S. A., & Hudspeth, A. J. (2013). *Principles of neural science* (5th ed.). McGraw–Hill.

Karikkineth, A. C., Scheibye-Knudsen, M., Fivenson, E., Croteau, D. L., & Bohr, V. A. (2017). Cockayne syndrome: Clinical features, model systems, and pathways. *Ageing Research Reviews, 33*, 3–17. https://doi.org/10.1016/j.arr.2016.08.002

Kauffman, S. A. (1993). *The origins of order: Self-organization and selection in evolution*. Oxford University Press.

Kauffman, S. (2000). *Investigations*. Oxford University Press.

Kaur, M., & Dhaliwal, H. S. (2016). *Interpretation of Fibonacci numbers in botany in the cross-sections and leafage of selected vegetables*. International Journal of Advanced Research, 4(10), 145–151.

Kelso, J. A. S. (1995). *Dynamic Patterns: The Self-Organization of Brain and Behavior*. MIT Press.

Kempkes, S.N., Slot, M.R., Freeney, S.E., Zevenhuizen, S.J.M., Vanmaekelbergh, D., Swart, I.

and Morais Smith, C., 2018. Design and characterization of electrons in a fractal geometry. Nature Physics, 15, 127–131.

Kennedy, B. K., Berger, S. L., Brunet, A., Campisi, J., Cuervo, A. M., Epel, E. S., … Sierra, F. (2014). Geroscience: Linking aging to chronic disease. *Cell, 159*(4), 709–713. https://doi.org/10.1016/j.cell.2014.10.039

Kitano, H. (2002). Systems biology: A brief overview. *Science, 295*(5560), 1662–1664. https://doi.org/10.1126/science.1069492

Kirkwood, T. B. L. (2005). Understanding the odd science of aging. *Cell, 120*(4), 437–447. https://doi.org/10.1016/j.cell.2005.01.027

Kirkwood, T. B. L., & Austad, S. N. (2000). Why do we age? *Nature, 408*(6809), 233–238.

Koblitz, N. (1994). *A course in number theory and cryptography* (2nd ed.). Springer.

Kuan, V., Fraser, H. C., Hingorani, M., Denaxas, S., Gonzalez-Izquierdo, A., Direk, K., & Hingorani, A. D. (2021). *Data-driven identification of ageing-related diseases from electronic health records.* Scientific Reports, 11, 2938.

Kültz, D. (2005). Molecular and evolutionary basis of the cellular stress response. *Annual Review of Physiology, 67*, 225–257. https://doi.org/10.1146/annurev.physiol.67.040403.103635

Larsen, S. H. (2021). *DNA structure and the golden ratio revisited*. *Symmetry, 13*(10), 1949. https://doi.org/10.3390/sym13101949

LeCun, Y., Bengio, Y., & Hinton, G. (2015). Deep learning. *Nature, 521*(7553), 436–444. https://doi.org/10.1038/nature14539

Lenstra, R. (2015). The graph, geometry and symmetries of the genetic code with Hamming metric. **Symmetry, 7**(3), 1211–1230. https://doi.org/10.3390/sym7031211

Levin, S. A. (1998). Ecosystems and the biosphere as complex adaptive systems. *Ecosystems, 1*(5), 431–436. https://doi.org/10.1007/s100219900037

Liddle, A. R., & Lyth, D. H. (2000). *Cosmological inflation and large-scale structure*. Cambridge University Press.

Lin, C. C., & Shu, F. H. (1964). On the spiral structure of disk galaxies. *The Astrophysical Journal, 140*, 646–655.

Linde, A. D. (1983). Chaotic inflation. *Physics Letters B, 129*(3–4), 177–181. https://doi.org/10.1016/0370-2693(83)90837-7

Livio, M. (2002). *The golden ratio: The story of phi, the world's most astonishing number*. Broadway Books.

López-Otín, C., Blasco, M. A., Partridge, L., Serrano, M., & Kroemer, G. (2013). The hallmarks of aging. *Cell, 153*(6), 1194–1217. https://doi.org/10.1016/j.cell.2013.05.039

Londono, J., Ghasmi, S., Lawand, G., Mirzaei, F., Akbari, F., & Dashti, M. (2022). Assessment of the golden proportion in natural facial esthetics: A systematic review. *The Journal of Prosthetic Dentistry*. https://doi.org/10.1016/j.prosdent.2022.04.026

Lorenz, E. N. (1963). Deterministic nonperiodic flow. *Journal of the Atmospheric Sciences, 20*(2), 130–141.

Lutz, A., Dunne, J. D., & Davidson, R. J. (2008). Meditation and the neuroscience of consciousness. In P. Zelazo, M. Moscovitch, & E. Thompson (Eds.), *The Cambridge handbook of consciousness* (pp. 497–549). Cambridge University Press.

Madau, P., & Dickinson, M. (2014). Cosmic star-formation history. *Annual Review of Astronomy and Astrophysics, 52*, 415–486. https://doi.org/10.1146/annurev-astro-081811-125615

Mandelbrot, B. B. (1982). *The fractal geometry of nature*. W. H. Freeman.

Margulis, L. (1970). *Origin of eukaryotic cells*. Yale University Press.

Mathur, S., García, R. A., Ballot, J., Ceillier, T., Salabert, D., & Metcalfe, T. S. (2014). Magnetic activity of F stars observed by Kepler. *Astronomy & Astrophysics, 562*, A124. https://doi.org/10.1051/0004-6361/201322552

Maynard Smith, J. (2000). The concept of information in biology. *Philosophy of Science, 67*(2), 177–194.

Maynard Smith, J., & Szathmáry, E. (1995). *The major transitions in evolution*. Oxford University Press.

Mayr, E. (2001). *What evolution is*. Basic Books.

McIntosh, S. W., Leamon, R. J., Krista, L. D., Title, A. M., Hudson, H. S., Riley, P., Harder, J. W., Kopp, G., Snow, M., Woods, T. N., Kasper, J. C., Stevens, M. L., & Ulrich, R. K. (2015). The solar magnetic activity band interaction and instabilities that shape quasi-periodic variability. *Nature Communications, 6*, 6491. https://doi.org/10.1038/ncomms7491

McKee, C. F., & Ostriker, E. C. (2007). Theory of star formation. *Annual Review of Astronomy and Astrophysics, 45*, 565–687. https://doi.org/10.1146/annurev.astro.45.051806.110602

Medzhitov, R. (2008). Origin and physiological roles of inflammation. *Nature, 454*(7203), 428–435. https://doi.org/10.1038/nature07201

Merrill, R. T., McElhinny, M. W., & McFadden, P. L. (1996). *The Magnetic Field of the Earth: Paleomagnetism, the Core, and the Deep Mantle*. Academic Press.

Mitchell, M. (2009). *Complexity: A guided tour*. Oxford University Press.

Mo, H., van den Bosch, F. C., & White, S. (2010). *Galaxy formation and evolution*. Cambridge University Press.

Moody, E.R., Alvarez-Carretero, S., Mahendrarajah, T., Clark, J.W., Betts, H., Dombrowski, N.,

Szánthó, L.L., Boyle, R., Daines, S., Chen, X. and Lane, N. (2024). The nature of the Last Universal Common Ancestor and its impact on the early Earth system. Nature Ecology and Evolution.

Morowitz, H. J. (1968). *Energy flow in biology: Biological organization as a problem in thermal physics*. Academic Press.

Murray, C. D., & Dermott, S. F. (1999). *Solar system dynamics*. Cambridge University Press.

Naylor, E. (1999). Marine animal behavior in relation to lunar phase. *Proceedings of the Royal Society B: Biological Sciences, 265*(1393), 1005–1010.

Newton, I. (1999). *The principia: Mathematical principles of natural philosophy* (I. B. Cohen & A. Whitman, Trans.). University of California Press. (Original work published 1687)

Nicholls, D. G., & Ferguson, S. J. (2013). *Bioenergetics 4*. Academic Press.

Nickerson, R. S. (1998). Confirmation bias: A ubiquitous phenomenon in many guises. *Review of General Psychology, 2*(2), 175–220. https://doi.org/10.1037/1089-2680.2.2.175

Nicolis, G., & Prigogine, I. (1989). *Exploring complexity: An introduction*. W. H. Freeman.

Noble, D. (2008). *The music of life: Biology beyond genes*. Oxford University Press.

Noether, E. (1971). Invariant variation problems (M. A. Tavel, Trans.). *Transport Theory and Statistical Physics, 1*(3), 186–207. (Original work published 1918)

Nosek, B. A., Ebersole, C. R., DeHaven, A. C., & Mellor, D. T. (2018). The preregistration revolution. *Proceedings of the National Academy of Sciences, 115*(11), 2600–2606. https://doi.org/10.1073/pnas.1708274114

Odum, H. T., & Pinkerton, R. C. (1955). Time's speed regulator: The optimum efficiency for maximum power output in physical and biological systems. *American Scientist, 43*(2), 331–343.

Oláh, K., Kővári, Z., Petrovay, K., Soon, W., Baliunas, S., Kolláth, Z. and Vida, K., (2016).

Magnetic cycles at different ages of stars. Astronomy & Astrophysics, 590, p.A133.

Olson, P., & Amit, H. (2014). Magnetic reversal frequency scaling in dynamos with thermochemical convection. *Physics of the Earth and Planetary Interiors*, 229, 122–133.

Orth, J. D., Thiele, I., & Palsson, B. Ø. (2010). What is flux balance analysis? *Nature Biotechnology, 28*(3), 245–248. https://doi.org/10.1038/nbt.1614

Ott, E. (2002). *Chaos in Dynamical Systems* (2nd ed.). Cambridge University Press.

Pagel, M. (1999). Inferring the historical patterns of biological evolution. *Nature, 401*, 877–884.

Pan, L., Yan, R., Li, W., & Xu, K. (2018). Super-resolution microscopy reveals the native

ultrastructure of the erythrocyte cytoskeleton. Cell Reports, 22(5), 1151-1158.

Panda, S. (2016). Circadian physiology of metabolism. *Science, 354*(6315), 1008–1015. https://doi.org/10.1126/science.aah4967

Parker, E. N. (1979). *Cosmical Magnetic Fields*. Oxford University Press.

Pathria, R. K., & Beale, P. D. (2011). *Statistical mechanics* (3rd ed.). Academic Press.

Paul, S. P. (2016). Golden spirals and scalp whorls: Nature's own design for rapid expansion. *PLoS ONE, 11*(9), e0162026. https://doi.org/10.1371/journal.pone.0162026

Peebles, P. J. E. (1993). *Principles of physical cosmology*. Princeton University Press.

Penrose, R. (2004). *The Road to Reality*. Jonathan Cape.

Persaud-Sharma, D. and O'Leary, J. P., 2015. Fibonacci series, golden proportions, and the human biology. Austin J Surg. 2, 1066.

Pietsch, M., Aguirre Dávila, L., Erfurt, P., Avci, E., Lenarz, T., & Kral, A. (2017). Spiral form of the human cochlea results from spatial constraints. *Scientific Reports, 7*, 7500. https://doi.org/10.1038/s41598-017-07795-4

Pikovsky, A., Rosenblum, M., & Kurths, J. (2001). *Synchronization: A universal concept in nonlinear sciences*. Cambridge University Press.

Pittendrigh, C. S. (1993). Temporal organization: Reflections of a Darwinian clock-watcher. *Annual Review of Physiology, 55*, 16–54.

Pletzer, B., Kerschbaum, H., & Klimesch, W. (2010). When frequencies never synchronize: The golden mean and the resting EEG. *Consciousness and Cognition, 19*(3), 856–864. https://doi.org/10.1016/j.concog.2010.05.004

Popper, K. R. (1959). *The logic of scientific discovery*. Routledge.

Prigogine, I., & Stengers, I. (1984). *Order out of chaos: Man's new dialogue with nature*. Bantam Books.

Raichle, M. E. (2015). The brain's default mode network. *Annual Review of Neuroscience, 38*, 433–447. https://doi.org/10.1146/annurev-neuro-071013-014030

Regula, B., & Lami, L. (2024). Reversibility of quantum resources through probabilistic protocols**.** *Nature Communications, 15*, Article 3096. https://doi.org/10.1038/s41467-024-47243-2

Riddle, L. (2019). *How to create Sierpinski triangle designs*. Agnes Scott College. https://larryriddle.agnesscott.org/ifskit/IFShelp/SierpinskiTriangles.html

Roberts, P. H., & King, E. M. (2013). On the genesis of the Earth's magnetism. *Reports on Progress in Physics*, 76(9), 096801.

Sacco, R. G., Beitman, B. B., & Marks-Tarlow, T. (2025). *Predicting mental health disorder onsets with Fibonacci sequencing: A genetic and epigenetic perspective.* Journal of Psychiatric Research, 183, 237–243.

Scerri, E. R. (2007). *The periodic table: Its story and its significance*. Oxford University Press.

Scheffer, M., Bascompte, J., Brock, W., Brovkin, V., Carpenter, S., Dakos, V., Held, H., van Nes, E., Rietkerk, M., & Sugihara, G. (2009). Early-warning signals for critical transitions. *Nature, 461*(7260), 53–59. https://doi.org/10.1038/nature08227

Scheibye-Knudsen, M., Fang, E. F., Croteau, D. L., Wilson, D. M., & Bohr, V. A. (2014). Protecting the mitochondrial powerhouse. *Trends in Cell Biology, 25*(3), 158–170. https://doi.org/10.1016/j.tcb.2014.11.002

Schneider, E. D., & Sagan, D. (2005). *Into the cool: Energy flow, thermodynamics, and life*. University of Chicago Press.

Schoenaker, D. A. J. M., Jackson, C. A., Rowlands, J. V., & Mishra, G. D. (2014). Socioeconomic position, lifestyle factors and age at natural menopause: A systematic review and meta-analyses of studies across six continents. *International Journal of Epidemiology, 43*(5), 1542–1562. https://doi.org/10.1093/ije/dyu094

Schrödinger, E. (1944). *What is life? The physical aspect of the living cell*. Cambridge University Press.

Sender, R., & Milo, R. (2021). The distribution of cellular turnover in the human body. *Nature Medicine, 27*(1), 45–48.

Sendker, F.L., Lo, Y.K., Heimerl, T., Bohn, S., Persson, L.J., Mais, C.N., Sadowska, W., Paczia,

N., Nußbaum, E., del Carmen Sánchez Olmos, M. and Forchhammer, K., 2024. Emergence of fractal geometries in the evolution of a metabolic enzyme. Nature, pp.1-7.

Shannon, C. E. (1948). A mathematical theory of communication. *Bell System Technical Journal, 27*, 379–423, 623–656. https://doi.org/10.1002/j.1538-7305.1948.tb01338.x

Simon, H. A. (1962). The architecture of complexity. *Proceedings of the American Philosophical Society, 106*(6), 467–482.

Sporns, O. (2011). *Networks of the brain*. MIT Press.

Springel, V., White, S. D. M., Jenkins, A., Frenk, C. S., Yoshida, N., Gao, L., … Evrard, A. E. (2005). Simulations of the formation, evolution and clustering of galaxies and quasars. *Nature, 435*, 629–636. https://doi.org/10.1038/nature03597

Stanley, H. E. (1999). Scaling, universality, and renormalization: Three pillars of modern critical phenomena. *Reviews of Modern Physics, 71*(2), S358–S366. https://doi.org/10.1103/RevModPhys.71.S358

Steriade, M. (2006). Grouping of brain rhythms in corticothalamic systems. *Neuroscience, 137*(4), 1087–1106. https://doi.org/10.1016/j.neuroscience.2005.10.029

Stewart, I. (2016). *The mathematics of life*. Basic Books.

Strogatz, S. H. (2015). *Nonlinear dynamics and chaos* (2nd ed.). Westview Press.

Suri, M. (2022). *The big bang of numbers: How to build the universe using only maths*. Bloomsbury Publishing.

Tegmark, M. (2000). Importance of quantum decoherence in brain processes. *Physical Review E, 61*(4), 4194–4206. https://doi.org/10.1103/PhysRevE.61.4194

The Event Horizon Telescope Collaboration, Akiyama, K., Alberdi, A., Alef, W., Algaba, J. C., Anantua, R., Asada, K., Azulay, R., Bach, U., & Baczko, A.-K., et al. (2024). First Sagittarius A* Event Horizon Telescope results. VIII. Physical interpretation of the polarized ring. *The Astrophysical Journal Letters, 964*(2), L26. https://doi.org/10.3847/2041-8213/ad2df1

Theiler, J., Eubank, S., Longtin, A., Galdrikian, B., & Farmer, J. D. (1992). Testing for nonlinearity in time series: The method of surrogate data. *Physica D: Nonlinear Phenomena, 58*(1–4), 77–94. https://doi.org/10.1016/0167-2789(92)90102-S

Thompson, D. W. (1942). *On growth and form* (2nd ed.). Cambridge University Press.

Tononi, G. (2008). Consciousness as integrated information: A provisional manifesto. *Biological Bulletin, 215*(3), 216–242.

Tononi, G., Boly, M., Massimini, M., & Koch, C. (2016). Integrated information theory: From consciousness to its physical substrate. *Nature Reviews Neuroscience, 17*(7), 450–461. https://doi.org/10.1038/nrn.2016.44

Torday, J. S. (2018). Quantum mechanics predicts evolutionary biology. *Progress in Biophysics and Molecular Biology, 135*, 11–15. https://doi.org/10.1016/j.pbiomolbio.2017.11.001

Torday, J. S. (2019). Evolution, the 'mechanism' of big history—the grande synthesis. *Journal of Big History, 3*(2), 17–24.

Torday, J.S. (2023). Symbiogenesis Redicts the Monism of the Cosmos, Progress in Biophysics and Molecular Biology, 191, 58–62.

Torday, J. S., & Rehan, V. K. (2012). *Evolutionary biology, cell–cell communication, and complex disease*. Wiley.

Torday, J. S., & Rehan, V. K. (2017). Evolution, the logic of biology. John Wiley & Sons.

Torday, J. S., & Sacco, R. G. (2023). Systems biology of human aging: A Fibonacci time series model. Progress in Biophysics and Molecular Biology, 177, 24-33.

Torday, J. S., & Sacco, R. G. (2024). Fibonacci's blueprint in lifespan: Integrating mathematical predictions with RNA dynamics and DNA heritability in systems biology. In J. Barciszewski (Ed.), *Systems biology II* (2nd ed.). Springer.

Valet, J.-P. (2003). Time variations in geomagnetic intensity. *Reviews of Geophysics*, 41(1).

Vogel, H. (1979). A better way to construct the sunflower head. *Mathematical Biosciences, 44*, 179–189.

Weinberg, S. (2008). *Cosmology*. Oxford University Press.

West, G. B. (2014). *Scale: The universal laws of growth, innovation, sustainability, and the pace of life in organisms, cities, economies, and companies*. Penguin Press.

West, B. J., Bhargava, V., & Goldberger, A. L. (1986). Beyond the principle of similitude: Renormalization in the bronchial tree. *Journal of Applied Physiology, 60*(3), 1089–1097. https://doi.org/10.1152/jappl.1986.60.3.1089

West, G. B., Brown, J. H., & Enquist, B. J. (1997). A general model for the origin of allometric scaling laws in biology. *Science, 276*(5309), 122–126. https://doi.org/10.1126/science.276.5309.122

West, G. B., Brown, J. H., & Enquist, B. J. (2001). A general model for ontogenetic growth. Nature, 413(6856), 628-631.

West-Eberhard, M. J. (2003). *Developmental plasticity and evolution*. Oxford University Press.

White, J., & Lloyd, M. (1979). 17-year cicadas emerging after 18 years: A new brood? *Evolution*, 1193–1199.

Wikipedia. (2021). Romanesco broccoli (Brassica oleracea). Wikipedia. Retrieved from https://en.wikipedia.org/wiki/Romanesco_broccoli#/media/File:Romanesco_broccoli_(Brassica_oleracea).jpg

Wilson, B. T., Stark, Z., Sutton, R. E., Danda, S., Ekbote, A. V., Elsayed, S. M., … Ganesan, V. (2016). The Cockayne syndrome natural history (CoSyNH) study: Clinical findings in 102 individuals and recommendations for care. *Genetics in Medicine, 18*(5), 483–493. https://doi.org/10.1038/gim.2015.109

Wilson, K. G. (1979). Problems in physics with many scales of length. *Scientific American, 241*(2), 158–179.

Wolfram, S. (2002). *A new kind of science*. Wolfram Media.

Wolfram Research, Inc. (n.d.). Galton board. MathWorld—A Wolfram Web Resource. https://mathworld.wolfram.com/GaltonBoard.html

Wolfram S. Pascal's Triangle Mod k. *Wolfram Demonstrations Project*. Available at: http://demonstrations.wolfram.com/PascalsTriangleModK/.2011.

Xiao, S., & Laflamme, M. (2009). On the eve of animal radiation: Phylogeny, ecology and evolution of the Ediacara biota. *Trends in Ecology & Evolution, 24*(1), 31–40. https://doi.org/10.1016/j.tree.2008.07.015

Young, M. W., & Kay, S. A. (2001). Time zones: A comparative genetics of circadian clocks. *Nature Reviews Genetics, 2*(9), 702–715.